uc3m | Universidad Carlos III de Madrid

e-Archivo

This is a postprint version of the following published document:

Salameh, S., Gómez-Hernández, J., Goulas, A., Van Bui, H. & van Ommen, J. R. (2017). Advances in scalable gas-phase manufacturing and processing of nanostructured solids: A review. *Particuology*, vol. 30, pp. 15–39.

Review

Advances in scalable gas-phase manufacturing and processing of nanostructured solids: A review

Samir Salameh[a], Jesús Gómez-Hernández[a,b], Aristeidis Goulas[a,c], Hao Van Bui[a], J. Ruud van Ommen[a,*]

[a]Delft University of Technology; Julianalaan 136, 2628 BL Delft, The Netherlands
[b]Carlos III University of Madrid; Avda. de la Universidad 30, 28911 Leganés, Madrid, Spain
[c]Delft IMP B.V.; Mekelweg 2, 2628 CD, Delft, The Netherlands
[*]Corresponding author. E-mail: J.R.vanOmmen@tudelft.nl

Abstract: Although the gas-phase production of nanostructured solids has already been carried out in industry for decades, only in recent years has research interest in this topic begun to increase. Nevertheless, despite the remarkable scientific progress made recently, many long-established processes are still used in industry. Scientific advancements can potentially lead to the improvement of existing industrial processes, but also to the development of completely new routes. This paper aims to review state-of-the-art synthesis and processing technologies, as well as the recent developments academic research. Flame reactors that produce inorganic nanoparticles on industrial- and lab-scales are described, alongside a detailed overview of the different systems used for the production of carbon nanotubes and graphene. We discuss the problems of agglomeration and mixing of nanoparticles, which are strongly related to synthesis and processing. Finally, we focus on two promising processing techniques, namely nanoparticle fluidization and atomic layer deposition.

Keywords: Nanoparticle synthesis; Gas-phase process; Nanoparticle fluidization; Atomic layer deposition; Agglomeration

Contents

1. Introduction

In recent years, chemistry has focused much attention on large molecules and supramolecular assemblies thereof, while engineering has become able to create increasingly smaller devices. They meet each other naturally at the nanometre scale, in the field known as nanoscience or nanotechnology. Great advances have been made, yielding all kinds of novel, nanostructured materials such as graphene, nanowires, and quantum dots. Such nanostructured materials are of great importance; they have the potential to significantly contribute to solutions to the great challenges faced by society today, e.g. energy conversion and storage. The building blocks of such materials are often nanostructured solids or particles: solid objects with a size <1 mm, consisting of multiple elements and/or multiple materials, at least one of the elements of which has a nanoscale dimension. These elements can be classified as 0D, 1D or 2D depending on the number of dimensions in which they have a size smaller than a threshold $d*$. This threshold $d*$ is defined by a critical characteristic of some physical phenomenon (free path length of electrons, phonons, length of de Broglie wave, length of external electromagnetic or acoustic waves, correlation length, penetration length, diffusion length, etc.) that gives rise to size-effects (Pokropivny & Skorokhod, 2007). However, in this review we will focus on the generic, commonly used value of 100 nm for $d*$.

Nanostructured solids exhibit extraordinary properties compared with those of their bulk counterparts. To give a few examples, nanoparticles have lower melting points and higher solubilities than bulk materials; quantum dots emit specific photons depending on their size; carbon and inorganic nanotubes exhibit high mechanical strength and controllable electric conductivity; graphene has a very high electrical and thermal conductivity. However, to fully exploit these special properties it is crucial that the material has a high level of quality, reflected by demanding specifications. For example, for quantum dots to emit well-defined photons, it is crucial that the standard deviation in their size is less than 5%. This corresponds to a precision of a single consistent atom layer throughout the 1–15-nm range (Pokropivny & Skorokhod, 2007). Such precision can now only be achieved in small-scale ultra-fast processes, using tricks from colloidal chemistry. This generates samples for R&D, but there is no clear route to a scalable commercial

process. In catalyst preparation, synthetic strategies based on molecular principles yield better-defined catalyst structures than traditional and cruder catalyst preparation techniques such as impregnation and deposition/precipitation. This can aid mechanism determination and the development of novel catalytic routes in several classes of reactions (Murray, Kagan, & Bawendi, 2000). Additionally, for consumer products based on nanostructured materials it is of utmost importance that morphology is precisely controlled. For example, the fabrication of transparent electrodes requires high-quality large-area graphene sheets (Wegener, Marks, & Stair, 2012). The strength of ultra-strong nanostructured materials is largely determined by the extent to which the amount of defects present can be minimized (Li et al., 2009a). A high level of control over morphology is thus crucial, both in fundamental studies and in the application of such materials.

Many of the current methods for manufacturing nanostructured materials do not lend themselves to large-scale production, which greatly inhibits innovation and actual use in society instead of in the lab (Roebben et al., 2014; Wegner, Schimmoeller, Thiebaut, Fernandez, & Rao, 2011; Zhu & Li, 2010). Large-scale production with high quality is required to achieve breakthroughs in seemingly unrelated fields, from the nanostructured materials required for personalized medicine without side-effects to those for high-power, fast-charging batteries. The technologies used to manufacture such materials expected to impact global problems related to food, water, energy and the environment must be scalable. "The main reason that these problems are so grand is that they are ubiquitous and therefore the related commercial markets have become commoditized. Very often, a technology that exploits a unique attribute of a nanomaterial can offer improvements in functional or engineering performance, but almost as often, these technologies require scarce materials (and therefore expensive) or slow or complicated manufacturing processes (and also expensive)" (Giges, 2013). The scaling-up of nanotechnology is not just something that remains to be done after all the interesting scientific work has been carried out; it should be an integral part of the scientific process leading to breakthrough solutions. When nanostructured materials are synthesized in such a way that the relevant processes concerning kinetics, thermodynamics and transport phenomena are known and controlled, then the knowledge is intrinsically scale-independent. In other words, rational design facilitates large-scale production. The urgent need to pay more attention to this topic is also reflected by the title of the Kavli Futures Symposium four years ago: "Plenty of Room in the Middle", paraphrasing Feynman's famous quote. With this title the organizers implied the need to master mesoscale structures and to bring nanoscientific discoveries to scale, bringing them to devices that can affect our everyday lives. It was concluded that "great opportunities that lie in scaling up from atomic assembly and individual nanodevices to macroscopic systems and structures with emergent properties and functionality" (Kavli Foundation, 2011).

While the majority of researchers currently working on nanostructured materials focus on liquid-phase synthesis, it is our firm belief that gas-phase routes deserve more attention if scalable processes are to be achieved. Currently, most single-material nanoparticles are commercially produced via gas-phase processes (Teoh, 2013). In this review, we discuss gas-phase approaches used to produce, transport and functionalize

nanostructured solids, focusing on methods that have good prospects for scale-up. First, we discuss the gas-phase synthesis of nanoparticles (0D materials), with a strong emphasis on the use of flame reactors because this is the most widely used technique at the industrial scale. We then address the synthesis of carbon nanotubes and graphene as examples of 1D and 2D materials that can already be produced at a relatively large scale. This is followed by a section on the subsequent physical processing of nanoparticles, discussing agglomeration, fluidization and mixing. Finally, we look into structuring at the nanoscale involving multiple materials (e.g., a host nanoparticle with a film or nanoclusters on its surface) using atomic layer deposition. It is certainly not our ambition to discuss all the developments in the field. We rather focus on a number of developments that we see as promising ways to produce nanostructured solids at the industrial scale that are already in use or are expected to find their way to industry in the short term.

2. Gas-phase synthesis of nanoparticles

In the following section we give an overview of gas-phase (aerosol) methods that are used to synthesize nanoparticles (0D materials) and are promising for industrial-scale synthesis. Because up to 90% of the commercially available aerosol-made products are synthesized using methods based on flame reactors (Mueller, Mädler, & Pratsinis, 2003; Wegner & Pratsinis, 2003), this review concentrates on this reactor type, although various gas-phase methods such as hot wall reactors (Weiss, Ly, Wegner, Pratsinis, & Steinfeld, 2005), laser ablation (Ullmann, Friedlander, & Schmidt-Ott, 2002), and plasma reactors (Vollath, 2008) are described in the literature. This chapter is by far too limited to give a comprehensive overview of all the problems and possibilities of flame reactors, but excellent reviews that report on this reactor type and the arising nanoparticles in much more detail are already available (Buesser & Pratsinis, 2012; Eggersdorfer & Pratsinis, 2014; Teoh, Amal, & Mädler, 2010). Herein, we first describe the established industrial processes for the gas-phase synthesis of nanoparticles to depict the state-of-the-art. Then, we discuss flame reactors and their development over the few last decades in detail to reveal the gap between current industrial processes and lab-scale developments. Finally, we give a short overview of spray drying as an additional promising technique for nanoparticle synthesis.

2.1. Industrial synthesis of nanoparticles

One of the oldest nanomaterials produced on an industrial scale is carbon black. Its production is dated back to ancient China, where it was used as a black pigment (Donnet, 1993). Nowadays this material is mainly used as a filler material in tires. Nevertheless, to a small extent carbon black is still used as a pigment as it was thousands of years ago (Donnet, 1993; Friedlander, 2000). The size of carbon black particles can vary between a few and a few hundred nanometres, depending on the conditions of the production process and the desired properties of the product. In contrast to the combustion of coal, which was the main production method used in the past, over 95% of carbon black is nowadays produced by the furnace process (see Fig. 1) (Addison et al., 2013; Donnet, 1993). In total, over 8 million tons of carbon black are produced per year (International Carbon Black Association, 2014).
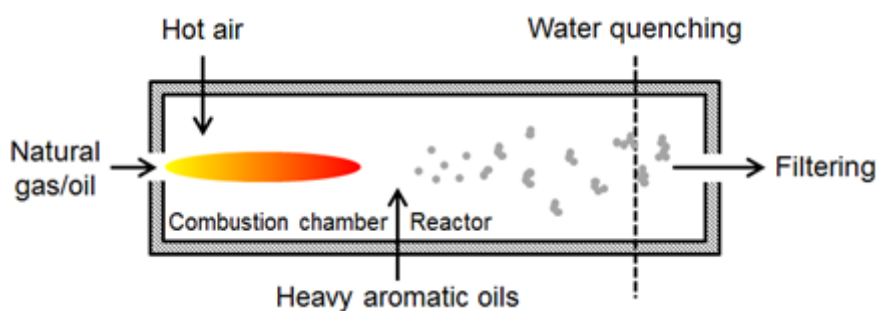
Fig. 1. Schematic representation of the furnace process used to synthesize carbon black on an industrial scale. The atomization and pyrolyzation of heavy aromatic oils lead to the formation of primary particles, which aggregate/agglomerate and can be separated at the end of the process.

In the furnace process, heavy aromatic oils are decomposed to carbon black using a hot gas stream. The exact furnace dimensions and structure can vary between different producers, but the process generally proceeds in the same way. To initiate the chemical reaction, the furnace is first heated by burning natural gas or oil inside a combustion chamber, leading to a temperature of about 1300 °C. The hot combustion gas produced passes into the reactor, where heavy aromatic oils are introduced. The atomized oil is vaporized and pyrolyzed, and particle formation occurs through the processes of nucleation, coalescence and aggregation. The properties of the synthesized particles can be controlled by the temperature and the pressure of the furnace, which is typically between 4 and 10 bars. At the end of the furnace the particles are quenched to about 200 °C using a water spray. Finally, they can be separated using a combination of electric filters, cyclones and bag filters, and further treatments can be performed as desired (Burke, 1933; Donnet, 1993; Friedlander, 2000; Gerhard, Gerhard, Gerhard, & Heinrich, 1972; Larson, 1957; Loving, 1947; Matlock, 1931; Pollock, 1957; Roger, 1969; Stokes, 1951, 1954; Voll, Rothbuhr, & Kuhner, 1984). Because the furnace process has been used for decades, it is now quite well understood. As a result, the discharge of soot can be easily controlled and prevented, and the production costs are very low. However, the process still does not operate at desired efficiency levels, and so its improvement is still ongoing (Davis, Nicholas, Smith, Wang, & Wright, 1991; Rumpf, Taylor, & Toombs, 2010; Schwaiger et al., 2014).

Another important nanomaterial synthesized on an industrial scale is TiO_2. It is mostly used as a white pigment in paints and coatings (Braun, Baidins, & Marganski, 1992). It is also used in sun crèmes (Singh & Nanda, 2014), as a photocatalyst (Fujishima & Honda, 1972; Gupta & Tripathi, 2011), and in dye-sensitized solar cells (Grätzel, 2003). However, the particle sizes needed for different applications vary strongly. For pigments the ideal particle size is about 200 nm (Knauth, Bouchet, Schaf, Weibel, & Auer, 2003), while for solar cells a particle size of about 25 nm is favourable (Chou, Zhang, Russo, Fryxell, & Cao, 2007). The worldwide production of TiO_2 is 4.5 million tons per year, about 50% that of carbon black (Robichaud, Uyar, Darby, Zucker, & Wiesner, 2009). Two essential processes, the sulfate process and the chloride process, are used to synthesize TiO_2 in industry (Braun et al., 1992; Knauth et al., 2003).

5

In the sulfate process, mined ore (mostly $FeTiO_3$) is digested with concentrated sulfuric acid. The resulting liquid contains titanyl sulfate and iron sulfate. The iron sulfate is removed through crystallization. In the next step, TiO_2 is formed by hydrolysis and heated in a calciner to evaporate water and the remaining sulfuric acid from the solids. Depending on the temperature in the calciner, either the anatase (~800 °C) or rutile (~900 °C) crystal phase is formed. After cooling, the crystals can be milled to achieve the desired size for each particular application. However, this process creates a large amount of acidic waste and runs as a batch process. Also, the minimum crystal size is limited by the milling process, which restricts the usability of this process to the production of very small primary particle sizes as required, e.g. in catalysis (Braun et al., 1992; Buxbaum, 2008; Gazquez, Bolivar, Garcia-Tenorio, & Vaca, 2014; Knauth et al., 2003).

In the chloride process, commercialized by Du Pont in the early 1950s (Schaumann, 1949a, 1949b), titanium (IV) chloride is formed by the reaction of ore, coke and chlorine at about 1000 °C. The resulting vapour stream is then cooled to purify it from other metal chlorides. Second, the liquid titanium (IV) chloride is vaporized and burned in an oxygen-rich environment at temperatures above 1500 °C. To achieve the high temperatures necessary for the chemical reaction, hydrocarbons (commonly methane) are added to the reaction zone. There, TiO_2 is formed as fine crystals in the gas stream, and can be filtered with cyclones or filters (Boeer, 1996; Braun et al., 1992; Buxbaum, 2008; Gazquez et al., 2014; Knauth et al., 2003; Lange, Diether, Volling, & Klebe, 1976; Schaumann, 1949a, 1949b; Tully & Olsen, 1954). However, this process requires high-purity ore and can only produce rutile pigments. Nevertheless, it has advantages in process cost and waste management compared with the sulfate process, and is therefore the most widely used industrial process (Gazquez et al., 2014).

For the manufacture of very fine oxide nanoparticles, an adapted version of the chloride process was patented in 1952 (Kloepfer, 1952). The process is similar to the manufacturing of industrial carbon black, as is obvious by comparing Fig. 1 and Fig. 2. Gases such as hydrogen are burned to create a hot flame and are mixed with preheated oxygen. Then, $TiCl_4$ (or a different precursor in the case of different oxide particles such as SiO_2) is vaporized and introduced into the reaction chamber, in which particles form through nucleation, coagulation and aggregation. To prevent further particle growth, the reaction time is limited to under 1 s using the gas stream and by quenching the hot particles at the end of the reaction chamber using an inert gas stream (Beumer, Brandle, Weidmann, & Zirngibl, 1969; Kloepfer, 1952; Macwan, Dave, & Chaturvedi, 2011). The above-described processes are under continuous improvement. A major challenge in the synthesis of both very fine and pigment powders is the pollution of the reactor walls with particles, which can strongly influence the properties of the product (Gruber & Malcharek, 2011; Rick, 1955; Yuill, Natalie, Flynn, & Fillipi, 2002). Another focus of new reactors is the production of mixed oxide powders such as TiO_2/ZnO, TiO_2/MgO, TiO_2/Al_2O_3, or TiO_2/Fe_2O_3 (Hemme, Mangold, Geissen, & Moiseev, 2003; Habermann, Hasenzahl, & Hemme, 2011; Hartmann & Kerner, 2002; Hartmann, Mangold, & Kerner, 1997, 1998; Kleinschmit & Schwarz, 1981; Mangold, Golchert, Katusic, & Janzon, 2001; Schumacher, Schilling, Alff, & Roth, 2006), which can be used in applications such as coatings (Petersen, Sale, & Reardon, 2007) or catalysts (Wachs, 2005).
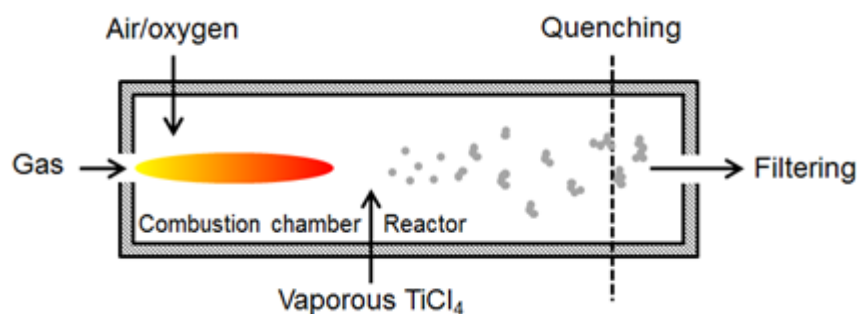
Fig. 2. Schematic representation of the synthesis of fine oxide nanoparticles by a vapour-assisted flame process.

2.2. Flame reactors

As described in the previous section, flame reactors are often used in industry to produce various types of nanoparticles. In general, the advantages of flame reactors are high purity, nonporous primary particles and small sizes with relatively narrow size distributions, while the disadvantages include difficulties in producing unagglomerated particles and multicomponent materials (Mädler, Kammler, Mueller, & Pratsinis, 2002a; Mädler, Stark, & Pratsinis, 2002b; Strobel, Baiker, & Pratsinis, 2006). Flame reactors can be classified into several types. Flame aerosol reactors are based on the use of gaseous precursors and the resulting gas-to-particle conversion. In these reactors the precursor is vaporized and burned in an air or oxygen environment. The heat needed for this reaction is achieved by burning natural gases (mostly methane) or oil as described in the previous section for carbon black and titania. A new generation of flame reactors, flame spray pyrolysis (FSP) reactors, have been intensively investigated during the last two decades (Baranwal, Villar, Garcia, & Laine, 2001; Bickmore et al., 1998; Bickmore, Waldner, Treadwell, & Laine, 1996; Chiarello, Selli, & Forni, 2008; Height, Mädler, Pratsinis, & Krumeich, 2006; Hembram, Sivaprakasam, Rao, & Wegner, 2013; Mädler et al., 2002a, 2006; Mädler & Pratsinis, 2002; Marchal, John, Baranwal, Hinklin, & Laine, 2004; Pawinrat, Mekasuwandumrong, & Panpranot, 2009; Pokhrel, Birkenstock, Schowalter, Rosenauer, & Mädler, 2010; Strobel et al., 2006; Strobel & Pratsinis, 2009; Teoh et al., 2010; Teoh, Amal, Mädler, & Pratsinis, 2007; Tian et al., 2009; Tok, Boey, & Zhao, 2006). In this reactor type, a liquid precursor is dispersed and the resulting droplets are burned. The heat necessary for the synthesis of the nanoparticles is directly provided from the combustion of the liquid precursor. The advantages of these reactors are that they are relatively simple, use cheap precursors, can produce multiple component systems (see Fig. 3) and have a high-temperature gradient (Kammler, Mädler, & Pratsinis, 2001; Mädler et al., 2002b; Teoh et al., 2010).
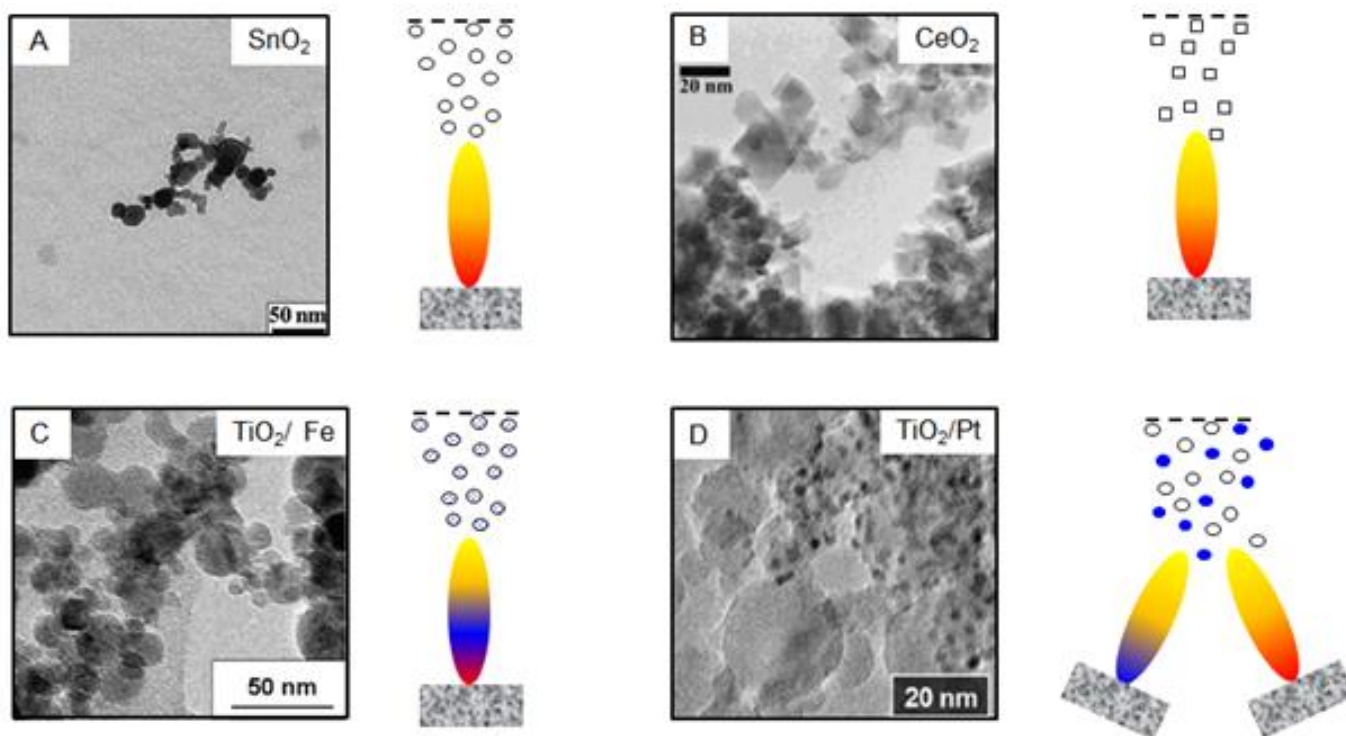
Fig. 3. Schematic representation of the flame spray pyrolysis (FSP) reactor producing spherical (A) or cubic (B) nanoparticles, or synthesizing multicomponent nanomaterials by doping (C) or using multiple flames (D). (All TEM images are reprinted with permission from the respective references: (A) Elsevier (Sahm et al., 2004), (B) Material Research Society (Mädler et al., 2002b), (C) Elsevier (Teoh et al., 2007), and (D) Springer Science and Business Media (Grossmann et al., 2015).)

In FSP reactors, the size of the synthesized nanoparticles depends on the temperature and the residence time of the particles in the flame. Both parameters can easily be controlled via the ratio of the precursor flow rate to the oxygen dispersion flow rate (Mädler et al., 2002a, 2002b). This gives a high flexibility for the adjustment of primary particle sizes during the FSP process. Furthermore, multicomponent systems can be easily synthesized by doping the basic material (Mädler et al., 2006; Pawinrat et al., 2009; Teoh et al., 2007; Tian et al., 2009) or using a multiple flame set-up (see Fig. 3C and D) (Grossmann et al., 2015; Minnermann et al., 2013). The reported advantages have recently motivated the first companies to implement the FSP reactor to synthesize nanopowders on an industrial scale (Hembram et al., 2013; Mueller et al., 2003). However, the FSP process is not completely understood and research is ongoing to understand coalescence and coagulation as the dominant mechanism to predict and control the aggregation of the particles (Buesser & Pratsinis, 2012; Eggersdorfer & Pratsinis, 2014) and the burning of droplets in the flame (Noriler, Rosebrock, Mädler, Meier, & Fritsching, 2014; Rosebrock, Riefler, Wriedt, Mädler, & Tse, 2013).

2.3. Spray drying

Another established process used to synthesize particles by dispersing a liquid precursor is spray drying (Fogler & Kleninschmidt, 1938; Gharsallaoui, Roudaut, Chambin, Voilley, & Saurel, 2007). This process is not yet used to synthesize nanoparticles on an industrial scale, but recent developments have revealed the scale-up potential of this technique. In spray drying, the liquid is dispersed into droplets with an atomizer or spray nozzle. Unlike in flame reactors, the droplets are evaporated under mild heating conditions in a hot gas stream, leading to the formation of particles (see Fig. 4). Because the temperatures used are much lower (typically 40–300 °C) than those in flame reactors, spray drying is widely used for the synthesis of temperature-sensitive powders, e.g. in food or pharmaceutical applications (Gharsallaoui et al., 2007; Tsapis, Bennett, Jackson, Weitz, & Edwards, 2002; Vehring, 2008; Vehring, Foss, & Lechuga-Ballesteros, 2007). The size of the particles depends strongly on the size of the dispersed droplets and therefore on the type of atomizer. Spray drying is usually used to synthesize micron-sized particles. However, new systems are also able to produce particles down to the nanoscale, as reviewed by Nandiyanto and Okuyama (2011). The decrease in particle size is achieved by very fine dispersion of the liquid using assisting methods such as pressure or centrifugal, electrostatic or ultrasonic forces (Nandiyanto & Okuyama, 2011). Kaluza and Muhler (2009) used spray drying with a two-fluid nozzle to synthesize nanosized Al_2O_3, ZnO and a composite of both materials. Additionally, Mei et al. (2011) reported the synthesis of Nb-doped TiO_2 using a two-fluid nozzle.
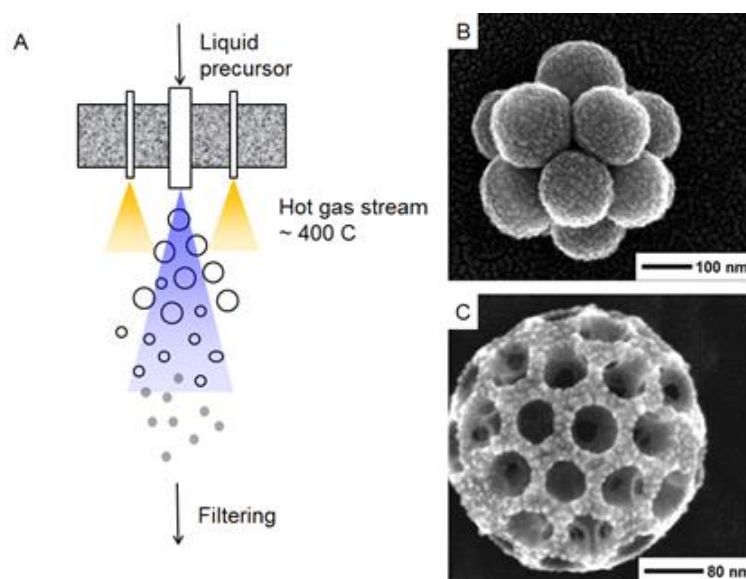
Fig. 4. (A) Schematic of the spray-drying process showing mild drying of the dispersed droplets. Depending on the droplet size and chemistry used, different particle shapes and sizes (down to the nanoscale) can be achieved. (B and C are reprinted with the permission of Elsevier (Nandiyanto & Okuyama, 2011).)

In a conventional spray-dryer, the concentration of the precursor in each droplet has to be very low to synthesize particles of tens to hundreds of nanometres in size. This is a large drawback for industrial-scale production. Therefore, new enhancements of the traditional spray drying process have been developed. The

most promising approaches are the rapid-solvent evaporation technique and the additive-assisted spray method (Mei et al., 2011; Nandiyanto & Okuyama, 2011). A unique property of spray drying is that particles with complex shapes can be synthesized (Fig. 4B and C) by tuning the precursor and drying conditions. The resulting diversely shaped particles can be hundreds of nanometres to microns in size. Their high porosity and therefore large accessible surface area makes them interesting for various applications and easy to scale up (Ariga, Vinu, Yamauchi, Ji, & Hill, 2012; Nandiyanto & Okuyama, 2011; Sathe, Agrawal, & Nie, 2006; Tsapis et al., 2002).

3. Gas-phase synthesis of carbon nanotubes and graphene

While nanoparticles are already widely produced in industry, the industrial manufacturing of 1D and 2D materials is still very limited; only carbon nanotubes and graphene are produced on relatively large scales. In the context of this review, we discuss the recent achievements in the large-scale gas-phase synthesis of CNTs and graphene from the viewpoint of powder technology (i.e., 1D (CNTs) and 2D (graphene) powders). Most attention will be given to carbon nanotube (CNT) synthesis. While commercial applications of graphene are still in their infancy, CNT powders have been applied in several commercial products (De Volder, Tawfick, Baughman, & Hart, 2013) since the hallmark paper by Iijima (1991).

3.1. Synthesis of CNTs by arc-discharge

In 1991, Iijima reported the synthesis of multi-walled CNTs (MWCNTs) by arc-discharge, which created enormous attention for these structures. Later, it was noted that CNTs had already been observed much earlier (Oberlin, Endo, & Koyama, 1976; Radushkevich & Lukyanovich, 1952), but had remained largely unnoticed. Single-walled CNTs (SWCNTs) synthesized by arc-discharge were reported by Iijima and Ichihashi (1993) and Bethune et al. (1993). Based on experimental observations, various models have been developed to explain the growth mechanism of CNTs in arc-discharge (Ajayan & Ebbesen, 1997; Amelinckx, Bernaerts, Zhang, Van Tendeloo, & Van Landuyt, 1995; Colbert et al., 1994; de Heer, et al., 2005; Gamaly & Ebbesen, 1995; Gavillet et al., 2001; Iijima, Ajayan, & Ichihashi, 1992; Kukovitsky, L'vov, & Sainov, 2000). For example, a vapor-solid phase mechanism for CNT formation in arc-discharge was proposed by Colbert et al. (1994) and Gamaly and Ebbesen (1995). A vapor-liquid-solid model was developed by Kukovitsky et al. (2000) and Gavillet et al. (2001), while a liquid-phase growth mechanism was proposed by de Heer et al. (2005). However, each of these models only explains the growth of CNTs under certain experimental conditions, and does not provide a general mechanism (Ajayan & Ebbesen, 1997).

The properties of CNTs synthesized by arc-discharge are strongly dependent on experimental conditions such as power supply and temperature, carbon sources, catalyst type and properties, pressure, and electrode size and shape (Arora & Sharma, 2014; Keidar, 2007). In arc-discharge, a high temperature is required for the ionization of the gas to form plasma. This is controlled by the current density between the

two electrodes and the thermal properties of the reaction atmosphere. For example, hydrogen plasma can generate temperatures in the range of 3300–3500 °C, whereas argon plasma can only reach 1900–2100 °C (Arora & Sharma, 2014). The temperature variation significantly influences the quality and size of the CNTs (Kim, Sugime, Hasegawa, Osawa, & Noda, 2012; Song, Liu, & Zhu, 2007; Zhao & Liu, 2004; Zhao, Liu, & Zhu, 2005). However, there is no clear trend in the influence of temperature on CNT size. An increase in temperature can increase CNT diameter (Zhao & Liu, 2004; Zhao et al., 2005) but can also reduce CNT diameter (Song et al., 2007). The use of a catalyst plays a crucial role in controlling the quality, size and properties of the synthesized CNTs. Without a catalyst, mostly MWCNTs are formed (Arora & Sharma, 2014; Kim, Muramatsu, Hayashi, & Endo, 2012; Liang, Shimizu, Tanaka, Choi, & Watanabe, 2012). For the synthesis of SWCNTs, transition metals are commonly used, such as Fe (Ando, Zhao, Inoue, Suzuki, & Kadoya, 2005; Ha, Yeom, & Lee, 2009; Qiu, Wang, Zhao, & Wang, 2007), Ni (Sano, Nakano, & Kanki, 2004), Co (Bethune et al., 1993), or their alloys (Hoa, Van Quy, Cho, & Kim, 2009; Hou et al., 2001; Itkis et al., 2004).

Owing to its high growth temperature, arc-discharge produces high-quality and highly crystalline SWCNTs, which show excellent performance in electronic device applications (Biswas & Lee, 2011). However, a major disadvantage of arc-discharge is its low yield of pure CNTs owing to the difficulties in controlling the experimental conditions. New approaches have been developed in the last two decades to improve the quality, size and yield of CNTs, including modification of the arc-discharge apparatus by adding more anodes (Zhao & Liu, 2004) or using a rotating carbon cathode (Joshi, Engstler, Nair, Haridoss, & Schneider, 2008; Lee, Baik, Yoo, & Han, 2002), using pulsed arc-discharge (Roch, Jost, Schultrich, & Beyer, 2007; Roch et al., 2009), using novel catalysts (Journet et al., 1997; Lv, Du, Ma, Wu, & Chen, 2005; Shi et al., 2000; Sun, Bao, Lv, Deng, & Wang, 2007), working at low pressure (Su, Zhou, Zhao, Yang, & Zhang, 2013) or using different gases and carbon sources (Shimotani, Anazawa, Watanabe, & Shimizu, 2014; Zhao et al., 2006). Nevertheless, arc-discharge is not considered to be a suitable method for the large-scale synthesis of CNTs.

3.2. Synthesis of CNTs by laser ablation

The synthesis of CNTs by laser ablation was first reported in 1995 by Guo, Nikolaev, Thess, Colbert, and Smalley (1995), in which a metal-graphite composite target was sublimed under high temperature generated by a YAG laser source. The vaporized carbon was cooled rapidly with an argon flow and SWCNTs were deposited on a water-cooled copper collector positioned downstream of the flow. The SWCNTs produced by this method were shown to be of better quality and higher yield (Guo et al., 1995; Thess et al., 1996) than those produced by arc-discharge. The properties of CNTs prepared by laser ablation are strongly influenced by the laser source, such as the type of laser, Nd:YAG or CO_2 (Maser et al., 1998; Yudasaka et al., 1999a), KrF (Lebel, Aissa, Khakani, & Therriault, 2010), XeCl (Kusaba & Tsunawaki, 2006), Tm:Ho:LuLF (Stramel, Gupta, Lee, Yu, & Edwards, 2010), the laser wavelength (Chrzanowska et al., 2015), the laser power (Yudasaka, Ichihashi, & Iijima, 1998; Zhang, Gu, & Iijima, 1998), the structural

and chemical composition of the target (Bandow et al., 1998; Maser et al., 1998; Yudasaka et al., 1999b), the chamber temperature (Bandow et al., 1998; Hinkov et al., 2004; Kokai et al., 1999; Yudasaka et al., 1998), the chamber pressure and ambient gases (Munoz, Maser, Benito, de la Fuente, & Martinez, 1999; Nishide et al., 2003; Zhang et al., 1998), and the carrier gas flow rate and pressure (Gorbunov et al., 1999). The fundamental aspects of CNT formation by laser ablation are the same as those in the arc-discharge method. Therefore, laser ablation is also commonly used to produce high-quality CNTs (Guo et al., 1995). However, compared with the arc-discharge and CVD methods, laser ablation is more laborious and expensive, and therefore not suitable for large-scale production.

3.3. Synthesis of CNTs by chemical vapour deposition

CVD methods are more attractive for large-scale manufacturing than the other techniques owing to their efficiency of CNT production and controllable growth (De Volder et al., 2013; Kong, Cassell, & Dai, 1998; Yan, Miao, et al., 2015; Zhang, Huang, Zhao, Qian, & Wei, 2011). The CVD of MWCNTs was first realized by Endo et al. (1993), and was further developed to enable the production of SWCNTs (Dai et al., 1996). The principle of CNT CVD is based on the decomposition of carbon precursors at high temperature in the presence of transition metal catalysts (Dai et al., 1996). Two main growth mechanisms of CNTs by CVD methods, determined by the catalyst-support interaction, have been widely accepted (Fig. 5, Kumar & Ando, 2010). When the catalyst-support interaction is weak, carbon precursors decompose on the catalyst surface, and the carbon atoms diffuse through the metal catalyst. In this case, CNTs are formed from the bottom of the metal, lifting the particle up (step i, Fig. 5(a)). This is known as the "tip-growth model", which was first observed by (Baker, Barber, Harris, Feates, & Waite, 1972). In this model, the growth of the CNTs will continue as long as hydrocarbon decomposition and diffusion are still possible (step ii, Fig. 5(a)). When the concentration of carbon on top of the catalyst reaches saturation, growth will stop (step iii, Fig. 5(a)). In contrast, when the catalyst-support interaction is strong, the diffused carbon atoms are not able to push the metal particle up. Instead, they emerge from the top of the metal surface (Fig. 5(b)). In this case, the so-called "base-growth model" occurs (Baker & Waite, 1975).
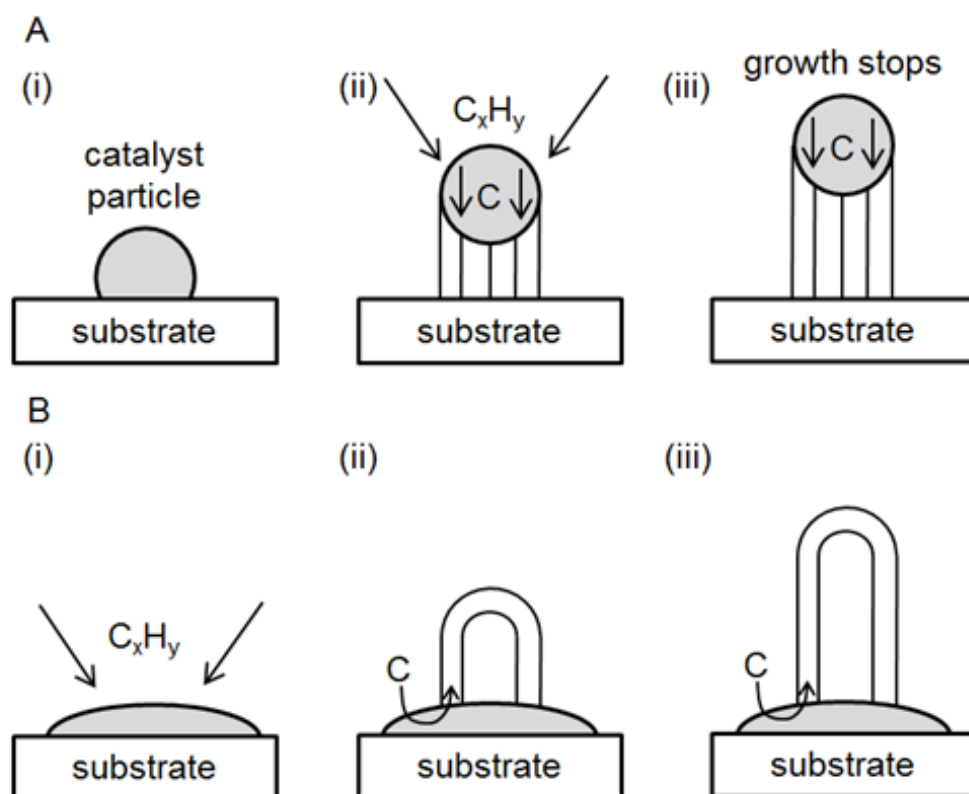
Fig. 5. Growth mechanism of CNTs: (A) tip-growth caused by weak catalyst-support interactions and (B) base-growth mechanism for strong catalyst-support interactions. (schematic redrawn based on Kumar and Ando (2010))

The properties, quality and yield of CNTs synthesized by CVD are strongly affected by the carbon precursor, temperature and catalyst (Yan, Miao, et al., 2015). In fact, the temperature of the CNT-CVD process is determined by the decomposition temperature of the precursor used. Methane (CH_4) has a high thermal stability, and CVD processes using this precursor are usually carried out above 800 °C (Abdullahi, Sakulchaicharoen, & Herrera, 2014; Cassell, Raymakers, Kong, & Dai, 1999; Kong et al., 1998; Li et al., 2004; Ning et al., 2006; Li, Yan, Cheng, Zhang, & Liu, 2002). This is similar to carbon monoxide-based CVD, which requires a very high temperature, i.e. up to 1200 °C (Dai et al., 1996). In contrast, CVD processes using ethylene (C_2H_4), acetylene (C_2H_2) and benzene (C_6H_6) are commonly performed at lower temperatures (i.e. 500–800 °C) owing to their lower stability, which leads to the deposition of large amounts of carbonaceous compounds rather than nanotubes at high temperatures (Chen, Liu, Yang, Wang, & Wang, 2008; Corrias et al., 2003; Endo et al., 1993; Escobar et al., 2007; Kim, Sugime, et al., 2012; Kumar & Ando, 2010; Mukhopadhyay et al., 1999; Qian et al., 2003; Sen, Govindaraj, & Rao, 1997; Tian et al., 2004; Wang, Wei, Luo, Yu, & Gu, 2002a; Zhang et al., 2009; Zhong et al., 2009). As a consequence of high-temperature processing, CVD using methane or carbon monoxide usually produces SWCNTs, whereas MWCNTs are formed in low-temperature processes. However, in some cases SWCNTs can also be grown at low temperatures (Kim, Sugime, et al., 2012; Zhong et al., 2009). In 2002, Maruyama,

Kojima, Miyauchi, Chiashi, and Kohno (2002) demonstrated that high-quality SWCNTs can be synthesized at a relatively low temperature (700 °C) using alcohol (ethanol, methanol). Since then, alcohol has been widely used as a carbon precursor for the CVD of CNTs (Fukuoka, Mizutani, Naritsuka, Maruyama, & Iijima, 2012; Grüneis et al., 2006; Kozawa et al., 2016; Maruyama et al., 2016; Maruyama, Mizutani, Naritsuka, & Iijima, 2011; Nasibulin, Moisala, Jiang, & Kauppinen, 2006; Okubo et al., 2004). The advantages of using ethanol for SWCNT synthesis rely on the role of decomposed OH radicals on the catalyst surface in the removal of amorphous carbon, which initiates the formation of MWCNTs. Hence, OH radicals prevent the generation of side-products and hinder the formation of MWCNTs (Maruyama et al., 2002).

Catalysts play a major role in determining the size of CNTs synthesized by CVD. Fe, Ni, and Co are most popularly used owing to the high solubility and high diffusion rate of carbon atoms in these metals. Additionally, their low equilibrium vapor pressure and high melting point enable a wide temperature range to be used in the CVD process (Yan, Miao, et al., 2015). SWCNTs with small diameters are formed on catalyst particles containing a small number of atoms. With increasing particle size, SWCNTs with larger diameters are formed. Further increases in particle size (to a few tens of nm wide) result in the formation of MWCNTs (Kumar & Ando, 2010; Sinnott et al., 1999). A summary of popular carbon precursors, temperature ranges and catalysts used in CNT-CVD processes is presented in Table 1.

Table 1 Popular carbon precursors, temperature ranges and catalysts used in CNT-CVD

Carbon source	Temperature	Catalyst	Support	CNT products	Reference
CH_4	1200 °C	Fe_2O_3	Al_2O_3 SiO_2	SWCNTs	(Kong et al., 1998)
CH_4	850–900 °C	Fe	MgO	SWCNTs	(Abdullahi et al., 2014)
CH_4	900 °C	Fe	MgO	SWCNTs	(Ning et al., 2006)
CH_4	850 °C	Fe	MgO	SWCNTs	(Li et al., 2002)
CH_4	900 °C	FeMo	SiO_2–Al_2O_3	SWNTs	(Cassell et al., 1999)
CH_4	760 °C	$Ni(NO_3)_2$	SiO_2	SWNTs	(Li et al., 2004)
CH_4	550–850 °C	Co Ni	Al_2O_3 Al_2O_3	MWCNTs	(Qian et al., 2004)
C_2H_4	615–705 °C	Co	La_2O_3	MWCNTs	(Chen et al., 2008)
C_2H_4	500–700 °C	Fe	Al_2O_3	MWCNTs	(Wang et al., 2002a)
C_2H_4	550 °C	Fe	Al_2O_3	MWCNTs	(Qian et al., 2003)
C_2H_4	650 °C	Fe	Al_2O_3	MWCNTs	(Corrias et al., 2003)
C_2H_4	650 °C	FeMo	Vermiculite	MWCNTs	(Zhang et al., 2009)
C_2H_2	700 °C	Co Fe CoFe	CaO MgO $Ca(OH)_2$ $Mg(OH)_2$ $CaCO_3$ $MgCO_3$	MWCNTs	(Kathyayini et al., 2004)
C_2H_2	720 °C	FeCo	$CaCO_3$	MWCNTs	(Couteau et al., 2003)
C_2H_2	600–700 °C	Co–Fe Co–V Co–Ni Co–Pt Co–Y Co–Cu Co–Sn	Zeolite	MWCNTs	(Mukhopadhyay et al., 1999)

C$_2$H$_2$	800 °C	Fe Ni Co	Al$_2$O$_3$	MWCNTs	(Weidenkaff et al., 2002)
C$_2$H$_2$	750 °C	Fe	SiO$_2$	MWCNTs	(Venegoni et al., 2002)
C$_2$H$_2$	600 °C	Fe	SiO$_2$	MWCNTs	(Escobar et al., 2007)
C$_2$H$_2$	650–700 °C	Fe	Al$_2$O$_3$	SWCNTs	(Zhong et al., 2009)
C$_2$H$_2$	820 °C	Fe/Al$_2$O$_x$	Al$_2$O$_3$	SWCNTs	(Kim, Sugime, et al., 2012)
CO	1200 °C			SWCNTs	(Dai et al., 1996)
Benzene	1000 °C	N/A	C	MWCNTs	(Endo et al., 1993)
Benzene	900 °C	Fe, Ni, Co		MWCNTs	(Sen et al., 1997)
Benzene	650 °C	Fe–Co	Al$_2$O$_3$	MWCNTs	(Tian et al., 2004)
Xylene	800 °C	Fe	SiO2	MWCNTs	(Wei, Vajtai, et al., 2002)
Xylene/C$_2$H$_2$	800 °C	Fe	Quartz	MWCNTs	(Li et al., 2010)
CH$_3$OH/ C$_2$H$_5$OH	700–800 °C	Fe–Co	Zeolite	SWCNTs	(Maruyama et al., 2002)
C$_2$H$_5$OH	600 °C	Rh	SiO$_2$	SWCNTs	(Kozawa et al., 2016)
C$_2$H$_5$OH	850 °C	Fe–Co	Zeolite	SWCNTs	(Okubo et al., 2004)
C$_2$H$_5$OH	300–700 °C	Pt	SiO$_2$	SWCNTs	(Maruyama et al., 2016)

The simplest system for CNT synthesis via CVD is a horizontal furnace, as shown in Fig. 6. However, this system is inefficient for large-scale production owing to the limited diffusion of the carbon precursors into the support powders (Kathyayini et al., 2004; Zeng, Sun, Cheng, Yan, & Xu, 2002). Kathyayini et al. (2004) have shown that the amount of CNTs produced using 1 g of catalyst was almost the same as the amount obtained using 0.5 g of catalyst placed in the same quartz boat (Kathyayini et al., 2004). With the same amount of catalyst, the yield of CNTs was increased by over three times when two quartz boats were used instead of a single boat (Zeng et al., 2002). This indicates that larger contact areas produce higher yields. For this reason, fluidized-bed reactors have been widely used for the mass production of CNTs.
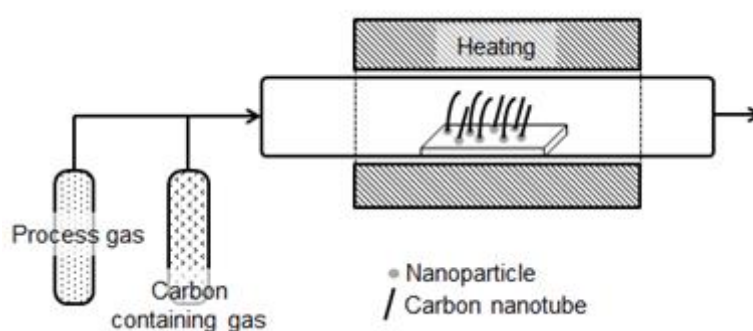

Fig. 6. Schematic representation of a horizontal furnace CVD apparatus. Carbon nanotubes grow on catalyst particles such as Fe, Ni, and Co. The drawback of this system is the limitation of the diffusion of the carbon precursor.

Fluidized-bed CVD (FBCVD) is performed with a bed of particles fluidized by a continuous upward gas flow (Fig. 7). FBCVD is one of the most popular techniques for the mass production of CNTs because of its advantages in terms of providing a sufficient surface area of supporting catalysts for CNT growth, excellent mass and heat transfer, easy up-scaling and continuous operation (Chen, Kim, Hasegawa, Osawa, & Noda, 2014; Kim, Sugime, Hasegawa, Osawa, & Noda, 2011, 2012; Philippe et al., 2007; See & Harris, 2007; Zhang, Zhao, Huang, Nie, & Wei, 2010). The mixing of the support powder caused by the fluidization allows for excellent exposure of the catalyst particles to the carbon precursor. This results in a more homogeneous growth of CNTs on the catalyst surface and provides a higher yield compared with those of fixed-bed reactors. Additionally, uniform temperature distribution can be achieved in fluidized-bed reactors, which is crucial for CNT quality control (Morancais et al., 2007). However, homogeneous fluidization can only be obtained for micron-sized particles. The high surface area and high mobility of nanoparticles result in their cohesion and agglomeration (see Chapter 4). To enhance the fluidization of nanoparticles, external forces such as vibration, ultrasonic or acoustic waves, and direct stirring have been used. However, these techniques have not been used for CNT synthesis so far (Yan, Miao, et al., 2015).
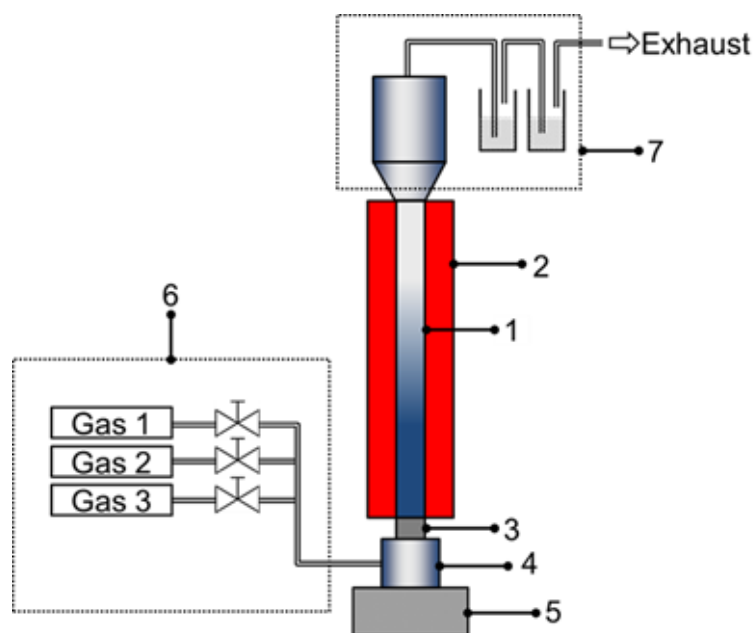
Fig. 7. Schematic drawing of fluidized-bed reactor showing the main components: (1) reactor, (2) heating system, (3) gas distributor, (4) wind box, (5) reactor support, (6) gas inlet system, (7) by-product gas treatment system. In the fluidized-bed reactor, the catalysts are fluidized by an upward flow of carrier and reactant gases.

Recently, many other CVD alternatives have also been developed. Plasma-enhanced CVD is used to increase the efficiency of CNT synthesis (Mao & Bogaerts, 2010; Wang & Moore, 2012). However, this method is usually applied to flat substrates and causes damage to the CNTs owing to the use of plasma (Chiu, Yoshimura, & Ueda, 2008; Mao & Bogaerts, 2010). Laser-assisted CVD is usually employed to synthesize high-purity CNTs (Akahane et al., 2014; Bondi, Lackey, Johnson, Wang, & Wang, 2006). Aerosol-assisted CVD combines spray pyrolysis and thermal CVD, in which the catalytic and carbon precursors are injected simultaneously into the reactor (Castro, Pinault, Porterat, Reynaud, & Mayne-L'Hermite, 2013; Meysami, Koós, Dillon, Dutta, & Grobert, 2015). This allows for the continuous formation of high-purity CNTs. However, owing to the high reaction rate and continuous change of catalyst size and shape, it is difficult to control the size and length of the synthesized CNTs, as well as their agglomeration (Yan, Miao, et al., 2015).

3.4. Flame synthesis of CNTs

Besides the three popularly used methods, a flame pyrolysis technique has also been developed for synthesizing CNTs (Height, Howard, Tester, & Vander Sande, 2004; Liu, Sun, & Ding, 2011; Liu, Zheng, Huang, & Sun, 2011; Merchan-Merchan, Saveliev, & Kennedy, 2004; Van der Wal, Hall, & Berger, 2002; Van der Wal & Ticich, 2001). In this method, a carbon precursor such as methane, ethylene or acetylene is reacted with an oxidizer (typically O_2 from air) in a flame to produce a complex gaseous mixture that includes carbon dioxide, water vapour, carbon monoxide, hydrogen, other hydrocarbons (C_2H_2, C_2H_4,

C_2H_6, etc.) and radicals. These hydrocarbons and carbon monoxide are the carbon sources for CNT formation on metal catalyst particles that are introduced to the flame either in the form of a substrate coating or as aerosolized particles (Gopinath & Gore, 2007). The structure of CNTs (MWCNTs and/or SWCNTs) produced by flame synthesis methods depends on the catalyst particle size and carbon deposition rate. This technique could be applied for large-scale production of CNTs. However, owing to the presence of various hydrocarbons in the flame, it is extremely difficult to control the growth and properties of the CNTs. Therefore, further work on optimizing the experimental conditions is essential before this method can be deployed for industrial-scale synthesis.

3.5. Gas-phase synthesis of graphene

Graphene, a single layer of carbon atoms arranged in a honeycomb structure, has attracted much attention owing to its superior properties such as large specific surface area, high charge carrier mobility, high thermal conductivity, and high thermal, mechanical and chemical stability. These properties make graphene an excellent material for many applications in various fields (Novoselov et al., 2012). The first graphene was produced by micromechanical cleavage of highly oriented pyrolytic graphite using Scotch tape (Novoselov et al., 2004). This method is a simple way of obtaining high-quality graphene with low defect density, and thus has been popularly used for studying the properties of graphene. However, the method is not scalable and not suitable for large-scale production.

Many techniques have been developed for the synthesis of graphene and its derivatives (multilayer graphene, graphene oxide, etc.). These can be divided into two groups: top-down and bottom-up approaches. This has been reviewed (Choi, Lahiri, Seelaboyina, & Kang, 2010; Li & Chopra, 2014a, 2014b). The top-down techniques include chemical or mechanical exfoliation (Liu et al., 2014; Paton et al., 2014) and reduction of graphene oxide (Feng, Cheng, Zhao, Duan, & Li, 2013; Zhou, Cui, Xiao, Jiang, & Han, 2014). The main advantages of these methods include their simplicity, low production cost, low-temperature operation and high feasibility for large-scale production. However, they also have several shortcomings, such as long process time and the generation of impurities and low-quality graphene (Li & Chopra, 2014a). The bottom-up approaches using gas-phase methods include two main techniques: epitaxial growth (Aristov et al., 2010; Emtsev et al., 2009) and chemical vapour deposition (Lee et al., 2014; Li et al., 2009b; Yang et al., 2013). These are also known as high-temperature techniques, and produce high-quality graphene. Epitaxial growth involves the graphitization of carbon atoms on a carbon-enriched surface at high temperature in ultrahigh vacuum (Emtsev et al., 2009; Li & Chopra, 2014b); this can only be used for producing graphene on the lab-scale. The CVD of graphene is generally carried out at atmospheric pressure at lower temperatures (<1000 °C) using hydrocarbons as the carbon source. Nowadays, CVD is the most commonly used technique for producing high-quality graphene on flat surfaces.

The synthesis of graphene powder on a large scale still relies on the top-down approaches using exfoliation and chemical reduction methods; the gas-phase approach is still challenging owing to the strict requirements of the catalytic surface to grow the 2D material. Nevertheless, recent developments show that scalable gas-phase synthesis of graphene powders is achievable. Shen and Lua (2013) have demonstrated a facile approach for the large-scale continuous synthesis of graphene by a thermocatalytic method using Fe nanoparticles as the catalyst and CH_4 as the carbon precursor. Dervishi et al. (2009) employed a radio frequency catalytic CVD (RF-cCVD) method using Fe-Co/MgO as the catalyst and acetylene as the carbon source. The use of RF-cCVD prevented the formation of amorphous carbon and other unwanted products while increasing the yield of the product. Dato et al. (2009) and Dato, Radmilovic, Lee, Phillips, and Frenklach (2008) reported a substrate-free gas-phase graphene synthesis involving the introduction of an aerosol containing ethanol droplets and argon gas into an atmospheric pressure microwave-generated plasma. When passing through the plasma, the ethanol droplets rapidly ($\sim 10^{-10}$ s) evaporated and decomposed, forming graphene. This method produces clean and highly ordered graphene sheets comparable to the graphene obtained by the mechanical exfoliation method (Dato et al., 2009). Nevertheless, the technique still needs further development and optimization to enable the large-scale production of high-quality graphene powder.

4. Agglomeration, fluidization and mixing of nanoparticles

The transport and mixing of nanoparticles are often crucial steps in the manufacturing and processing of nanostructured materials. However, handling dry nanoparticles is still difficult owing to their natural tendency to form large micron-sized agglomerates with very low density, reducing their surface area per unit volume and hindering their use in large-scale processes. In this section, we discuss the clustering tendency of primary nanoparticles, focusing on the cohesive forces that cause agglomerates to form. Then, we address gas-phase processing methods, with a focus on fluidization: suspension of particles in an upward-flowing gas. The characteristics and advantages of this method are described in detail owing to its wide applications in industry. Other mixing methods, such as dry particle coating and rapid expansion of supercritical suspensions (RESS), are finally compared with the fluidization approach.

4.1. Agglomeration behavior of nanoparticles in the gas phase

Nanoparticles encountered in the gas phase form agglomerates of small size, with void fractions of up to 98%–99% and low bulk densities (Jung & Gidaspow, 2002; Wang, Gu, Wei, & Wu, 2002b). The primary nanoparticles can be bonded together by aggregation and/or agglomeration. We use the term aggregation for cases where the nanoparticles are attached to each other by chemical forces (metallic, ionic or covalent bonds). Aggregation typically takes place in the large-scale, high-temperature production methods described in chapter 2. Agglomeration refers to adhesion between particles caused by physical forces (Eggersdorfer & Pratsinis, 2014), and is mostly unavoidable when nanoparticles are kept in high concentration. In many practical situations, aggregation and agglomeration both play a role. In a fluidized

bed, nanoparticles have been found to be in a dynamic equilibrium between disintegration forces (e.g. drag, collision, and gravitational) and cohesive forces (e.g., capillary, van der Waals, and electrostatic) (Matsuda, Hatano, Muramoto, & Tsutsumi, 2004). Such bonds lead to the formation of complex agglomerates of hundreds of micrometers in size that are composed of both aggregates and primary nanoparticles. Thus, knowledge of the nanoparticle characteristics that lead to agglomerate formation will also reveal the resulting agglomerate structure. When particles are in contact in the gas phase, there are three main interactions between them that influence their cohesion behavior: capillary, electrostatic and van der Waals interactions (Seville, Willett, & Knight, 2000). Fig. 8 summarizes the magnitude of these forces.
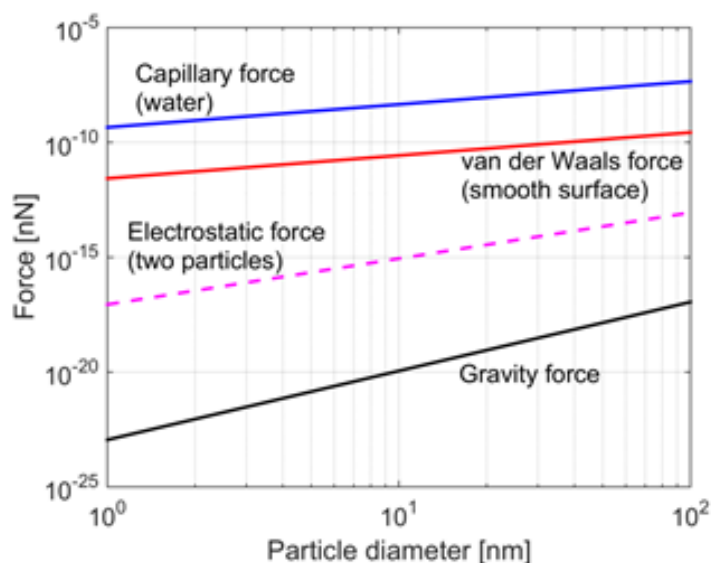

Fig. 8. Comparison of attractive forces between two identical silica particles (ρ = 2200 kg/m^3) as a function of particle diameter. The capillary force is obtained for water; the van der Waals force assumes a distance of 1 nm between particles and the electrostatic force is between two particles carrying opposite charges separated by 1 nm.

Capillary forces are caused by the presence of liquid bridges that originate from the adsorption and condensation of molecules on a particle surface. When these forces appear, they are dominant at the nanoscale (Farshchi-Tabrizi, Kappl, Cheng, Gutmann, & Butt, 2006). The surface tension, viscosity of the liquid and surface properties of the particles (i.e. hydrophobicity) strongly influence the magnitude of the interaction (Seville et al., 2000). For example, a high relative humidity of the surrounding air can promote sintering if the particle material is soluble, enhance particle cohesiveness or reduce the friction between particles (Podczeck, Newton, & James, 1997; Rondet, Ruiz, & Cuq, 2013). Recently Salameh et al. (2012) reported the importance of structural forces (solvation forces) between nanoparticles. Atomic force spectroscopy studies in combination with all-atom molecular dynamic simulations showed that these forces are of the same magnitude as capillary forces (Laube, Salameh, Kappl, Mädler, & Colombi Ciacchi, 2015; Salameh et al., 2012). These results were supported by Tahmasebpoor, de Martin, Talebi, Mostoufi, and van Ommen (2013), who described the formation of hydrogen bonds between hydrophilic nanoparticles in

dry and dense suspensions. They showed that dry nanoparticles with a polar surface form direct hydrogen bonds, increasing the cohesion force.

Van der Waals forces are always present between particles. Owing to the small size of nanoparticles, it is generally accepted that this force is more significant than the others in the absence of water bridges (Shabanian, Jafari, & Chaouki, 2012). The magnitude of van der Waals forces depends on structural and material properties such as size, separation, Hamaker coefficient and contact geometry. In particular, surface roughness is the key factor that determines the magnitude of the forces (Castellanos, 2005; Li, Rudolph, & Peukert, 2006; van Ommen, Valverde, & Pfeffer, 2012).

Electrostatic forces are present when the particles are charged. These have been typically neglected because the adhesion force between particles of ≤ 5 μm in size is dominated by the other forces (Zhang & Ahmandi, 2011), although they can be present between agglomerates owing to triboelectric charges. The charge distribution of nanoparticles has been measured by Lamminen (2011). Hakim, Blackson, George, and Weimer (2005a) reduced the electrostatic forces between agglomerates in a fluidized bed by applying an antistatic surfactant to the column wall, decreasing the minimum fluidization velocity. Similarly, Quevedo and Pfeffer (2010) obtained an improved fluidization by bubbling the gas flow through an ethyl alcohol-water solution. Further analysis of this effect showed that the presence of isopropanol vapour weakens the cohesion between particles (Tahmasebpoor et al., 2013).

Owing to these strong cohesive forces, nanoparticles are commonly found as agglomerates in the gas phase. The structure of these agglomerates corresponds to the well-known fractal geometry theory developed by Mandelbrot (1982). The concept of a fractal is associated with geometrical objects that satisfy self-similarity and fractional dimensionality, such as a snowflake. The former property means that a fractal is formed of similar sub-units on multiple levels, while the fractal dimension gives information about the agglomerate structure and its growth mechanism (Nam, Pfeffer, Dave, & Sundaresan, 2004; Quevedo et al., 2006; Wang, Palero, Soria, & Rhodes, 2006). The scaling law for the number of particles involved in an agglomerate is often written as:

$$N_{\mathrm{p}} = k_{\mathrm{n}} \left(\frac{d_{\mathrm{a}}}{d_{\mathrm{p}}} \right)^{D_{\mathrm{f}}}, \tag{1}$$

where d_{p} is the diameter of the primary particles, d_{a} is the diameter of gyration of the agglomerate, k_{n} is a structural prefactor, and D_{f} is the mass fractal dimension.

Many authors have analysed the structure of agglomerates from a fractal point of view. The experiments of Forrest and Witten (1979) were the first to describe the clustering of nanoparticles as chain-like agglomerates of primary particles formed by Brownian collisions. They reported a fractal dimension of $D_{\mathrm{f}} \sim 2$ for smoke-particle aggregates. For fluidized beds, more recent works have obtained a fractal dimension of about 2.5 (Nakamura & Watano, 2008; Nam et al., 2004; Quevedo et al., 2006; Valverde &

Castellanos, 2008; Valverde et al., 2008; Wang et al., 2006). In these works, the fractal dimension was measured indirectly using image analysis or bed expansion measurements owing to the difficulty of measuring the properties of fluidized agglomerates in situ. Furthermore, the studies employed Eq. (1) with $k_n = 1$, assuming mono-dimensional clusters for all scales. This value implies that the nanoparticle agglomerates are built from single nanoparticles and on all scales may be described with only one fractal dimension. However, the multi-stage structure of the nanoparticle agglomerates shown in Fig. 9 contradicts the common assumption of $k_n = 1$.
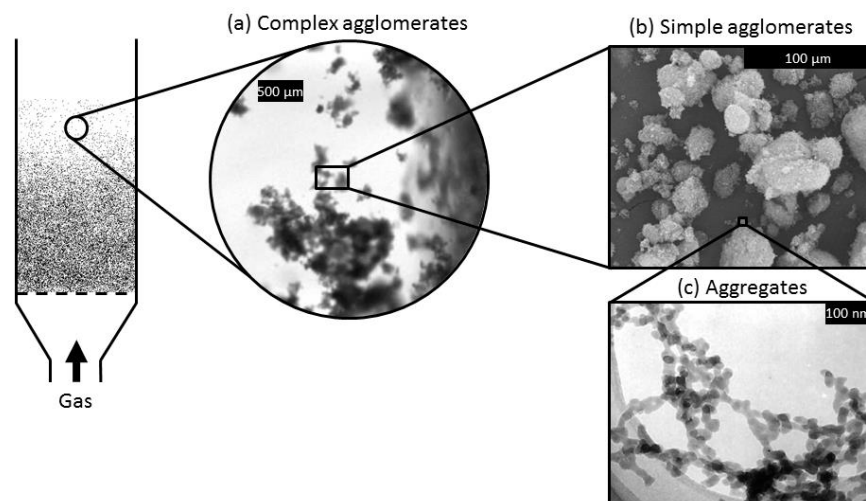

Fig. 9. Multi-level structure of fluidized agglomerates showing the differences for complex agglomerates, simple agglomerates and aggregates (SEM/TEM images). (pictures reprinted with permission from Elsevier ((a) (Hakim et al., 2005b; (b) Wang et al., 2007; (c) Wang et al., 2002b))

A three-stage agglomerate formation mechanism has been widely accepted in the literature (Shabanian et al., 2012; van Ommen et al., 2012; Wang et al., 2002b). For the multi-stage agglomerate (MSA) structure, the agglomerates are formed by three subsequent mechanisms: (i) the formation of 3D net-like aggregates during particle production, Fig. 9(a), (ii) the formation of so-called simple agglomerates by the linking of the aggregates, Fig. 9(b), and (iii) the combination of the simple agglomerates and aggregates into complex agglomerates, Fig. 9(c) (Wang et al., 2002b). However, this cascade of clustering mechanisms has been described using only one fractal dimension. Whether this approach is valid for the overall agglomeration mechanism has been recently addressed by the works of de Martin, Bouwman, and van Ommen (2014a) and de Martín, Fabre, and van Ommen (2014b). They used in situ spin-echo neutron small-angle neutron scattering (SESANS) to measure the structure of agglomerates under stagnant and fluidizing conditions. With these experiments, they demonstrated that the structure prefactor k_n that relates the size of the complex agglomerate to the nanoparticle can vary with size. This implies that the agglomerate structure can be described by a sequentially formed three-level fractal. From a practical point of view, the prefactor and fractal dimension values can be used as a quality index to determine whether the agglomerate scale changed during the processing of nanoparticles (de Martín et al., 2014b). A subsequent

approach (de Martin et al., 2014a) linked the multifractal structure of the agglomerates to the synthesis, storage and fluidization of the powder. Fig. 10 shows the gyration diameter dependency of the multifractal nature of agglomerates with multi-stage agglomerate structure proposed by Wang et al. (2002b):

  i.   Aggregates (1–100 nm), which are characteristic of stored and fluidized agglomerates formed by in-flame processes and showing a fractal dimension of about 2.

 ii.   Simple agglomerates (1–10 µm), which are related to unbreakable clusters during fluidization that could be responsible for the memory effect of nanopowders in a fluidized bed. This scale is characterized by a large fractal dimension of ~2.7.

iii.   Complex agglomerates (>10 µm), which are large agglomerates characterized by low relative strength and a fractal dimension of about 2.
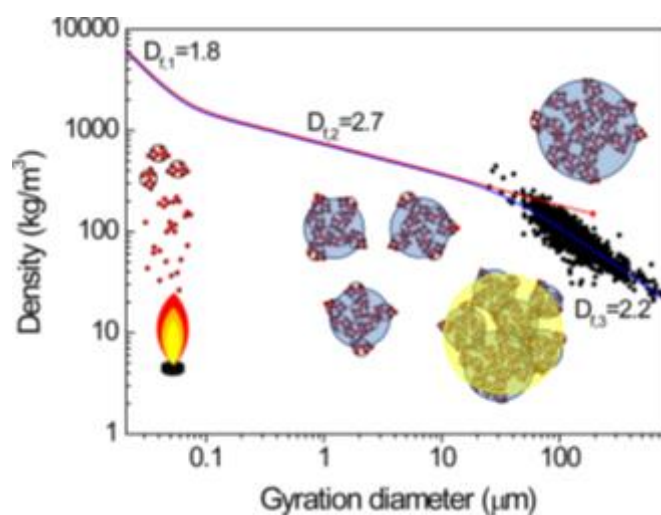

Fig. 10. Conceptual evolution of agglomerate density as a function of gyration diameter. The blue line represents fluidized agglomerates, while the red line indicates stored TiO_2 P25. Black dots are experimental data for fluidized tests. (reprinted with permission from the American Chemical Society (de Martin et al., 2014a))

4.2. Fluidization of nanoparticles

High heat and mass transfer coefficients, together with the possibility of processing large amounts of materials, make fluidization a suitable technology for handling nanoparticles. Recently, multiple reviews have pointed out the rise of this technology in nanoparticle research (Shabanian et al., 2012; van Ommen et al., 2012; Zhu, Zhang, Wang, & Wei, 2015). Here, we highlight the main features of nanoparticle fluidization.

Based on their size and density, nanoparticles fall under Geldart group C (< 30 µm) classification, indicating unfavorable fluidization characteristics. However, when nanoparticles are suspended in an upward flow of gas, they can be fluidized owing to the formation of micron-sized agglomerates. In fact,

Wang, Rahman, and Rhodes (2007) showed that nanoparticle agglomerates exhibit both Group A and Group C characteristics. These agglomerates are formed by the strong cohesive forces between the nanoparticles, and thus the properties of these agglomerates rather than the properties of the primary nanoparticles determine their fluidization behavior. Fluidized nanoparticles are found to appear as large clusters (100–400 μm) with fractal structure, low bulk density and a high void fraction of about 98%–99% (Wang et al., 2002b).

Two different types of fluidization behavior have been reported in the literature for nanoparticles: agglomerate particulate fluidization (APF) and agglomerate bubbling fluidization (ABF) (Wang et al., 2002b). APF refers to a smooth and bubbleless fluidization with high bed expansion ratio and low fluidization velocity. The fluidization of nanoparticles at very low gas velocities results in the formation of weak channels, which collapse with increasing gas velocity, leading to a smooth fluidization without dead regions. In contrast, bubbles, a low bed expansion ratio (less than 50%) and segregation of particles with large agglomerates at the bottom of the bed are observed in ABF. As a result, stable channels are formed throughout the bed, causing the stratification of the agglomerates along the bed height. Typically, a defluidized region of large agglomerates is present at the bottom of the bed, while a fluidized region with smaller agglomerates is found in the upper part (Hakim, Portman, Casper, & Weimer, 2005b; Nam et al., 2004; Wang et al., 2002b; Zhu, Yu, Dave, & Pfeffer, 2005). The ABF regime can also be found in fluidized beds containing micron-sized particles and high-viscosity gas (Valverde & Castellanos, 2007). A comprehensive comparison of both fluidization types can be found in Zhu et al. (2005).

There are two main classification criteria used to discriminate between APF and ABF behavior. Zhu et al. (2005) proposed the definition of a dimensionless number based on the work of Romero and Johanson (1958). However, more research is needed to generalize this classification. Valverde and Castellanos (2007) proposed a different approach based on the modification of empirical relationships used to describe liquid fluidization. They adapted these equations to micro- and nanopowders in the gas phase to replace Geldart type C behavior with solid-like to fluid-like elutriation (SFE) behavior and fluid-like to bubbling (SFB) behavior (Fig. 11).
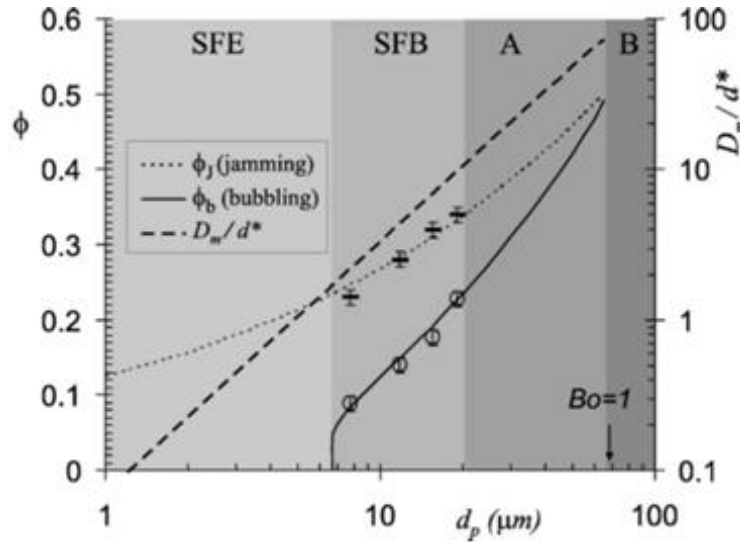
Fig. 11. Types of fluidization behavior as a function of particle size. (reprinted with permission from the American Physical Society (Valverde & Castellanos, 2007))

Many authors have studied the properties of agglomerates owing to their relevance to fluidization behavior. SEM analysis has been widely applied to measure the size of agglomerates. For this procedure, the agglomerates are usually sampled from the bed with adhesive tape or by aspiration (Shabanian et al., 2012). However, this involves the physical manipulation of the porous and fragile agglomerates, which can modify their structural properties. Other methods that measure the size of agglomerates without altering their structure have been reported. Agglomerate size can be indirectly estimated from the bed expansion (Quintanilla et al., 2008; Quintanilla, Valverde, Espin, & Castellanos, 2012; Wang et al., 2002b; Yu, Dave, Zhu, Quevedo, & Pfeffer, 2005), bed settling (Quintanilla et al., 2008; Valverde & Castellanos, 2006), and/or the minimum fluidization velocity (Matsuda et al., 2004). The size data are obtained either using the modified Richardson-Zaki equation or by semi-empirical models (Tahmasebpoor et al., 2013; Valverde & Castellanos, 2008; Yang, 2005). Other approaches employ image techniques to visualize individual agglomerates, such as particle/droplet image analysis (PDIA), in which a laser is used to illuminate the agglomerates and measure their size from their projection (Zhu et al., 2005). Recently, de Martín, Sánchez-Prieto, Hernández-Jiménez, and van Ommen (2014c) proposed the use of a settling tube to collect fluidized agglomerates in the splash zone and visualize them using a boroscope attached to a high-speed camera. Furthermore, the fractal dimension can also be used to estimate agglomerate size. The value of this parameter may be obtained through scattering techniques (de Martín et al., 2014b, 2014c; de Martín & van Ommen, 2013). Recently, such a technique was used together with a nanoparticle spectrometer and an optical particle counter to measure the particle size distribution from 5 nm to 4 mm in the freeboard (Fabre et al., 2016). Other works have employed radioactive techniques, such as X-ray microtomography (Gundogdu, Jenneson, & Tuzun, 2006) or γ-ray densitometry (Esmaeili, Chaouki, & Dubois, 2008; Jung & Gidaspow, 2002), to evaluate solid hold-up during the fluidization of nanoparticles.

Typically, the pressure drop in the bed is measured to determine the fluidization quality. The measurement of pressure fluctuations has also been employed to understand the fluidized-bed dynamics of nanoparticles. For example, time and frequency domain techniques together with state space analyses were studied in Ajbar, Bakhbakhi, Ali, and Asif (2011). The dominant frequency was used to determine the influence of the rotation speed of a rotary reactor coupled with an atomic layer deposition process (Duan, Liu, Shan, & Chen, 2015). However, in spite of efforts to determine the hydrodynamics of nanoparticle fluidization from pressure signals (Tamadondar, Zarghami, Tahmasebpoor, & Mostoufi, 2014), further research is needed to give a complete view for both ABF and APF behavior.

Independently of the fluidization regime, hard agglomerates will retain the memory of their loaded state before fluidization (Valverde & Castellanos, 2006; Wang et al., 2002b). As pointed out by Wang et al. (2002b), some of these hard agglomerates are formed during storage owing to van der Waals forces, solvation forces and water adsorption (Laube et al., 2015; Salameh et al., 2012). Because of this, it is common practice to sieve the powder to remove agglomerates larger than 500 μm before fluidization (van Ommen et al., 2012). Large agglomerates can also form during fluidization (Wang et al., 2002b). As reported by Nam et al. (2004), large agglomerates of Aerosil R974 hydrophobic silica powder cannot be fluidized by simply aerating the bed. However, the application of vibration causes the interparticle networks to break and the resulting agglomerates can be fluidized using aeration alone. Similarly, assistance methods have focused on the breakage of the initial network to further improve the fluidization quality (Ammendola, Chirone, & Raganati, 2011a). These methods include mechanical vibration, stirring, sound waves, magnetic/electric fields, centrifugal fields, pulsed flows, secondary gas from microjets and addition of particles. The excellent reviews of Shabanian et al. (2012), van Ommen et al. (2012), and Zhu et al. (2015) detail the characteristics of each of these methods.

External force generated by sound can break up a significant number of large agglomerates, reducing channelling and the minimum fluidization velocity, and increasing bed expansion (Ajbar et al., 2011; Guo, Li, Wang, Shen, & Yang, 2006; Zhu et al., 2004). Recently, Chirone and co-workers have reviewed their main results in the field of CO_2 adsorption using sound-assisted fluidized beds (Raganati, Ammendola, & Chirone, 2015). They optimized the capture of CO_2 by fine activated carbon using a sound intensity of 125 dB in a frequency range of 50–120 Hz. A further work employing activated carbon studied the effect of temperature swing adsorption (TSA) on CO_2 adsorption, in which the sorbent and CO_2 recovery were regenerated with a temperature increase and gas (Raganati et al., 2015). They were able to perform adsorption/desorption cycles at 140 dB and 80 Hz under different temperatures and flow rates.

An alternating electric field has been used to agitate heavy agglomerates settled at the bottom of a bed by enhancing its gas distribution (Quintanilla et al., 2012). However, the bed showed stratification by agglomerate weight, with the lightest agglomerates located in the freeboard. A detailed comparison of electric and vibration assistance methods is reported in Quintanilla et al. (2008).

Pulsation of the fluidizing gas is another method used to overcome the gas bypass and gas channelling usually observed during the fluidization of ABF nanoparticles. This results in periodic expansion and contraction of the bed height, which reduces hysteresis effects and the minimum fluidization velocity (Akhavan, Rahman, Wang, & Rhodes, 2015; Ali & Asif, 2012; Ali, Asif, & Ajbar, 2014). Tiznado et al. (2014) used a pulsed bed to process powder supports synthesized by atomic layer deposition. They employed different powders (carbon nanotubes of 50–100 nm in diameter, $YCrO_3$ of ~1 μm in diameter, and ZnO of ~10 μm in diameter) in a modified version of a standard atomic layer deposition reactor.

The improvement of nanoparticle fluidization by particle addition may be advantageous for applications in powder coating. For example, the addition of sand particles (Geldart A) to a bed of Aerosil 200 (Ajbar et al., 2011) was reported to reduce powder entrainment and increase the bed pressure drop. Duan, Liang, Zhou, Wang, and Tang (2014) analysed the influence of adding catalyst particles (FCC) and coarse Al_2O_3 particles to a single type or a binary mixture of nanoparticles. The minimum fluidization value was substantially reduced when 30%–40% of FCC particles were added to the system.

Another method used to transport nanoparticles is pneumatic conveying. Recently, Anantharaman, van Ommen, and Chew (2015) reported the effect of nanoparticle properties on transport behavior. Also in these cases, the nanoparticles move as agglomerates. Several researchers have studied the flow properties of nanoparticles in the absence of a gas flow. For example, investigations of the flowability of micron-sized materials coated with nanoparticles by dry particle-coating devices (Yang, Sliva, Banerjee, Dave, & Pfeffer, 2005), or mixed (Kojima & Elliott, 2013; Perez-Vaquero, Valverde, & Quintanilla, 2013), have shown that the addition of smaller-sized silica nanoparticles reduces the internal friction of a powder, but increasing their concentration can also reduce the flowability. Recently, some authors have studied the flow properties of several oxide nanoparticles (Xanthakis, van Ommen, & Ahrné, 2015), carbon black and silica nanopowders (Jacques, François, & Philippe, 2014), and mixtures of silica nanoparticles with fine cohesive powders (Kojima & Elliott, 2013). In the same way, Xanthakis et al. (2015) showed with shear tests that hydrophobic nanopowders behave more cohesively than their hydrophilic counterparts.

4.3. Mixing of nanoparticles

The tendency of nanoparticles to agglomerate reduces their high surface area per unit volume and therefore decreases their potential use in industrial applications. In well-mixed nanocomposites, the loss of surface area is prevented, and thus special properties can be obtained by the proper dispersion and mixture of the constituent nanoparticles. The degree of homogeneity of a given mixture is measured with the mixing index, which is a statistical quantification based on the composition of the mixture (Fan, Chen, & Watson, 1970; Fan, Chen, & Lai, 1990). However, the great number of methods available in the literature and the difficulties of obtaining reliable powder sample sizes make it hard to select a proper mixing index (Bridgwater, 2012; Huang & Kuo, 2014). To further increase the complexity, nanoparticle agglomerates are extremely fragile, which complicates their handling and sampling. Nevertheless, several imaging

techniques can be used to obtain images suitable for analyzing mixing quality, such as field emission scanning electron microscopy (FESEM) (Narh, Agwedicham, & Jallo, 2008; Scicolone, Lepek, Louie, & Davé, 2013), transmission electron microscopy (TEM) (Wei, Dave, & Pfeffer, 2002), electron energy loss spectroscopy (EELS) (Yang, Wang, Dave, & Pfeffer, 2003), atomic force microscopy (AFM) (Wei, Dave, et al., 2002) and energy-dispersive X-ray spectroscopy (EDS) (Sanganwar, Gupta, Ermoline, Scicolone, & Dave, 2009; To, Dave, Yin, & Sundaresan, 2009; To, Sundaresan, & Dave, 2011). Among them, it has been shown that EELS can be used to characterize binary mixtures of nanoparticles (Yang et al., 2003), while EDS provides information on a scale of about 1 μm (Wei, Dave, et al., 2002).

Yang et al. (2003) measured the atomic ratio at randomly chosen spots along a sample to calculate its standard deviation as an indication of the mixing index. A more standardized procedure was used (Sanganwar & Gupta, 2008; Sanganwar et al., 2009; To et al., 2009, 2011). They differentiated between multiple high-quality mixtures using the intensity of the segregation index, which was determined using EDS data measured at 400 random points with a resolution of ~2 μm, and coarse-scale mixtures using the scale of the segregation index, determined using EDS-based maps of elemental concentration for areas of 75×50 μm^2. In a similar way, Scicolone et al. (2013) employed the homogeneity of mixing index (HoM), which is the complement of the intensity of segregation. The homogeneity or mixing efficiency, fractal dimension and agglomerate size were measured by Daumann, Weber, Anlauf, and Nirschl (2011) to analyze the mixing quality of dry nanoparticle mixtures.

For proper dry particle mixing at the aggregate scale, the first step is deagglomeration: the disintegration of the agglomerates into smaller aggregates. The degree of mixing depends on the competition between shear and cohesive forces. Thus, if the external forces are large enough to break up the agglomerates, mixing will occur at the scale of the aggregates. Otherwise, only the agglomerates will be mixed, at larger-length scales (Wei, Dave, et al., 2002). Traditional methods used to create nanocomposites involve the use of liquid solvents with additives and the application of high shear forces. In these techniques, two-component powders are suspended in a liquid solvent inside a beaker. After the breakage of the agglomerates, which can be done either by high shear mixing or ultrasonic cavitation, the colloidal suspension is dried and collected (Oliveira, Chen, & Ferreira, 2002). Nanoparticle agglomerates can be broken to below 100 nm in size using wet methods (Seekkuarachchi & Kumazawa, 2008). However, these processes involve the use of solvents and surfactants, require additional steps of filtration and drying, and are often environmentally unfriendly owing to volatile organic compound emissions (To et al., 2009; Wei, Dave, et al., 2002). Other works have tried to overcome these drawbacks of wet mixing using nanoparticle fluidization, dry particle mixing, mixing with supercritical fluids and sonication in supercritical CO$_2$.

Coarse-scale mixing of nanoparticles can be achieved during fluidization with relatively low energy cost (To et al., 2009). Huang, Wang, and Wei (2008) studied the mixing quality of SiO$_2$ in a conventional fluidized bed by adding a phosphor tracer at less than 5 wt%. Their results showed that both the axial and radial mixing coefficients were two orders of magnitude lower than those in FCC systems owing to the

extremely loose structure and low density of the agglomerates. Recently, assistance methods have been applied to improve the mixing of nanoparticles. The influence of processing time on the degree of mixing has been studied at different length scales in a vibrating fluidized bed (Liang, Duan, Zhou, & Kong, 2014; Liang, Duan, Wang, & Zhou, 2014, 2015; Nam et al., 2004), in a rotating or centrifugal bed (Nakamura & Watano, 2008), and in a sound-assisted bed (Ammendola & Chirone, 2010; Ammendola et al., 2011a, 2011b). From a macroscopic point of view, only a few minutes are required to mix two nanopowders above agglomerate-scale lengths in vibrated (Nam et al., 2004), rotating (Nakamura & Watano, 2008) and sound-assisted beds (Ammendola et al., 2011b). From a microscopic point of view, larger processing times (80–150 min) are needed to mix at the aggregate scale (Ammendola et al., 2011a). In a similar way, Quevedo and Pfeffer (2010) showed that microjets can promote the mixing of alumina and iron oxide nanoparticles at the aggregate scale. Furthermore, the effect of processing time was also addressed for a magnetically fluidized bed by Scicolone et al. (2013). This method achieved mixing results comparable with those obtained with the rapid expansion of high-pressure suspension processes.

In 1975, Hersey (1975)[missing in References] introduced the idea of ordered mixing, such as the use of finer particles that form a loose layer around larger particles. One step further is to use large mechanical forces to perform dry particle-coating processes in which the guest particles are physically or chemically bonded to the host particles, making the surface cover more permanent, as shown in Fig. 12 (Pfeffer, Dave, Wei, & Ramlakhan, 2001).
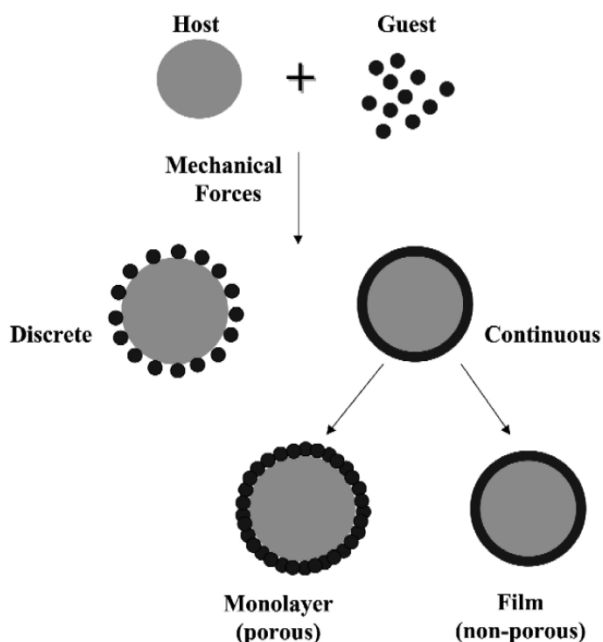

Fig. 12. Dry particle-coating process involving the creation of a layer of guest particles on the surface of host particles. Depending on the forces between particles, a discrete or continuous layer can be formed. (reprinted with permission from Elsevier (Pfeffer et al., 2001))

Magnetically assisted impaction mixing (MAIM) has been applied to dry particle mixing, and has also been used for dry particle coating (Pfeffer et al., 2001; Yang et al., 2003). In this technique, the two component powders are placed together with larger magnetic particles in a container, which is then subjected to an oscillating magnetic field. As a result, the whole system acts as if it is fluidized, although no fluidizing gas is present (Wei, Dave, et al., 2002). An optimization of this method is reported in Scicolone, Mujumdar, Sundaresan, and Davé (2011), where a mixing quality comparable to that achieved with the RESS was obtained. Similarly, carbon nanotubes were dry coated on polyethylene oxide particles in a MAIM (Narh et al., 2008), although the carbon nanotubes were previously deagglomerated using both RESS and high-intensity ultrasonic techniques.

Other dry particle mixing techniques employ high centrifugal forces to break up the agglomerates. Perez-Vaquero et al. (2013) mixed silica nanoparticles with limestone in a ball mill for CO_2 adsorption in a fluidized bed. Wei, Dave, et al. (2002) and Yang et al. (2005) reported other methods, such as a hybridization system consisting of a cylindrical chamber with high-speed blades that produced high centrifugal forces and high-intensity collisions. Another technique is mechanofusion, which involves the use of a cylindrical drum that rotates at high speed (up to 3000 rpm) to produce high-intensity compressive forces. Compared with the solvent-based methods, this hybrid system achieved similar mixing performance.

In mixing by RESS or rapid expansion of high-pressure suspensions (REHPS), the nanoparticles are first pressurized with supercritical carbon dioxide and then rapidly depressurized through a nozzle (To et al., 2009; Wei, Dave, et al., 2002; Yang et al., 2003). The resulting deagglomeration can be attributed to the penetration of supercritical CO_2 into the nanopores of agglomerates and its subsequent rapid expansion, which breaks the agglomerates, as shown in Fig. 13.
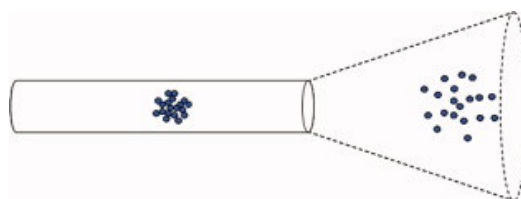
Fig. 13. In the rapid expansion of supercritical suspensions or high-pressure suspensions (RESS/REHPS) technique, the powder sample to be deagglomerated is suspended in supercritical or high-pressure CO_2, and the mixture is expanded through a capillary nozzle, breaking the nanoparticle agglomerates. (image reprinted with permission from Wiley-VCH (To et al., 2009))

This method showed better mixing performance than solvent-based methods (Wei, Dave, et al., 2002). As shown by Sanganwar & Gupta (2008), the mixing of silica nanoparticles with itraconazole nanoflakes reduced the growth of the drug particles during storage and improved their flow properties. The mixing of silica, titania and alumina was achieved through this method even though the surface of the

particles was not modified (Ghoroi et al., 2013). This method can also be used to deagglomerate carbon nanotube bundles and mix them at the sub-micron scale (To et al., 2011).

The sonication of nanoparticle suspensions is similar to REHPS. In this case, ultrasound is applied to a suspension of nanopowder in supercritical carbon dioxide (Sanganwar et al., 2009). The pressure waves propagate through the gaseous and supercritical CO_2, inducing particle collisions that result in the breakage of loose agglomerates and mixing of dissimilar particles. The final mixture is separated from the CO_2 by depressurization. Recently, this method has been used to create a hydrophobic surface on cellulose and polyester fibers by effectively coating them with titania nanoparticles (Matsuyama, Tanaka, & Okuyama, 2014).

5. Atomic layer deposition for particle nanostructuring

Currently, several gas-phase techniques are applied for the coating of micron-sized particles with films of comparable thickness. When it comes to growing much thinner features (nanometer-sized films or particles), however, only a few techniques are suitable. Multimaterial particles can be made with advanced flame spray pyrolysis (see Fig. 3), but making core-shell particles is not straightforward with this technique, although a few examples have been published (Choi, Lee, & Chan Kang, 2013; Waser, Büchel, Hintennach, Novák, & Pratsinis, 2011). Atomic layer deposition (ALD) is a versatile technique that can be used to apply a variety of ultrathin coatings around particles of nano- to micrometer-size. This is a gas-phase technique relying on the distinct, consecutive binding of two (or more) compounds in a combined structure under a self-limiting chemisorption/reaction scheme. Intermediate purging of the reactor volume ensures that excess reactants and process by-products are effectively removed (see illustration in Fig. 14). A simplified reaction scheme for aluminium oxide ALD using trimethylaluminium (TMA) and water is shown below (Puurunen, 2005) (// denotes the solid surface). Carrying out reactions (A) and (B) constitutes one A-B ALD cycle:
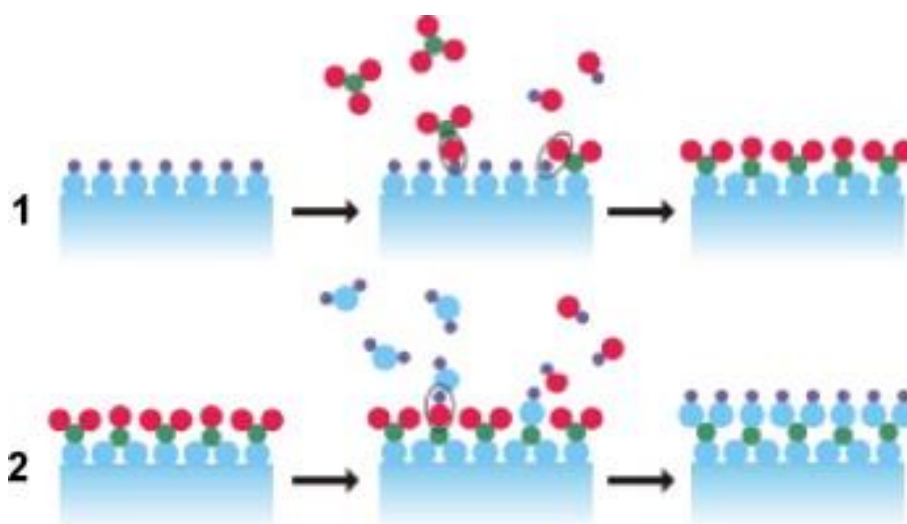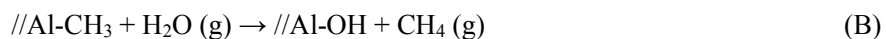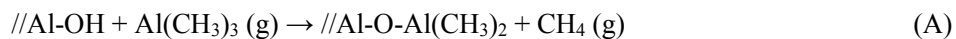
Fig. 14. Schematic representation of atomic layer deposition (ALD) half-reactions: (1) chemisorption of precursor (e.g. trimethylaluminium) at the sample surface and (2) reaction of adsorbed species with the co-reactant (e.g. water) resulting in ligand removal and re-population of the surface with the initial active sites. (reprinted with permission from Wiley-VCH (van Ommen et al., 2010))

$$//Al\text{-}OH + Al(CH_3)_3 \ (g) \rightarrow //Al\text{-}O\text{-}Al(CH_3)_2 + CH_4 \ (g) \tag{A}$$
$$//Al\text{-}CH_3 + H_2O \ (g) \rightarrow //Al\text{-}OH + CH_4 \ (g) \tag{B}$$

The principle and application of ALD were initially established in the former Soviet Union, under the term molecular layering (ML) (Puurunen, 2014), by V. B. Aleskovskii during the formulation of his matrix (or framework) hypothesis. In this section of the review, we focus on the development of ALD technology (and its organic counterpart molecular layer deposition, MLD) for the processing of nanostructured solids, excluding this early work in the former Soviet Union. Additionally, we have not considered applications of ALD on supported powders (e.g. powders on wafers, TEM grids, etc.) but focus on cases where the application potential can be clearly assessed from the reactors used and the batch sizes processed.

To our knowledge, the first reported application of ALD (or atomic layer epitaxy, ALE, as it was called at the time) to powder nanostructuring was the work of Lakomaa, Haukka, and Suntola (1992) on the modification of a small batch of micron-sized porous SiO_2 powder with TiO_2. The first application of MLD implemented in a hybrid mode (using an ALD inorganic precursor with an organic co-reactant) was reported by Liang, King, Li, and Weimer (2009b), who modified SiO_2 and TiO_2 cohesive nanoparticles by the growth of alucone polymeric films. So far, ALD nanostructuring of solids has mostly found applications in the fields of catalysis and energy storage (battery cathodes and capacitors). Using ALD, superior heterogeneous catalysts with ultrahigh dispersion of the active phase (down to the level of single metal atoms) (Yan, Miao, et al., 2015) and stable performance realized by protective accessible overcoats (Lu et al., 2012) have been obtained. Enhanced battery materials with improved cyclability and performance characteristics produced by careful encapsulation of nanosized cathode powders (Xiao et al., 2015) have also been reported. Other fields that have demonstrated the benefits of ALD include the preparation of improved fillers/nanocomposites (Kilbury et al., 2012), phosphorescent materials (Yoon, Jung, & Kim, 2011), passivation/barrier films for reactive powders (Zhou et al., 2010a) including thermites (Qin, Gong, Hao, Wang, & Feng, 2013), and electronic components (e.g. varistors) (Weimer et al., 2008).

In the near future, it is expected that the use of ALD (and hybrid ALD/CVD (Valdesueiro, Meesters, Kreutzer, & van Ommen, 2015)) schemes will expand to the manufacturing of nanostructured solids. The gas-phase preparation of support materials (e.g. carbon nanocoils (Gao et al., 2015) or $TiSi_2$ nanonets (Lin, Zhou, Sheehan, & Wang, 2011) made by CVD) and the modification or change of surface functionality (e.g. Ni nanocatalyst growth (Gao et al., 2015) or the deposition of Fe_2O_3 seeding layer by ALD (Lin et al., 2011)) can be carried out in one reactor vessel (Selvaraj, Jursich, & Takoudis, 2013), removing a number of separation-related unit operations and greatly simplifying the process.

5.1. ALD nanostructuring

With ALD it is possible to grow single-component or mixed-oxide films of sub-nanometer thickness. This has been evidenced by deposition of a ~0.3–0.4-nm-thick Al_2O_3 overcoat on $LiCoO_2$ particles after only two ALD cycles of alternating exposure to TMA and H_2O (Jung et al., 2010). However, this claim is somewhat controversial because it is generally accepted that a full Al_2O_3 monolayer (0.38 nm) can only be obtained after 3–4 ALD cycles (George, 2010). Similarly, for a material with a low growth-per-cycle (GPC), WO_x, a film of 0.46 nm was measured by TEM after 25 cycles of $W(CO)_6$ and H_2O_2 on commercial Degussa P25 TiO_2 nanoparticles (Jackson, Dunn, Guan, & Kuech, 2014). To our knowledge, the thickest ALD film grown on a powder support is a ~110 nm Al_2O_3 passivation barrier deposited onto Fe powder particles (Moghtaderi, Shames, & Doroodchi, 2006). By combining ALD and MLD in hybrid schemes, thin conformal films (~1–12 nm) of materials like alucone (Liang, King, Li, George, & Weimer, 2009b), titanicone (Patel, Jiang, & Liang, 2015), and zincone (Liang, Jiang, & Weimer, 2012) have been reported. The use of certain treatment schemes can induce porosity in the films, resulting in accessible overcoats that can stabilize underlying nanostructures.

In most ALD cases of metals on oxide supports, the difference between the surface energy of the deposited material and the support results in island growth. In that case, a single ALD cycle will generally yield the smallest metal particle (cluster) size. This opens up the possibility of atomic-level dispersion of the catalyst active phase as recently reported for single-atom Pd on graphene (Yan, Cheng, et al., 2015) and Pt (Li et al., 2015). Additionally, binary alloy nanoparticles (Christensen et al., 2010; Molenbroek, Haukka, & Clausen, 1998) and core-shell bimetallic particles (and multi-metallic particles) (Lei et al., 2012) can be prepared while effectively controlling their composition and structural characteristics. An indication of the particle sizes of several metals that can be obtained after a single ALD cycle on the most commonly used support materials is given in Table 2.

Table 2 Reported nanoparticle size (in nm) for a single ALD cycle of different metals/metal oxides onto commonly used support powders

Deposited material	Support			
	Al_2O_3	C	SiO_2	TiO_2
Co/CoO$_x$			2.7 (Backman et al., 2000)	
Cu/CuO$_x$			2.4 (Chen et al., 2006)	
Ir	1 (Cronauer et al., 2011)			
Ni/NiO$_x$	2.4 (Gould et al., 2013)		1.8 (Jeong et al., 2014)	
Pd	1 (Lu & Stair, 2010)	2.6 (Lei et al., 2013)		1 (Lu & Stair, 2010)
Pt	1 (Cronauer et al., 2011)	1.3 (Liang & Jiang, 2013)	3.1 (Lashdaf et al., 2004)	1 (Zhou et al., 2010b)

Ru	1 (Cronauer et al., 2011)	3.5 (Plomp et al., 2008)	

Although initial research focused on deposition in well-defined ceramic oxide supports (e.g. SiO_2 (Lakomaa et al., 1992), Al_2O_3 (Lindblad, Lindfors, & Suntola, 1994), ZrO_2 (Milt, Ulla, & Lombardo, 2000), TiO_2 (Keränen, Guimon, Iiskola, Auroux, & Niinistö, 2003)), other oxides such as MgO (He et al., 2010), ZnO (Longrie, Deduytsche, Haemers, Driesen, & Detavernier, 2012), and aluminosilicates (zeolites) (Silvennoinen et al., 2007; Vuori, Silvennoinen, Lindblad, Österholm, & Krause, 2009) have also been successfully coated. Unlike oxide materials, carbon-based and polymer supports have received less attention until recently (Cavanagh, Wilson, Weimer, & George, 2009; Devine, Oldham, Jur, Gong, & Parsons, 2011; Gong et al., 2015; King, Spencer, Liang, Hakim, & Weimer, 2007; Liang et al., 2007; Yan, Cheng, et al., 2015; Zang, Lu, Qi, & Wang, 2006; Zhan et al., 2008), mainly because of the lack of a well-defined initial concentration of active sites and subsequent nucleation inhibition behavior. The inert nature of carbon nanotubes (CNTs), graphene, and even activated carbon hinders the chemisorption of metal precursors, causing non-uniformity of thin films and nanoparticles grown by ALD, which mainly takes place at the defect sites. A pretreatment step is commonly applied to create a (homogeneous) reactive surface (Cavanagh et al., 2009; Devine et al., 2011; Gong et al., 2015; King et al., 2007; Yan, Chen, et al., 2015; Zhan et al., 2008). This can be performed either in aqueous phase using a mixture of chemicals such as $NaNO_3/H_2SO_4/KMnO_4$ (Yan, Chen, et al., 2015), ethanol and sodium dodecylsulfate (Zhan et al., 2008), and surfactants (King et al., 2007) or in the gas phase using reactive gases (e.g., NO_2 and TMA (Cavanagh et al., 2009) or ozone (Van Bui, Helmer, Goulas, Grillo, & van Ommen, 2015)). ALD on pretreated surfaces has resulted in conformal and smooth metal oxide films (Cavanagh et al., 2009; Devine et al., 2011; Zhan et al., 2008) and uniform and monodispersed nanoparticles (Gong et al., 2015; Yan, Cheng, et al., 2015). An ultrathin nucleation/seeding layer can be beneficial if the inclusion of aluminium on the support can be tolerated (Ban et al., 2013). Oxide-based seeding layers have been commonly implemented in the modification of Al_2O_3 (e.g. with TiO_2, ZrO_2 and CeO_2) (Korhonen, Airaksinen, Bañares, & Krause, 2007; Lobo et al., 2012) and SiO_2 (e.g. with TiO_2 and Al_2O_3) (Elam, Zinovev, Pellin, Comstock, & Hersam, 2007; Keränen et al., 2003), greatly improving noble metal nucleation and mitigating leaching problems under demanding process conditions. Additionally, non-porous metal powders (e.g. Fe, Ni, Al, Co, Ti, Zn) (Ferguson, Buechler, Weimer, & George, 2005; Kilbury et al., 2012; King et al., 2009; Longrie et al., 2012; Wank, Buechler, Hakim, George, & Weimer, 2004) of nano- or micron-size have been effectively nanostructured by ALD. Further, nanostructured functional materials can be enhanced by modification via ALD. Typical examples include the modification of supported base or noble metal catalysts (Cronauer et al., 2011; Ma, Brown, Howe, Overbury, & Dai, 2008), battery cathode materials (Beetstra, Lafont, Nijenhuis, Kelder, & van Ommen, 2009) and phosphors (Kim et al., 2006). Examples of ALD nanostructuring on powders for either support modification, metal or oxide support overcoating and metal cluster decoration are shown in Fig. 15.
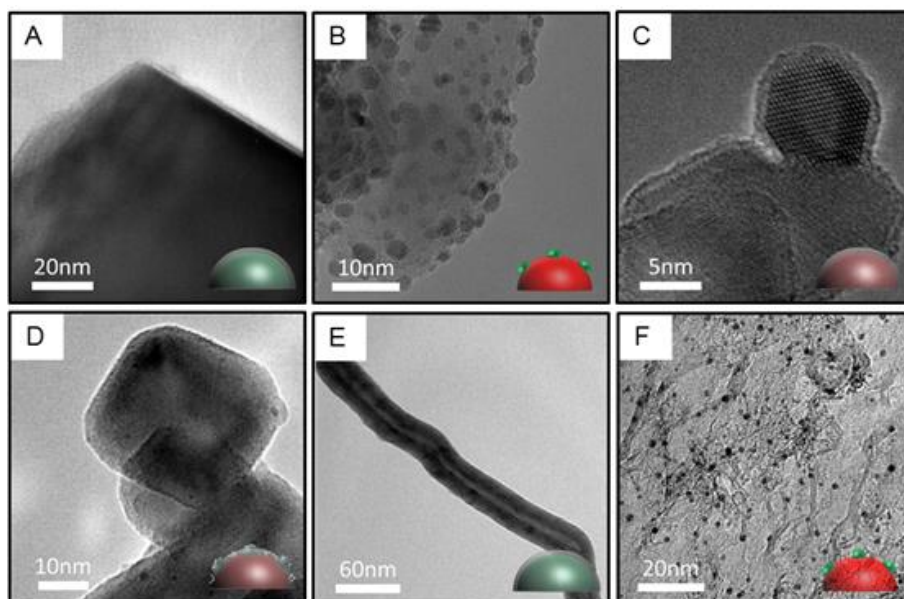
Fig. 15. Examples of ALD nanostructuring on powder supports, showing: (A) an ultrathin Al_2O_3 film (~1 nm) on $LiMn_2O_4$ nanoparticles, (B) Pt nanoparticles (2.3 nm) decorating the surface of TiO_2 nanoparticles (Goulas & van Ommen, 2013), (C) an ultrathin Al_2O_3 film (~1 nm) on the surface of TiO_2 nanoparticles (Valdesueiro et al., 2015), (D) a Pt/TiO_2 nanocatalyst overcoated with an ultrathin Al_2O_3 overcoat (~1.9 nm) (Goulas et al., 2015), (E) a CNT coated with a thin Al_2O_3 layer (6.8 nm) (Cavanagh et al., 2009) (© IOP Publishing reproduced with permission. All rights reserved), and (F) Monodispersed Pd nanoparticles (~1.5 nm) decorated graphene nanoplatelets (Van Bui et al., 2016).

5.2. Processing conditions

The first reactors used for ALD modification of powder materials were based on modifications of the F-120 flow-type reactor produced by Microchemistry Ltd., the first commercial ALD reactor (Puurunen, 2014). The quartz chamber of the reactor could contain up to ~10 g of powder supported on a sintered grid, and the reactions were carried out at 60–100 mbar of N_2 atmosphere. The vaporized precursor was fed through the powder bed and the reaction by-products and excess precursors were pumped out from the bottom of the bed (Haukka, Lakomaa, & Suntola, 1993). Despite the stationary state of the powder bed, sufficient sample uniformity for saturated surface coverage was obtained at both the top and bottom of the powder bed (Suntola, 1996). The process and reactor used are described in a patent assigned to Fortum Oil and Gas Oy (Finland) (Suntola et al., 2003). A similar vertical flow-type reactor has been reported (Milt, Ulla, & Lombardo, 2001), and a variation of the reactor with the precursor and co-reactant fed in counter-current mode through the powder bed has also been described (Kim et al., 2006).

A viscous flow reactor (Elam, Groner, & George, 2002) equipped with a fixed-bed powder holder that contained ~1 g of powder support was reported by Libera, Elam, & Pellin (2008). The top of the powder holder had an open structure that allowed precursor, co-reactant and gaseous by-product diffusion while preventing the disturbance of the flat powder layer. A similar powder holder was recently described by Van

Norman et al. (2015). Typically, viscous flow reactors are less efficient than normal flow-type reactors (Libera et al., 2008). However, for lab-scale material testing, flow-type ALD reactors are a facile option. An example of the coupling of a plug flow ALD reactor with in-situ catalytic testing of the prepared powdered materials was introduced recently by Arradiance Inc. (United States) (Camacho-Bunquin et al., 2015).

However, for treating larger batches, agitation of the powder bed is required in order to achieve uniform deposition characteristics and high precursor utilization (Longrie, Deduytsche, & Detavernier, 2014a). A fluidized-bed reactor can be used to realize proper gas-solid contact, ensuring sufficient precursor transport and uniform heat transfer in large batches of powders (King, Liang, & Weimer, 2012; van Ommen, Yurteri, Ellis, & Kelder, 2010). Efficient mixing in a fluidized-bed reactor enables the possibility of homogeneous sample preparation even for sub-saturation (non-ideal) ALD conditions, as demonstrated in the early 1990s (Suvanto & Pakkanen, 1998). Although the non-assisted fluidization and coating of well-flowing powders has been reported (Moghtaderi et al., 2006; Soria-Hoyo et al., 2015), several assistance techniques (see also chapter 4) can be used to improve the coating quality and fluidization of cohesive (nano)powders (King et al., 2007). Although most of the reported processes are operated under vacuum conditions (Gould et al., 2015; Lubers, Muhich, Anderson, & Weimer, 2015; Patel et al., 2015), large-scale processing under atmospheric pressure conditions has also been demonstrated (Beetstra et al., 2009; Goulas & van Ommen, 2013; Soria-Hoyo et al., 2015; Valdesueiro et al., 2015). Semi-fluidized-bed powder cell implementations have also been reported (Rauwel et al., 2012; Tiznado et al., 2014).

Another reactor concept that can facilitate powder agitation is the rotary reactor. This reactor uses a porous inner tube that contains the powder and can accommodate static reactant exposure, increasing the efficiency of precursor utilization because the carrier gas is not used – primarily – to agitate the particles (McCormick, Cloutier, Weimer, & George, 2007a). A similar reactor, operated under high-vacuum conditions (7–10 mbar) and capable of performing plasma-enhanced ALD (PEALD) on powders, has also been described (Longrie et al., 2012).

Rotary reactors are most commonly operated in a horizontal or inclined configuration, contrary to most flow-type, viscous flow and fluidized-bed reactors, which are arranged in a vertical alignment. Two configurations that deviate from this trend are the inclined fluidized-bed reactor (Moghtaderi et al., 2006) and the (horizontal) vibration reactor that implements a porous cylinder as a powder holder (Park, Kim, Choi, & Shim, 2014). Recently, a fluidized bed coupled with a rotary particle cartridge has been proposed to combine the strengths of the fluidized-bed reactor and rotary reactor technologies (Duan et al., 2015). Finally, a reactor based on the pneumatic conveying of powders that can be used for continuous ALD modification of powders was recently introduced (van Ommen, 2013; van Ommen, Kooijman, Niet, Talebi, & Goulas, 2015). Its main difference from all the previously mentioned reactors is that instead of separating the precursor and co-reactant dosage in the temporal domain (by introducing intermediate

purging/evacuating pulses), the separation of the injection of the chemical reactants is achieved in a spatial way, using injection ports that are located along the coiled reactor tube. In this manner, a production rate on the order of 1 g/min has been achieved for nanopowder processing on the lab-scale. A summary of the important processing characteristics of the main reactor types discussed above is shown in Table 3.

Table 3 Main powder ALD reactor types classified by their most important processing-related characteristics

Reactor	Processing ability	Gas-solid contact	Agglomeration prevention	Energy provision	Vacuum quality
Flow-type	medium	flow through	none (static bed)	thermal	medium
Viscous flow	low	flow over	none (static bed)	thermal	medium
Fluidized bed	high	mixed flow	mechanical & pneumatic vibration, stirring, microjet, pulsed flow	thermal	medium–atmospheric
Rotary	medium	mixed flow	rotational agitation	thermal & plasma	high–medium
Pneumatic conveying	high	local mix (jet)	none	thermal	atmospheric

5.3. Agglomeration during ALD processing of solids

Because ALD is not a line-of-sight limited technique, the range of powder supports it can handle spans from nano-sized to micron-sized porous particles. Especially for nanopowders, processing is done on the agglomerate level, while coating is achieved on the primary particle level. This unique characteristic is unparalleled by other techniques (e.g. CVD) and shows the real strength of ALD for solids processing. Complementary to the role of interparticle forces, surface modification by ALD can lead to interconnection of nanoparticles. Although (soft) agglomerates and (hard) aggregates are two terms often used to describe particle interconnection, the nature of the interconnecting forces' weak physical interactions for agglomeration and strong chemical interactions or sintering for aggregation should be clearly defined (Teleki, Wengeler, Wengeler, Nirschl, & Pratsinis, 2008) (also see chapter 4). Moreover, when we refer to particle agglomeration, we do not refer to the process that takes place during the growth of ALD-deposited material/active species but to the interconnection of primary support nanoparticles.

Initially applied for the coating of individual micron-sized non-porous Ni particles in a fluidized-bed reactor by Wank, George, & Weimer (2004a), ALD processing did not result in a statistically important change in the particle size distribution (PSD) of the support for a deposited layer of ~11.1 nm Al_2O_3 after 100 cycles. Two vibromotors attached to the reactor platform were used to provide external energy for the fluidization of the cohesive powders. Stirring has also been implemented as a means of particle agitation in fluidized-bed ALD reactors (King et al., 2008a). A different reactor module that uses vibration for particle agitation was recently proposed by Park et al. (2014). Increasing the vibration frequency allowed favourable transport of the reactants to the coated graphitic powder, resulting in a higher elemental content of the deposited material and an increased average particle size.

Measuring PSDs by laser diffractometry has some limits when it comes to agglomeration monitoring during ALD. In fluidized-bed reactors, the observed distributions can shift to larger particle sizes as a function of the ALD processing time owing to the elutriation of fines (Wank, George, & Weimer, 2004b). Especially for nanoparticles, only a certain agglomerate size, usually >100 nm, is taken into account, leaving out information on the primary particle level. In such cases, surface area measurements can be used to probe the degree of particle interconnection more accurately. Additionally, these measurements are often complemented by TEM or SEM characterization. The conformal Al_2O_3 coating of SiO_2 and ZrO_2 nanoparticles (<100 nm) with no particle aggregation, owing to dynamic agglomeration (the constant breaking and formation of agglomerates) during ALD, was first reported in the work of Hakim, Portman, Casper, and Weimer (2004).

Using a rotary reactor to agitate the particles, McCormick, Rice, Paul, Weimer, and George (2007b) achieved uniform Al_2O_3 coating on individual ZrO_2 nanoparticles while observing only a minor surface area loss. Variation of the rotational speed of the porous cylindrical drum of the reactor (100–200 rpm) was claimed not to affect the surface area of the coated powders (McCormick et al, 2007b). However, in another case (coating of MWCNTs) it was shown that operation within a well-defined regime of rotational frequencies (140–180 rpm) is essential for minimizing agglomeration (Cavanagh et al., 2009). Higher rotational frequencies will cause agglomeration because of the immobilization of the support on the walls of the porous reactor drum. At lower rotational frequencies, however, the powder will experience less agitation and thus will not be efficiently penetrated by the precursor gas molecules. A rotating reactor also capable of performing plasma-enhanced ALD has been successfully used to grow conformal ALD films of TiN on sub-micron ZnO powders without any reported agglomeration problems (Longrie et al., 2014b).

Inefficient mixing and operating near the decomposition temperature of ALD precursors (resulting in a parasitic CVD growth component) can be two major causes of particle aggregation. Certain supports can limit the reactor operating temperature owing to their heat-sensitive characteristics. As the reactor temperature is decreased, the removal of sticky precursors (including residual water) becomes extremely difficult. As shown by King, Liang, Li, and Weimer (2008b), ALD processes using H_2O-based co-reactants at temperatures lower than 125 °C will face liquid-bridging problems that will cause particle agglomeration (see chapter 4). The strong interparticle forces that develop will be responsible for a localized CVD effect of the remaining reactants in subsequent cycles, forming solid connector/bridges that lead to aggregate formation. This has also been shown in other studies on ALD processes carried out at low temperatures (Didden, Middelkoop, Besling, Nanu, & van de Krol, 2014), but also high temperatures (Wiedmann et al., 2012). The described behavior is not expected for larger micron-size particles, for which ALD can be implemented at low temperatures without the expectation of agglomeration problems (Liang et al., 2009b).

A similar behavior is expected in hybrid ALD/MLD schemes, which are typically operated at low temperatures. As shown by Liang et al. (2009a), although a sticky precursor (ethylene glycol) was used at a low deposition temperature, only a small degree of permanent aggregation was observed during the coating

of TiO$_2$ and SiO$_2$ sub-micron particles with alucone films. Diluting the precursor stream using N$_2$ bubbling is a straightforward way of limiting powder aggregation. The agglomeration behavior is sometimes even harder to monitor in these systems, because the hybrid ALD/MLD films obtained can have porous structures. One such example has been reported by Liang, Jiang, et al. (2012); during deposition of a zincone film, a decrease in the support surface area was observed during the first 20 cycles (corresponding to a film of ~1 nm thickness). However, above 20 cycles no further reduction in surface area was observed.

Coating micron-sized protein particles with a polyester film by an MLD scheme resulted in serious agglomeration (Vasudevan et al., 2015) that compromised the fluidization of the powder. Implementing vibration and a microjet, and using long intermediate purging pulses with high flow-rates of N$_2$, helped re-establish fluidization in the system. Finally, agglomeration has also been reported for ALD in a viscous-flow reactor (Qin et al., 2013). Studying the growth of two oxide coatings (ZnO and SnO$_2$) on Al nanopowder, Qin et al. came to the conclusion that the thickness of the coating relative to the primary particle size and film growth rate can also influence the agglomeration behavior.

ALD can alter the surface properties (e.g. surface termination/functionality, roughness, repulsion characteristics, flowability, etc.) of nanopowders, drastically changing the agglomeration behavior of the primary particles. In one example, the average agglomerate size of ZrO$_2$ nanoparticles was found to greatly decrease from ~25 μm to ~4 μm after the deposition of a SnO$_2$ coating (Ferguson et al., 2005). A similar trend was observed for TiO$_2$ nanoparticles coated with SiO$_2$ (Kim, Kang, Kim, & Choi, 2011) in a fixed bed (flow-type) reactor that facilitated counter-current injection of the precursors. For graphite particles, an even more pronounced effect was observed; the bimodal agglomerate size distribution of uncoated particles (with an average size of 47 μm) became unimodal after the ALD deposition of Al$_2$O$_3$, following a shift to 38 and 39 μm for 90 and 185 cycles, respectively (Lichty et al., 2013). In contrast, small ceramic oxide nanoparticles showed increased interactions (increase in aggregate size from 39 to 70 μm) after the deposition of a thin Al$_2$O$_3$ overcoat (Hakim, Blackson, & Weimer, 2007).

6. Concluding remarks

In recent years, there has been an increasing demand for materials and devices containing nanostructured solids, either nanoparticles (0D), nanotubes (1D) or nanoplatelets (2D). Such nanostructured solids can provide unique properties even at low contents. Furnace processes are typically used for the large-scale production of inorganic nanoparticles; carbon black and titania have already been produced in this way for decades. Currently, flame spray pyrolysis is being investigated as a related alternative that gives more control over particle size and provides the opportunity to produce multimaterial particles. Spray drying may provide a way to manufacture organic nanostructured particles. Of the 1D materials, only carbon nanotubes are already produced on a large scale. Of the many alternative synthesis approaches being researched, chemical vapour deposition in a fluidized bed is the most attractive way to make large amounts of this material. Many alternative approaches for graphene (2D material) synthesis are also being

investigated; its large-scale production is still in the early stages. Besides the synthesis of nanostructured solids, their processing also typically requires transport and mixing. Some first steps have already been taken in acquiring more insight into these processes for dry nanostructured solids, mostly aimed at fluidizing nanopowders, but there is still a long way to go in understanding and controlling them. To give the produced materials additional functionalities, it is often necessary to add nanostructures (film, nanoclusters, etc.) of a different material. Atomic layer deposition is a versatile and scalable method to achieve this. While most of the industrial production of nanomaterials is carried out in the gas phase, the majority of academic researchers focus on the liquid-phase synthesis of structures such as nanocrystals. In our view, increased attention to gas-phase routes is needed, and the scalability of such approaches should be considered from the very first stages.

Acknowledgements

References

Abdullahi, I., Sakulchaicharoen, N., & Herrera, J. E. (2014). Selective synthesis of single-walled carbon nanotubes on Fe–MgO catalyst by chemical vapor deposition of methane. *Diamond and Related Materials, 41*, 84-93.

Addison, R. F., McKague, A. B., Larsson, A., McLeay, D. J., Ney, P. E., & Parker, G. A., et al. (2013). *Anthropogenic compounds.* Berlin: Springer.

Ajayan, P. M., & Ebbesen, T. W. (1997). Nanometre-size tubes of carbon. *Reports on Progress in Physics, 60*, 1025-1062.

Ajbar, A., Bakhbakhi, Y., Ali, S., & Asif, M. (2011). Fluidization of nano-powders: Effect of sound vibration and pre-mixing with group A particles. *Powder Technology, 206*, 327-337.

Akahane, K., Yamamomto, N., Maeda, M., Takai, H., Nakamura, S., & Yamaguchi, H., et al. (2014). Synthesis of carbon nanotubes by laser-assisted alcohol chemical vapor deposition. *Physica E-Low-Dimensional Systems & Nanostructures, 56*, 452-455.

Akhavan, A., Rahman, F., Wang, S., & Rhodes, M. (2015). Enhanced fluidization of nanoparticles with gas phase pulsation assistance. *Powder Technology, 284*, 521-529.

Ali, S. S., & Asif, M. (2012). Fluidization of nano-powders: Effect of flow pulsation. *Powder Technology, 225*, 86-92.

Ali, S. S., Asif, M., & Ajbar, A. (2014). Bed collapse behavior of pulsed fluidized beds of nano-powder. *Advanced Powder Technology, 25*, 331-337.

Amelinckx, S., Bernaerts, D., Zhang, X. B., Van Tendeloo, G., & Van Landuyt, J. (1995). A structure model and growth mechanism for multishell carbon nanotubes. *Science, 267*, 1334-1338.

Ammendola, P., & Chirone, R. (2010). Aeration and mixing behaviors of nano-sized powders under sound vibration. *Powder Technology, 201*, 49-56.

Ammendola, P., Chirone, R., & Raganati, F. (2011a). Effect of mixture composition, nanoparticle density and sound intensity on mixing quality of nanopowders. *Chemical Engineering and Processing: Process Intensification, 50*, 885-891.

Ammendola, P., Chirone, R., & Raganati, F. (2011b). Fluidization of binary mixtures of nanoparticles under the effect of acoustic fields. *Advanced Powder Technology, 22*, 174-183.

Anantharaman, A., van Ommen, J. R., & Chew, J. W. (2015). Minimum pickup velocity (U-pu) of nanoparticles in gas-solid pneumatic conveying. *Journal of Nanoparticle Research, 17*(12), 1-10.

Ando, Y., Zhao, X., Inoue, S., Suzuki, T., & Kadoya, T. (2005). Mass production of high-quality single-wall carbon nanotubes by H_2–N_2 arc discharge. *Diamond and Related Materials, 14*, 729-732.

Ariga, K., Vinu, A., Yamauchi, Y., Ji, Q., & Hill, J. P. (2012). Nanoarchitectonics for mesoporous materials. *Bulletin of the Chemical Society of Japan, 85*, 1-32.

Aristov, V. Y., Urbanik, G., Kummer, K., Vyalikh, D. V., Molodtsova, O. V., & Preobrajenski, A. B.,et al. (2010). Graphene synthesis on cubic SiC/Si wafers. perspectives for mass production of graphene-based electronic devices. *Nano Letters, 10*, 992-995.

Arora, N., & Sharma, N. N. (2014). Arc discharge synthesis of carbon nanotubes: Comprehensive review. *Diamond and Related Materials, 50*, 135-150.

Backman, L. B., Rautiainen, A., Lindblad, M., & Krause, A. O. I. (2000). Effect of support and calcination on the properties of cobalt catalysts prepared by gas phase deposition. *Applied Catalysis A: General, 191*, 55-68.

Baker, R. T. K., Barber, M. A., Harris, P. S., Feates, F. S., & Waite, R. J. (1972). Nucleation and growth of carbon deposits from the nickel catalyzed decomposition of acetylene. *Journal of Catalysis, 26*, 51–62.

Baker, R. T. K., & Waite, R. J. (1975). Formation of carbonaceous deposits from the platinum-iron catalyzed decomposition of acetylene. *Journal of Catalysis, 37*, 101–105.

Ban, C., Xie, M., Sun, X., Travis, J. J., Wang, G., & Sun, H., et al. (2013). Atomic layer deposition of amorphous TiO_2 on graphene as an anode for Li-ion batteries. *Nanotechnology, 24*, 424002.

Bandow, S., Asaka, S., Saito, Y., Rao, A. M., Grigorian, L., & Richter, E., et al. (1998). Effect of the growth temperature on the diameter distribution and chirality of single-wall carbon nanotubes. *Physical Review Letters, 80*, 3779-3782.

Baranwal, R., Villar, M. P., Garcia, R., & Laine, R. M. (2001). Flame spray pyrolysis of precursors as a route to nano-mullite powder: Powder characterization and sintering behavior. *Journal of the American Ceramic Society, 84*, 951-961.

Beetstra, R., Lafont, U., Nijenhuis, J., Kelder, E. M., & van Ommen, J. R. (2009). Atmospheric pressure process for coating particles using atomic layer deposition. *Chemical Vapor Deposition, 15*, 227-233.

Bethune, D. S., Kiang, C. H., de Vries, M. S., Gorman, G., Savou, R., & Vazquez, J., et al. (1993). Cobalt-catalysed growth of carbon nanotubes with single-atomic-layer walls. *Nature, 363*, 605-607.

Beumer, P., Brandle, K., Weidmann, W., & Zirngibl, H. (1969). Vapour phase oxidation process. *U.S. Patent No. 3,485,584.* Bayer AG.Bickmore, C. R., Waldner, K. F., Baranwal, R., Hinklin, T., Treadwell, D. R., & Laine, R. M. (1998). Ultrafine titania by flame spray pyrolysis of a titanatrane complex. *Journal of the European Ceramic Society, 18*, 287-297.

Bickmore, C. R., Waldner, K. F., Treadwell, D. R., & Laine, R. M. (1996). Ultrafine spinel powders by flame spray pyrolysis of a magnesium aluminum double alkoxide. *Journal of the American Ceramic Society, 79*, 1419-1423.

Biswas, C., & Lee, Y. H. (2011). Graphene versus carbon nanotubes in electronic devices. *Advanced Functional Materials, 21*, 3806-3826.

Boeer, J. P. D. (1996). Verfahren zur Herstellung hochdisperser oxidischer Pulver und Brenner zur Durchführung des Verfahrens. *DE 19505133A1.* Hermsdorfer Inst. Tech. Ceramics.

Bondi, S. N., Lackey, W. J., Johnson, R. W., Wang, X., & Wang, Z. L. (2006). Laser assisted chemical vapor deposition synthesis of carbon nanotubes and their characterization. *Carbon, 44*, 1393-1403.

Braun, J. H., Baidins, A., & Marganski, R. E. (1992). TiO$_2$ pigment technology: A review. *Progress in Organic Coatings, 20*, 105-138.

Bridgwater, J. (2012). Mixing of powders and granular materials by mechanical means—A perspective. *Particuology, 10*, 397-427.

Buesser, B., & Pratsinis, S. E. (2012). Design of nanomaterial synthesis by aerosol processes. *Annual Review of Chemical and Biomolecular Engineering, 3*, 103-127.

Burke, S. P. (1933). Carbon black process and apparatus. *U.S. Patent 1,902,797.*

Buxbaum, G. (2008). *Industrial inorganic pigments.* New York: Wiley.

Camacho-Bunquin, J., Shou, H., Aich, P., Beaulieu, D. R., Klotzsch, H., & Bachman, S., et al. (2015). Catalyst synthesis and evaluation using an integrated atomic layer deposition synthesis–catalysis testing tool. *Review of Scientific Instruments, 86*, 084103.

Cassell, A. M., Raymakers, J. A., Kong, J., & Dai, H. (1999). Large scale CVD synthesis of single-walled carbon nanotubes. *The Journal of Physical Chemistry B, 103*, 6484-6492.

Castellanos, A. (2005). The relationship between attractive interparticle forces and bulk behavior in dry and uncharged fine powders. *Advances in Physics, 54*, 263-376.

Castro, C., Pinault, M., Porterat, D., Reynaud, C., & Mayne-L'Hermite, M. (2013). The role of hydrogen in the aerosol-assisted chemical vapor deposition process in producing thin and densely packed vertically aligned carbon nanotubes. *Carbon, 61*, 585-594.

Cavanagh, A. S., Wilson, C. A., Weimer, A. W., & George, S. M. (2009). Atomic layer deposition on gram quantities of multi-walled carbon nanotubes. *Nanotechnology, 20*, 255602.

Chen, C. S., Lin, J. H., You, J. H., & Chen, C. R. (2006). Properties of Cu(thd)$_2$ as a precursor to prepare Cu/SiO$_2$ catalyst using the atomic layer epitaxy technique. *Journal of the American Chemical Society, 128*, 15950-15951.

Chen, L., Liu, H., Yang, K., Wang, J., & Wang, X. (2008). The effect of reaction temperature on the diameter distribution of carbon nanotubes grown from ethylene decomposition over a Co-La-O catalyst. *Materials Chemistry and Physics, 112*, 407-411.

Chen, Z., Kim, D. Y., Hasegawa, K., Osawa, T., & Noda, S. (2014). Over 99.6wt%-pure, sub-millimeter-long carbon nanotubes realized by fluidized-bed with careful control of the catalyst and carbon feeds. *Carbon, 80*, 339-350.

Chiarello, G. L., Selli, E., & Forni, L. (2008). Photocatalytic hydrogen production over flame spray pyrolysis-synthesised TiO_2 and Au/TiO_2. *Applied Catalysis B: Environmental, 84*, 332-339.

Chiu, C. C., Yoshimura, M., & Ueda, K. (2008). Synthesis of carbon nanotubes by microwave plasma-enhanced hot filament chemical vapor deposition. *Diamond and Related Materials, 17*, 611-614.

Choi, S. H., Lee, J.-H., & Chan Kang, Y. (2013). One-pot rapid synthesis of core-shell structured $NiO@TiO_2$ nanopowders and their excellent electrochemical properties as anode materials for lithium ion batteries. *Nanoscale, 5*, 12645-12650.

Choi, W., Lahiri, I., Seelaboyina, R., & Kang, Y. S. (2010). Synthesis of graphene and its applications: A review. *Critical Reviews in Solid State and Materials Sciences, 35*, 52-71.

Chou, T. P., Zhang, Q., Russo, B., Fryxell, G. E., & Cao, G. (2007). Titania particle size effect on the overall performance of dye-sensitized solar cells. *The Journal of Physical Chemistry C, 111*, 6296-6302.

Christensen, S. T., Feng, H., Libera, J. L., Guo, N., Miller, J. T., & Stair, P. C., et al. (2010). Supported Ru−Pt bimetallic nanoparticle catalysts prepared by atomic layer deposition. *Nano Letters, 10*, 3047-3051.

Chrzanowska, J., Hoffman, J., Małolepszy, A., Mazurkiewicz, M., Kowalewski, T. A., & Szymanski, Z., et al. (2015). Synthesis of carbon nanotubes by the laser ablation method: Effect of laser wavelength. *Physica Status Solidi (B), 252*, 1860-1867.

Colbert, D. T., Zhang, J., McClure, S. M., Nikolaev, P., Chen, Z., & Hafner, J. H., et al. (1994). Growth and sintering of fullerene nanotubes. *Science, 266*, 1218-1222.

Corrias, M., Caussat, B., Ayral, A., Durand, J., Kihn, Y., & Kalck, P., et al. (2003). Carbon nanotubes produced by fluidized bed catalytic CVD: First approach of the process. *Chemical Engineering Science, 58*, 4475-4482.

Couteau, E., Hernadi, K., Seo, J. W., Thiên-Nga, L., Mikó, C., & Gaál, R., et al. (2003). CVD synthesis of high-purity multiwalled carbon nanotubes using $CaCO_3$ catalyst support for large-scale production. *Chemical Physics Letters, 378*, 9-17.

Cronauer, D. C., Jacobs, G., Linganiso, L., Kropf, A. J., Elam, J. W., & Christensen, S. T., et al. (2011). CO hydrogenation: Exploring iridium as a promoter for supported cobalt catalysts by TPR-EXAFS/XANES and reaction testing. *Catalysis Letters, 141*, 968-976.

Dai, H. J., Rinzler, A. G., Nikolaev, P., Thess, A., Colbert, D. T., & Smalley, R. E. (1996). Single-wall nanotubes produced by metal-catalyzed disproportionation of carbon monoxide. *Chemical Physics Letters, 260*, 471-475.

Dato, A., Lee, Z., Jeon, K. J., Erni, R., Radmilovic, V., & Richardson, T. J., et al. (2009). Clean and highly ordered graphene synthesized in the gas phase. *Chemical Communications,* (40), 6095-6097.

Dato, A., Radmilovic, V., Lee, Z., Phillips, J., & Frenklach, M. (2008). Substrate-free gas-phase synthesis of graphene sheets. *Nano Letters, 8*, 2012-2016.

Daumann, B., Weber, J. A., Anlauf, H., & Nirschl, H. (2011). Discontinuous powder mixing of nanoscale particles. *Chemical Engineering Journal, 167*, 377-387.

Davis, R. A., Nicholas, D. M., Smith, D. D., Wang, S. I., & Wright, R. A. (1991). Integrated reformer process for the production of carbon black. *U.S. Patent No. 5,011,670*. Air Products and Chemicals Inc.

de Heer, W. A., Poncharal, P., Berger, C., Gezo, J., Song, Z., & Bettini, J., et al. (2005). Liquid carbon, carbon-glass beads, and the crystallization of carbon nanotubes. *Science, 307*, 907-910.

de Martin, L., Bouwman, W. G., & van Ommen, J. R. (2014a). Multidimensional nature of fluidized nanoparticle agglomerates. *Langmuir, 30*, 12696-12702.

de Martín, L., Fabre, A., & van Ommen, R. J. (2014b). The fractal scaling of fluidized nanoparticle agglomerates. *Chemical Engineering Science, 112*, 79-86.

de Martín, L., Sánchez-Prieto, J., Hernández-Jiménez, F., & van Ommen, J. R. (2014c). A settling tube to determine the terminal velocity and size distribution of fluidized nanoparticle agglomerates. *Journal of Nanoparticle Research, 16,* 2183, doi:10.1007/s11051-013-2183-3.

de Martín, L., & van Ommen, J. R. (2013). A model to estimate the size of nanoparticle agglomerates in gas−solid fluidized beds. *Journal of Nanoparticle Research, 15,* 2055, doi:10.1007/s11051-013-2055-x.

De Volder, M. F. L., Tawfick, S. H., Baughman, R. H., & Hart, A. J. (2013). Carbon nanotubes: Present and future commercial applications. *Science, 339*, 535-539.

Dervishi, E., Li, Z., Watanabe, F., Biswas, A., Xu, Y., & Biris, A. R., et al. (2009). Large-scale graphene production by RF-cCVD method. *Chemical Communication,* (27), 4061-4063.

Devine, C. K., Oldham, C. J., Jur, J. S., Gong, B., & Parsons, G. N. (2011). Fibrous containment for improved laboratory handling and uniform nanocoating of milligram quantities of carbon nanotubes by atomic layer deposition. *Langmuir, 27*, 14497-14507.

Didden, A. P., Middelkoop, J., Besling, W. F. A., Nanu, D. E., & van de Krol, R. (2014). Fluidized-bed atomic layer deposition reactor for the synthesis of core-shell nanoparticles. *Review of Scientific Instruments, 85*, 013905.

Donnet, J. B. (1993). *Carbon black: Science and technology* (2nd Ed.). New York: Taylor & Francis.

Duan, C.-L., Liu, X., Shan, B., & Chen, R. (2015). Fluidized bed coupled rotary reactor for nanoparticles coating via atomic layer deposition. *Review of Scientific Instruments, 86*, 075101.

Duan, H., Liang, X., Zhou, T., Wang, J., & Tang, W. (2014). Fluidization of mixed SiO_2 and ZnO nanoparticles by adding coarse particles. *Powder Technology, 267*, 315-321.

Eggersdorfer, M. L., & Pratsinis, S. E. (2014). Agglomerates and aggregates of nanoparticles made in the gas phase. *Advanced Powder Technology, 25*, 71-90.

Elam, J. W., Groner, M. D., & George, S. M. (2002). Viscous flow reactor with quartz crystal microbalance for thin film growth by atomic layer deposition. *Review of Scientific Instruments, 73*(8), 2981-2987.

Elam, J. W., Zinovev, A. V., Pellin, M. J., Comstock, D. J., & Hersam, M. C. (2007). Nucleation and growth of noble metals on oxide surfaces using atomic layer deposition. *ECS Transactions, 3*, 271-278.

Emtsev, K. V., Bostwick, A., Horn, K., Jobst, J., Kellogg, G. L., & Ley, L.,et al. (2009). Towards wafer-size graphene layers by atmospheric pressure graphitization of silicon carbide. *Nature Materials, 8*, 203-207.

Endo, M., Takeuchi, K., Igarashi, S., Kobori, K., Shiraishi, M., & Kroto, H. W. (1993). The production and structure of pyrolytic carbon nanotubes (PCNTs). *Journal of Physics and Chemistry of Solids, 54*, 1841-1848.

Escobar, M., Moreno, M. S., Candal, R. J., Marchi, M. C., Caso, A., & Polosecki, P. I.,et al. (2007). Synthesis of carbon nanotubes by CVD: Effect of acetylene pressure on nanotubes characteristics. *Applied Surface Science, 254*, 251-256.

Esmaeili, B., Chaouki, J., & Dubois, C. (2008). An evaluation of the solid hold-up distribution in a fluidized bed of nanoparticles using radioactive densitometry and fibre optics. *The Canadian Journal of Chemical Engineering, 86*, 543-552.

Fabre, A., Clemente, A., Balas, F., Pilar Lobera, M., Santamaria, J., Kreutzer, M. T., & van Ommen, J. R. (2016). Entrainment of nanosized clusters from nanopowder fluidized bed. *Submitted to Environmental Science: Nano*.

Fan, L. T., Chen, S. J., & Watson, C. A. (1970). Solids mixing. *Industrial & Engineering Chemistry, 62*, 53-69.

Fan, L. T., Chen, Y.-M., & Lai, F. S. (1990). Recent developments in solids mixing. *Powder Technology, 61*, 255-287.

Farshchi-Tabrizi, M., Kappl, M., Cheng, Y. J., Gutmann, J., & Butt, H. J. (2006). On the adhesion between fine particles and nanocontacts: An atomic force microscope study. *Langmuir, 22*, 2171-2184.

Feng, H., Cheng, R., Zhao, X., Duan, X., & Li, J. (2013). A low-temperature method to produce highly reduced graphene oxide. *Nature Communications, 4*, 1539.

Ferguson, J. D., Buechler, K. J., Weimer, A. W., & George, S. M. (2005). SnO_2 atomic layer deposition on ZrO_2 and Al nanoparticles: Pathway to enhanced thermite materials. *Powder Technology, 156*, 154-163.

Fogler, B. B., & Kleninschmidt, R. V. (1938). Spray drying. *Industrial & Engineering Chemistry, 30*, 1372-1384.

Forrest, S. R., & Witten, T. A. J. (1979). Long-range correlations in smoke-particle aggregates. *Journal of Physics A: Mathematical and General, 12*, 109-117.

Friedlander, S. K. (2000). *Smoke, dust, and haze: Fundamentals of aerosol dynamics*. Oxford: Oxford University Press.

Fujishima, A., & Honda, K. (1972). Electrochemical photolysis of water at a semiconductor electrode. *Nature, 238*, 37-38.

Fukuoka, N., Mizutani, Y., Naritsuka, S., Maruyama, T., & Iijima, S. (2012). Low-temperature synthesis of single-walled carbon nanotubes in a high vacuum using pt catalyst in alcohol gas source method. *Japanese Journal of Applied Physics, 51*, 06FD23.

Gamaly, E. G., & Ebbesen, T. W. (1995). Mechanism of carbon nanotube formation in the arc discharge. *Physical Review B, 52*, 2083-2089.

Gao, Z., Dong, M., Wang, G., Sheng, P., Wu, Z., & Yang, H., et al. (2015). Multiply confined nickel nanocatalysts produced by atomic layer deposition for hydrogenation reactions. *Angewandte Chemie International Edition, 54*, 9006-9010.

Gavillet, J., Loiseau, A., Journet, C., Willaime, F., Ducastelle, F., & Charlier, J. C. (2001). Root-growth mechanism for single-wall carbon nanotubes. *Physical Review Letters, 87*, 275504.

Gazquez, M. J., Bolivar, J. P., Garcia-Tenorio, R., & Vaca, F. (2014). A review of the production cycle of titanium dioxide pigment. *Materials Sciences and Applications, 5*, 441-458.

George, S. M. (2010). Atomic layer deposition: An overview. *Chemical Reviews, 110*, 111-131.

Gerhard, D., Gerhard, J., Gerhard, K., & Heinrich, S. (1972). Apparatus and process for atomizing liquids, particularly carbon black raw materials. *U.S. Patent No. 3,701,480.* Degussa AG.

Gharsallaoui, A., Roudaut, G., Chambin, O., Voilley, A., & Saurel, R. (2007). Applications of spray-drying in microencapsulation of food ingredients: An overview. *Food Research International, 40*, 1107-1121.

Ghoroi, C., Han, X., To, D., Jallo, L., Gurumurthy, L., & Davé, R. N. (2013). Dispersion of fine and ultrafine powders through surface modification and rapid expansion. *Chemical Engineering Science, 85*, 11-24.

Giges, N.S. (2013). *Top 5 trends in nanotechnology*. ASME news. Retrieved from ASME website: https://www.asme.org/engineering-topics/articles/nanotechnology/top-5-trends-in-nanotechnology?cm_sp=Nanotechnology-_-Feataured%20Articles-_-Top%205%20Trends%20in%20Nanotechnology.

Gong, T., Qin, L., Zhang, W., Wan, H., Lu, J., & Feng, H. (2015). Activated carbon supported palladium nanoparticle catalysts synthesized by atomic layer deposition: Genesis and evolution of nanoparticles and tuning the particle size. *The Journal of Physical Chemistry C, 119*, 11544-11556.

Gopinath, P., & Gore, J. (2007). Chemical kinetic considerations for postflame synthesis of carbon nanotubes in premixed flames using a support catalyst. *Combustion and Flame, 151*, 542-550.

Gorbunov, A. A., Friedlein, R., Jost, O., Golden, M. S., Fink, J., & Pompe, W. (1999). Gas-dynamic consideration of the laser evaporation synthesis of single-wall carbon nanotubes. *Applied Physics A: Materials Science & Processing, 69*, S593-S596.

Goulas, A., Dokania, A., Grillo, F., van Ommen, J. R., & van Limpt, B. (2015). Scalable production of stabilized catalysts via atomic layer deposition. In *TechConnect World Innovation*. Washington, DC.

Goulas, A., & van Ommen, R. J. (2013). Atomic layer deposition of platinum clusters on titania nanoparticles at atmospheric pressure. *Journal of Materials Chemistry A, 1*, 4647-4650.

Gould, T. D., Lubers, A. M., Corpuz, A. R., Weimer, A. W., Falconer, J. L., & Medlin, J. W. (2015). Controlling nanoscale properties of supported platinum catalysts through atomic layer deposition. *ACS Catalysis, 5*, 1344-1352.

Gould, T. D., Lubers, A. M., Neltner, B. T., Carrier, J. V., Weimer, A. W., & Falconer, J. L., et al. (2013). Synthesis of supported Ni catalysts by atomic layer deposition. *Journal of Catalysis, 303*, 9-15.

Grätzel, M. (2003). Dye-sensitized solar cells. *Journal of Photochemistry and Photobiology C: Photochemistry Reviews, 4*, 145-153.

Grossmann, H. K., Grieb, T., Meierhofer, F., Hodapp, M. J., Noriler, D., & Gröhn, A., et al. (2015). Nanoscale mixing during double-flame spray synthesis of heterostructured nanoparticles. *Journal of Nanoparticle Research, 17*, 1-16.

Gruber, R., & Malcharek, F. (2011). Method for manufacturing titanium dioxide by oxidizing of titanium tetrachloride. *U.S. Patent No. 7,968,077*. Kronos International Inc.

Grüneis, A., Rümmeli, M. H., Kramberger, C., Barreiro, A., Pichler, T., & Pfeiffer, R., et al. (2006). High quality double wall carbon nanotubes with a defined diameter distribution by chemical vapor deposition from alcohol. *Carbon, 44*, 3177-3182.

Gundogdu, O., Jenneson, P. M., & Tuzun, U. (2006). Nano particle fluidisation in model 2-D and 3-D beds using high speed X-ray imaging and microtomography. *Journal of Nanoparticle Research, 9*, 215-223.

Guo, Q., Li, Y., Wang, M., Shen, W., & Yang, C. (2006). Fluidization characteristics of SiO_2 nanoparticles in an acoustic fluidized bed. *Chemical Engineering and Technology, 29*, 78-86.

Guo, T., Nikolaev, P., Thess, A., Colbert, D. T., & Smalley, R. E. (1995). Catalytic Growth of Single-Walled Nanotubes by Laser Vaporization. *Chemical Physics Letters, 243*, 49-54.

Gupta, S., & Tripathi, M. (2011). A review of TiO_2 nanoparticles. *Chinese Science Bulletin, 56*, 1639-1657.

Ha, B., Yeom, T. H., & Lee, S. H. (2009). Ferromagnetic properties of single-walled carbon nanotubes synthesized by Fe catalyst arc discharge. *Physica B: Condensed Matter, 404*, 1617-1620.

Habermann, H., Hasenzahl, S. D., & Hemme, I. D. (2011). Iron oxide- and silicon dioxide- titanium dioxide mixture. *EP 1197472B1*. Evonik Degussa GmbH.

Hakim, L. F., Blackson, J., George, S. M., & Weimer, A. W. (2005a). Nanocoating individual silica nanoparticles by atomic layer deposition in a fluidized bed reactor. *Chemical Vapor Deposition, 11*, 420-425.

Hakim, L. F., Blackson, J. H., & Weimer, A. W. (2007). Modification of interparticle forces for nanoparticles using atomic layer deposition. *Chemical Engineering Science, 62*, 6199-6211.

Hakim, L. F., Portman, J. L., Casper, M. D., & Weimer, A. W. (2004). Conformal coating of nanoparticles using atomic layer deposition in a fluidized bed reactor. In *Proceedings of AIChE Annual Meeting* (pp. 6543-6563).

Hakim, L. F., Portman, J. L., Casper, M. D., & Weimer, A. W. (2005b). Aggregation behavior of nanoparticles in fluidized beds. *Powder Technology, 160*, 149-160.

Hartmann, W., & Kerner, D. (2002). Titanium dioxide powder which contains iron oxide. *U.S. Patent No. 6,406,532*. Degussa AG.

Hartmann, W., Mangold, H., & Kerner, D. (1998). Flame-hydrolytically produced titanium dioxide mixed oxide, method of its production and its use. *U.S. Patent No. 5,762,914.* Degussa AG.

Hartmann, W. D., Mangold, H. D., & Kerner, D. D. (1997). Titandioxide mixed oxide prepared by flame hydrolysis, process for its preparation and its use. *EP 0595078B1*. Degussa AG.

Haukka, S., Lakomaa, E.-L., & Suntola, T. (1993). Analytical and chemical techniques in the study of surface species in atomic layer epitaxy. *Thin Solid Films, 225*, 280-283.

He, M., Chernov, A. I., Fedotov, P. V., Obraztsova, E. D., Sainio, J., & Rikkinen, E., et al. (2010). Predominant (6,5) single-walled carbon nanotube growth on a copper-promoted iron catalyst. *Journal of the American Chemical Society, 132*, 13994-13996.

Height, M. J., Howard, J. B., Tester, J. W., & Vander Sande, J. B. (2004). Flame synthesis of single-walled carbon nanotubes. *Carbon, 42*, 2295-2307.

Height, M. J., Mädler, L., Pratsinis, S. E., & Krumeich, F. (2006). Nanorods of ZnO made by flame spray pyrolysis. *Chemistry of Materials, 18*, 572-578.

Hembram, K., Sivaprakasam, D., Rao, T. N., & Wegner, K. (2013). Large-scale manufacture of ZnO nanorods by flame spray pyrolysis. *Journal of Nanoparticle Research, 15,* 1461, doi:10.1007/s11051-013-1461-4.

Hemme, I., Mangold, H., Geissen, S. U., & Moiseev, A. (2003). Doped titanium dioxide. *U.S. Patent No. 6,627,173*. Degussa AG.

Hinkov, I. , Grand, J., de La Chapelle, M. L., Farhat, S., Scott, C. D., & Nikolaev, P., et al. (2004). Effect of temperature on carbon nanotube diameter and bundle arrangement: Microscopic and macroscopic analysis. *Journal of Applied Physics, 95*, 2029-2037.

Hoa, N. D., Van Quy, N., Cho, Y., & Kim, D. (2009). Porous single-wall carbon nanotube films formed by in Situ arc-discharge deposition for gas sensors application. *Sensors and Actuators B: Chemical, 135*, 656-663.

Hou, P. X., Liu, C., Tong, Y., Xu, S. T., Liu, M., & Cheng, H. M. (2001). Purification of single-walled carbon nanotubes synthesized by the hydrogen arc-discharge method. *Journal of Materials Research, 16*, 2526-2529.

Huang, A.-N., & Kuo, H.-P. (2014). Developments in the tools for the investigation of mixing in particulate systems – A review. *Advanced Powder Technology, 25*, 163-173.

Huang, C., Wang, Y., & Wei, F. (2008). Solids mixing behavior in a nano-agglomerate fluidized bed. *Powder Technology, 182*, 334-341.

Iijima, S. (1991). Helical microtubules of graphitic carbon. *Nature, 354*, 56-58.

Iijima, S., Ajayan, P. M., & Ichihashi, T. (1992). Growth model for carbon nanotubes. *Physical Review Letters, 69*, 3100-3103.

Iijima, S., & Ichihashi, T. (1993). Single-shell carbon nanotubes of 1-nm diameter. *Nature, 363*, 603-605.

International Carbon Black Association. (2014). http://www.carbon-black.org.

Itkis, M. E., Perea, D. E., Niyogi, S., Love, J., Tang, J., & Yu, A., et al. (2004). Optimization of the Ni-Y catalyst composition in bulk electric Arc synthesis of single-walled carbon nanotubes by use of near-infrared spectroscopy. *Journal of Physical Chemistry B, 108*, 12770-12775.

Jackson, D. H. K., Dunn, B. A., Guan, Y., & Kuech, T. F. (2014). Tungsten hexacarbonyl and hydrogen peroxide as precursors for the growth of tungsten oxide thin films on titania nanoparticles. *AIChE Journal, 60*, 1278-1286.

Jacques, B., François, H., & Philippe, M. (2014). Rheology of powders and nanopowders through the use of a Couette four-bladed vane rheometer: Flowability, cohesion energy, agglomerates and dustiness. *Journal of Nanoparticle Research, 16,* 2558, doi:10.1007/s11051-014-2558-0.

Jeong, M.-G., Park, E. J., Jeong, B., Kim, D. H., & Kim, Y. D. (2014). Toluene combustion over NiO nanoparticles on mesoporous SiO_2 prepared by atomic layer deposition. *Chemical Engineering Journal, 237*, 62-69.

Joshi, R., Engstler, J., Nair, P. K., Haridoss, P., & Schneider, J. J. (2008). High yield formation of carbon nanotubes using a rotating cathode in open air. *Diamond and Related Materials, 17*, 913-919.

Journet, C., Maser, W. K., Bernier, P., Loiseau, A., de la Chapelle, M. L., & Lefrant, S., et al. (1997). Large-scale production of single-walled carbon nanotubes by the electric-arc technique. *Nature, 388*, 756-758.

Jung, J., & Gidaspow, D. (2002). Fluidization of nano-size particles. *Journal of Nanoparticle Research, 4*, 483-497.

Jung, Y. S., Cavanagh, A. S., Dillon, A. C., Groner, M. D., George, S. M., & Lee, S. H. (2010). Enhanced stability of $LiCoO_2$ cathodes in lithium-ion batteries using surface modification by atomic layer deposition. *Journal of the Korean Ceramic Society, 47*, 61-65.

Kaluza, S., & Muhler, M. (2009). On the precipitation mechanism and the role of the post-precipitation steps during the synthesis of binary $ZnO-Al_2O_3$ composites with high specific surface area. *Journal of Materials Chemistry, 19*, 3914-3922.

Kammler, H. K., Mädler, L., & Pratsinis, S. E. (2001). Flame synthesis of nanoparticles. *Chemical Engineering & Technology, 24*, 583-596.

Kathyayini, H., Nagaraju, N., Fonseca, A., & Nagy, J. B. (2004). Catalytic activity of Fe, Co and Fe/Co supported on Ca and Mg oxides, hydroxides and carbonates in the synthesis of carbon nanotubes. *Journal of Molecular Catalysis A: Chemical, 223*, 129-136.

Kavli Foundation. (2011). *Scaling up: The future of nanoscience*. Retrieved from http://www.kavlifoundation.org/science-spotlights/caltech-kavli-futures-symp-nanoscience#.VukZAE32apo.

Keidar, M. (2007). Factors affecting synthesis of single wall carbon nanotubes in arc discharge. *Journal of Physics D: Applied Physics, 40*, 2388-2393.

Keränen, J., Guimon, C., Iiskola, E., Auroux, A., & Niinistö, L. (2003). Atomic layer deposition and surface characterization of highly dispersed titania/silica-supported vanadia catalysts. *Catalysis Today, 78*, 149-157.

Kilbury, O. J., Barrett, K. S., Fu, X., Yin, J., Dinair, D. S., & Gump, C. J., et al. (2012). Atomic layer deposition of solid lubricating coatings on particles. *Powder Technology, 221*, 26-35.

Kim, D. Y., Sugime, H., Hasegawa, K., Osawa, T., & Noda, S. (2011). Sub-millimeter-long carbon nanotubes repeatedly grown on and separated from ceramic beads in a single fluidized bed reactor. *Carbon, 49*, 1972-1979.

Kim, D. Y., Sugime, H., Hasegawa, K., Osawa, T., & Noda, S. (2012). Fluidized-bed synthesis of sub-millimeter-long single walled carbon nanotube arrays. *Carbon, 50*, 1538-1545.

Kim, H. J., Kang, I. G., Kim, D. H., & Choi, B. H. (2011). Dispersion characteristics of TiO_2 particles coated with the SiO_2 nano-film by atomic layer deposition. *Journal of Nanoscience and Nanotechnology, 11*, 10344-10348.

Kim, H. J., Kim, M. W., Kim, H. S., Kim, H. S., Kim, S. H., & Lee, S. W., et al. (2006). Atomic layer deposition of aluminum oxide thin film on $BaMgAl_{10}O_{17}$:Eu^{2+} phosphor. *Molecular Crystals and Liquid Crystals, 459*, 239-245.

Kim, Y. A., Muramatsu, H., Hayashi, T., & Endo, M. (2012). Catalytic metal-free formation of multi-walled carbon nanotubes in atmospheric arc discharge. *Carbon, 50*, 4588-4595.

King, D. M., Liang, X., Carney, C. S., Hakim, L. F., Li, P., & Weimer, A. W. (2008a). Atomic layer deposition of UV-absorbing ZnO films on SiO_2 and TiO_2 nanoparticles using a fluidized bed reactor. *Advanced Functional Materials, 18*, 607-615.

King, D. M., Liang, X., Li, P., & Weimer, A. W. (2008b). Low-temperature atomic layer deposition of ZnO films on particles in a fluidized bed reactor. *Thin Solid Films, 516*, 8517-8523.

King, D. M., Liang, X., & Weimer, A. W. (2012). Functionalization of fine particles using atomic and molecular layer deposition. *Powder Technology, 221*, 13-25.

King, D. M., Spencer, J. A., Liang, X., Hakim, L. F., & Weimer, A. W. (2007). Atomic layer deposition on particles using a fluidized bed reactor with in situ mass spectrometry. *Surface and Coatings Technology, 201*, 9163-9171.

King, D. M., Zhou, Y., Hakim, L. F., Liang, X., Li, P., & Weimer, A. W. (2009). In situ synthesis of TiO_2-functionalized metal nanoparticles. *Industrial & Engineering Chemistry Research, 48*, 352-360.

Kleinschmit, P., & Schwarz, R. (1981). Temperature stabilized, pyrogenically produced aluminum oxide-mixed oxide, the process for its production and use. *U.S. Patent No. 4,286,990.* Degussa AG.

Kloepfer, H. (1952). Verfahren zur Herstellung von feinverteilten Oxyden. *DE 830786C.* Degussa AG.

Knauth, P., Bouchet, R., Schaf, O., Weibel, A., & Auer, G. (2003). Functionalized TiO_2 nanoparticles for pigments, photoelectrochemistry, and solid state chemical sensors. *ChemInform, 34,* doi: 10.1002/chin.200327196.

Kojima, T., & Elliott, J. A. (2013). Effect of silica nanoparticles on the bulk flow properties of fine cohesive powders. *Chemical Engineering Science, 101,* 315-328.

Kokai, F., Takahashi, K., Yudasaka, M., Yamada, R., Ichihashi, T., & Iijima, S. (1999). Growth dynamics of single-wall carbon nanotubes synthesized by CO_2 laser vaporization. *The Journal of Physical Chemistry B, 103,* 4346-4351.

Kong, J., Cassell, A. M., & Dai, H. (1998). Chemical vapor deposition of methane for single-walled carbon nanotubes. *Chemical Physics Letters, 292,* 567-574.

Korhonen, S. T., Airaksinen, S. M. K., Bañares, M. A., & Krause, A. O. I. (2007). Isobutane dehydrogenation on zirconia-, alumina-, and zirconia/alumina-supported chromia catalysts. *Applied Catalysis A: General, 333,* 30-41.

Kozawa, A., Kiribayashi, H., Ogawa, S., Saida, T., Naritsuka, S., & Maruyama, T. (2016). Single-walled carbon nanotube growth on SiO_2/Si using Rh catalysts by alcohol gas source chemical vapor deposition. *Diamond and Related Materials, 63,* 159-164.

Kukovitsky, E. F., L'vov, S. G., & Sainov, N. A. (2000). VLS-growth of carbon nanotubes from the vapor. *Chemical Physics Letters, 317,* 65-70.

Kumar, M., & Ando, Y. (2010). Chemical vapor deposition of carbon nanotubes: A review on growth mechanism and mass production. *Journal of Nanoscience and Nanotechnology, 10,* 3739-3758.

Kusaba, M., & Tsunawaki, Y. (2006). Production of single-wall carbon nanotubes by a XeCl excimer laser ablation. *Thin Solid Films, 506-507,* 255-258.

Lakomaa, E.-L., Haukka, S., & Suntola, T. (1992). Atomic layer growth of TiO_2 on silica. *Applied Surface Science, 60-61,* 742-748.

Lamminen, E. (2011). Accurate measurement of nanoparticle charge, number and size with the ELPI+™ instrument. In *Journal of Physics: Conference Series* (Vol. 304, No. 1, p. 012064).

Lange, L., Diether, J., Volling, A., & Klebe, H. (1976). Process for the production of finely divided oxides. *U.S. Patent No. 3,954,945* Deutsche Gold- und Silber-Schneideanstalt.

Larson, H. A. (1957). Carbon black process and apparatus. *U.S. Patent No. 2,809,098*. Phillips Petroleum Co.

Lashdaf, M., Lahtinen, J., Lindblad, M., Venäläinen, T., & Krause, A. O. I. (2004). Platinum catalysts on alumina and silica prepared by gas- and liquid- phase deposition in cinnamaldehyde hydrogenation. *Applied Catalysis A: General, 276*, 129-137.

Laube, J., Salameh, S., Kappl, M., Mädler, L., & Colombi Ciacchi, L. (2015). Contact forces between TiO_2 nanoparticles governed by an interplay of adsorbed water layers and roughness. *Langmuir, 31*, 11288-11295.

Lebel, L. L., Aissa, B., Khakani, M. A. E., & Therriault, D. (2010). Preparation and mechanical characterization of laser ablated single-walled carbon-nanotubes/polyurethane nanocomposite microbeams. *Composites Science and Technology, 70*, 518-524.

Lee, J. H., Lee, E. K., Joo, W. J., Jang, Y., Kim, B. S., & Lim, J. Y., et al. (2014). Wafer-scale growth of single-crystal monolayer graphene on reusable hydrogen-terminated germanium. *Science, 344*, 286-289.

Lee, S. J., Baik, H. K., Yoo, J. E., & Han, J. H. (2002). Large scale synthesis of carbon nanotubes by plasma rotating arc discharge technique. *Diamond and Related Materials, 11*, 914-917.

Lei, Y., Liu, B., Lu, J., Lobo-Lapidus, R. J., Wu, T., & Feng, H., et al. (2012). Synthesis of Pt–Pd core–shell nanostructures by atomic layer deposition: application in propane oxidative dehydrogenation to propylene. *Chemistry of Materials, 24*, 3525-3533.

Lei, Y., Lu, J., Zhao, H., Liu, B., Low, K.-B., & Wu, T., et al. (2013). Resolving Precursor Deligation, Surface Species Evolution, and Nanoparticle Nucleation during Palladium Atomic Layer deposition. *The Journal of Physical Chemistry C, 117*, 11141-11148.

Li, H., He, D., Li, T., Genestoux, M., & Bai, J. (2010). Chemical kinetics of catalytic chemical vapor deposition of an acetylene/xylene mixture for improved carbon nanotube production. *Carbon, 48*, 4330-4342.

Li, J., Zhang, B., Chen, Y., Zhang, J., Yang, H., & Zhang, J., et al. (2015). Styrene hydrogenation performance of Pt nanoparticles with controlled size prepared by atomic layer deposition. *Catalysis Science & Technology, 5*, 4218-4223.

Li, Q., Rudolph, V., & Peukert, W. (2006). London-van der Waals adhesiveness of rough particles. *Powder Technology, 161*, 248-255.

Li, Q., Yan, H., Cheng, Y., Zhang, J., & Liu, Z. (2002). A scalable CVD synthesis of high-purity single-walled carbon nanotubes with porous MgO as support material. *Journal of Materials Chemistry, 12*, 1179-1183.

Li, X., Zhu, Y., Cai, W., Borysiak, M., Han, B., & Chen, D., et al. (2009a). Transfer of large-area graphene films for high-performance transparent conductive electrodes. *Nano Letters, 9*, 4359-4363.

Li, X. S., Cai, W. W., An, J. H., Kim, S., Nah, J., & Yang, D. X., et al. (2009b). Large-area synthesis of high-quality and uniform graphene films on copper foils. *Science, 324*, 1312-1314.

Li, Y.-L., Kinloch, I. A., Shaffer, M. S. P., Geng, J., Johnson, B., & Windle, A. H. (2004). Synthesis of single-walled carbon nanotubes by a fluidized-bed method. *Chemical Physics Letters, 384*, 98-102.

Li, Y., & Chopra, N. (2014a). Progress in large-scale production of graphene. Part 1: Chemical methods. *JOM, 67*, 34-43.

Li, Y., & Chopra, N. (2014b). Progress in large-scale production of graphene. Part 2: Vapor methods. *JOM, 67*, 44-52.

Liang, F., Shimizu, T., Tanaka, M., Choi, S., & Watanabe, T. (2012). Selective preparation of polyhedral graphite particles and multi-wall carbon nanotubes by a transferred arc under atmospheric pressure. *Diamond and Related Materials, 30*, 70-76.

Liang, X., Duan, H., Zhou, T., & Kong, J. (2014). Fluidization behavior of binary mixtures of nanoparticles in vibro-fluidized bed. *Advanced Powder Technology, 25*, 236-243.

Liang, X., Duan, H., Wang, J., & Zhou, T. (2014). Agglomerate sizes of binary nanoparticle mixtures in a vibro-fluidized bed. *Chemical Engineering and Technology, 37*, 20-26.

Liang, X., Duan, H., Wang, J., & Zhou, T. (2015). Agglomerating Vibro-fluidization Behavior of Binary Nanoparticles Mixtures. *Procedia Engineering, 102*, 887-892.

Liang, X., Hakim, L. F., Zhan, G.-D., McCormick, J. A., George, S. M., & Weimer, A. W., et al. (2007). Novel processing to produce polymer/ceramic nanocomposites by atomic layer deposition. *Journal of the American Ceramic Society, 90*, 57-63.

Liang, X., & Jiang, C. (2013). Atomic layer deposited highly dispersed platinum nanoparticles supported on non-functionalized multiwalled carbon nanotubes for the hydrogenation of xylose to xylitol. *Journal of Nanoparticle Research, 15*, 1-9.

Liang, X., Jiang, Y.-B., & Weimer, A. W. (2012). Nanocoating zinc alkoxide (zincone) hybrid polymer films on particles using a fluidized bed reactor. *Journal of Vacuum Science & Technology A, 30,* 01A108.

Liang, X., King, D. M., Li, P., George, S. M., & Weimer, A. W. (2009a). Nanocoating hybrid polymer films on large quantities of cohesive nanoparticles by molecular layer deposition. *AIChE Journal, 55,* 1030-1039.

Liang, X., King, D. M., Li, P., & Weimer, A. W. (2009b). Low-Temperature Atomic Layer-Deposited TiO_2 Films with Low Photoactivity. *Journal of the American Ceramic Society, 92,* 649-654.

Libera, J. A., Elam, J. W., & Pellin, M. J. (2008). Conformal ZnO coatings on high surface area silica gel using atomic layer deposition. *Thin Solid Films, 516,* 6158-6166.

Lichty, P., Wirz, M., Kreider, P., Kilbury, O., Dinair, D., & King, D., et al. (2013). Surface modification of graphite particles coated by atomic layer deposition and advances in ceramic composites. *International Journal of Applied Ceramic Technology, 10,* 257-265.

Lin, Y., Zhou, S., Sheehan, S. W., & Wang, D. (2011). Nanonet-based hematite heteronanostructures for efficient solar water splitting. *Journal of the American Chemical Society, 133,* 2398-2401.

Lindblad, M., Lindfors, L. P., & Suntola, T. (1994). Preparation of Ni/Al_2O_3 catalysts from vapor-phase by atomic layer epitaxy. *Catalysis Letters, 27,* 323-336.

Liu, X., Zheng, M., Xiao, K., Xiao, Y., He, C., & Dong, H., et al. (2014). Simple, green and high-yield production of single- or few-layer graphene by hydrothermal exfoliation of graphite. *Nanoscale, 6,* 4598-4603.

Liu, Y. C., Sun, B. M., & Ding, Z. Y. (2011). Effect of helium on synthesis of carbon nanotubes from the V-Type pyrolysis flame. *Advanced Materials Research, 221,* 540-544.

Liu, Y. C., Zheng, N. N., Huang, J. D., & Sun, B. M. (2011). Synthesis of carbon nanotubes with typical structure from the pyrolysis flame. *Advanced Materials Research, 221,* 99-103.

Lobo, R., Marshall, C. L., Dietrich, P. J., Ribeiro, F. H., Akatay, C., & Stach, E. A., et al. (2012). Understanding the chemistry of H_2 production for 1-propanol reforming: Pathway and support modification effects. *ACS Catalysis,* 2316-2326.

Longrie, D., Deduytsche, D., & Detavernier, C. (2014a). Reactor concepts for atomic layer deposition on agitated particles: A review. *Journal of Vacuum Science & Technology A, 32*(1), 010802.

Longrie, D., Deduytsche, D., Haemers, J., Driesen, K., & Detavernier, C. (2012). A rotary reactor for thermal and plasma-enhanced atomic layer deposition on powders and small objects. *Surface and Coatings Technology, 213*, 183-191.

Longrie, D., Deduytsche, D., Haemers, J., Smet, P. F., Driesen, K., & Detavernier, C. (2014b). Thermal and plasma-enhanced atomic layer deposition of TiN using TDMAT and NH_3 on particles agitated in a rotary reactor. *ACS Applied Materials & Interfaces, 6*, 7316-7324.

Loving, W. (1947). Apparatus for the manufacture of carbon black. *U.S. Patent No. 2,418,475*. Cabot Godfrey L Inc.

Lu, J., Fu, B., Kung, M. C., Xiao, G., Elam, J. W., & Kung, H. H., et al. (2012). Coking- and sintering-resistant palladium catalysts achieved through atomic layer deposition. *Science, 335*, 1205-1208.

Lu, J., & Stair, P. C. (2010). Low-temperature ABC-type atomic layer deposition: Synthesis of highly uniform ultrafine supported metal nanoparticles. *Angewandte Chemie International Edition, 49*, 2547-2551.

Lubers, A. M., Muhich, C. L., Anderson, K. M., & Weimer, A. W. (2015). Mechanistic studies for depositing highly dispersed Pt nanoparticles on carbon by use of trimethyl(methylcyclopentadienyl)platinum(IV) reactions with O_2 and H_2. *Journal of Nanoparticle Research, 17*, 1-16.

Lv, X., Du, F., Ma, Y., Wu, Q., & Chen, Y. (2005). Synthesis of high quality single-walled carbon nanotubes at large scale by electric arc using metal compounds. *Carbon, 43*, 2020-2022.

Ma, Z., Brown, S., Howe, J. Y., Overbury, S. H., & Dai, S. (2008). Surface modification of Au/TiO_2 catalysts by SiO_2 via atomic layer deposition. *The Journal of Physical Chemistry C, 112*, 9448-9457.

Macwan, D. P., Dave, P., & Chaturvedi, S. (2011). A review on nano-TiO_2 sol-gel type syntheses and its applications. *Journal of Materials Science, 46*, 3669-3686.

Mädler, L., Kammler, H. K., Mueller, R., & Pratsinis, S. E. (2002a). Controlled synthesis of nanostructured particles by flame spray pyrolysis. *Journal of Aerosol Science, 33*, 369-389.

Mädler, L., & Pratsinis, S. E. (2002). Bismuth oxide nanoparticles by flame spray pyrolysis. *Journal of the American Ceramic Society, 85*, 1713-1718.

Mädler, L., Roessler, A., Pratsinis, S. E., Sahm, T., Gurlo, A., & Barsan, N., et al. (2006). Direct formation of highly porous gas-sensing films by in situ thermophoretic deposition of flame-made Pt/SnO_2 nanoparticles. *Sensors and Actuators B: Chemical, 114*, 283-295.

Mädler, L., Stark, W. J., & Pratsinis, S. E. (2002b). Flame-made ceria nanoparticles. *Journal of Materials Research, 17*, 1356-1362.

Mandelbrot, B. (1982). *The fractal geometry of nature*. New York: W. H. Freeman and Company.

Mangold, H., Golchert, R., Katusic, S., & Janzon, K. (2001). Doped, pyrogenically prepared oxides. *U.S. Patent No. 6,328,944*. Degussa AG.

Mao, M., & Bogaerts, A. (2010). Investigating the plasma chemistry for the synthesis of carbon nanotubes/nanofibres in an inductively coupled plasma enhanced CVD system: The effect of different gas mixtures. *Journal of Physics D-Applied Physics, 43*(20), 205201.

Marchal, J., John, T., Baranwal, R., Hinklin, T., & Laine, R. M. (2004). Yttrium aluminum garnet nanopowders produced by liquid-feed flame spray pyrolysis (LF-FSP) of metalloorganic precursors. *Chemistry of Materials, 16*, 822-831.

Maruyama, S., Kojima, R., Miyauchi, Y., Chiashi, S., & Kohno, M. (2002). Low-temperature synthesis of high-purity single-walled carbon nanotubes from alcohol. *Chemical Physics Letters, 360*, 229-234.

Maruyama, T., Kondo, H., Ghosh, R., Kozawa, A., Naritsuka, S., & Iizumi, Y., et al. (2016). Single-walled carbon nanotube synthesis using Pt catalysts under low ethanol pressure via cold-wall chemical vapor deposition in high vacuum. *Carbon, 96*, 6-13.

Maruyama, T., Mizutani, Y., Naritsuka, S., & Iijima, S. (2011). Single-walled carbon nanotube growth in high vacuum using Pt catalyst in alcohol gas source method. *Materials Express, 1*, 267-272.

Maser, W. K., Munoz, E., Benito, A. M., Martinez, M. T., de la Fuente, G. F., & Maniette, Y., et al. (1998). Production of high-density single-walled nanotube material by a simple laser-ablation method. *Chemical Physics Letters, 292*, 587-593.

Matlock, C. (1931). Process and apparatus for producing carbon black. *U.S. Patent NO. 1798614A*. Monroe Louisiana Carbon Compan.

Matsuda, S., Hatano, H., Muramoto, T., & Tsutsumi, A. (2004). Modeling for size reduction of agglomerates in nanoparticle fluidization. *AIChE Journal, 50*, 2763-2771.

Matsuyama, K., Tanaka, S., & Okuyama, T. (2014). Hydrophobic modification of fibers by pressure-induced phase-separation coupled with ultrasonic irradiation in high-pressure liquid carbon dioxide. *Chemical Engineering Journal, 246*, 106-113.

McCormick, J. A., Cloutier, B. L., Weimer, A. W., & George, S. M. (2007a). Rotary reactor for atomic layer deposition on large quantities of nanoparticles. *Journal of Vacuum Science & Technology A: Vacuum, Surfaces, and Films, 25*, 67-74.

McCormick, J. A., Rice, K. P., Paul, D. F., Weimer, A. W., & George, S. M. (2007b). Analysis of Al_2O_3 atomic layer deposition on ZrO_2 nanoparticles in a rotary reactor. *Chemical Vapor Deposition, 13*, 491-498.

Mei, B., Sanchez, M. D., Reinecke, T., Kaluza, S., Xia, W., & Muhler, M. (2011). The synthesis of Nb-doped TiO_2 nanoparticles by spray drying: an efficient and scalable method. *Journal of Materials Chemistry, 21*, 11781-11790.

Merchan-Merchan, W., Saveliev, A. V., & Kennedy, L. A. (2004). High-rate flame synthesis of vertically aligned carbon nanotubes using electric field control. *Carbon, 42*, 599-608.

Meysami, S. S., Koós, A. A., Dillon, F., Dutta, M., & Grobert, N. (2015). Aerosol-assisted chemical vapour deposition synthesis of multi-wall carbon nanotubes: III. Towards upscaling. *Carbon, 88*, 148-156.

Milt, V. G., Ulla, M. A., & Lombardo, E. A. (2000). Cobalt-containing catalysts for the high-temperature combustion of methane. *Catalysis Letters, 65*, 67-73.

Milt, V. G., Ulla, M. A., & Lombardo, E. A. (2001). Zirconia-supported cobalt as a catalyst for methane combustion. *Journal of Catalysis, 200*, 241-249.

Minnermann, M., Grossmann, H. K., Pokhrel, S., Thiel, K., Hagelin-Weaver, H., & Bäumer, M., et al. (2013). Double flame spray pyrolysis as a novel technique to synthesize alumina-supported cobalt Fischer–Tropsch catalysts. *Catalysis Today, 214*, 90-99.

Moghtaderi, B., Shames, I., & Doroodchi, E. (2006). Combustion prevention of iron powders by a novel coating method. *Chemical Engineering and Technology, 29*, 97-103.

Molenbroek, A. M., Haukka, S., & Clausen, B. S. (1998). Alloying in Cu/Pd nanoparticle catalysts. *The Journal of Physical Chemistry B, 102*, 10680-10689.

Morancais, A., Caussat, B., Kihn, Y., Kalck, P., Plee, D., & Gaillard, P., et al. (2007). A parametric study of the large scale production of multi-walled carbon nanotubes by fluidized bed catalytic chemical vapor deposition. *Carbon, 45*, 624-635.

Mueller, R., Mädler, L., & Pratsinis, S. E. (2003). Nanoparticle synthesis at high production rates by flame spray pyrolysis. *Chemical Engineering Science, 58*, 1969-1976.

Mukhopadhyay, K., Koshio, A., Sugai, T., Tanaka, N., Shinohara, H., & Konya, Z., et al. (1999). Bulk production of quasi-aligned carbon nanotube bundles by the catalytic chemical vapour deposition (CCVD) method. *Chemical Physics Letters, 303*, 117-124.

Munoz, E., Maser, W. K., Benito, A. M., de la Fuente, G. F., & Martinez, M. T. (1999). Single-walled carbon nanotubes produced by laser ablation under different inert atmospheres. *Synthetic Metals, 103*, 2490-2491.

Murray, C. B., Kagan, C. R., & Bawendi, M. G. (2000). Synthesis and characterization of monodisperse nanocrystals and close-packed nanocrystal assemblies. *Annual Review of Materials Science, 30*, 545-610.

Nakamura, H., & Watano, S. (2008). Fundamental particle fluidization behavior and handling of nano-particles in a rotating fluidized bed. *Powder Technology, 183*, 324-332.

Nam, C. H., Pfeffer, R., Dave, R. N., & Sundaresan, S. (2004). Aerated vibrofluidization of silica nanoparticles. *AIChE Journal, 50*, 1776-1785.

Nandiyanto, A. B. D., & Okuyama, K. (2011). Progress in developing spray-drying methods for the production of controlled morphology particles: From the nanometer to submicrometer size ranges. *Advanced Powder Technology, 22*, 1-19.

Narh, K. A., Agwedicham, A.-T., & Jallo, L. (2008). Dry coating polymer powder particles with deagglomerated carbon nanotubes to improve their dispersion in nanocomposites. *Powder Technology, 186*, 206-212.

Nasibulin, A. G., Moisala, A., Jiang, H., & Kauppinen, E. I. (2006). Carbon nanotube synthesis from alcohols by a novel aerosol method. *Journal of Nanoparticle Research, 8*, 465-475.

Ning, G. Q., Wei, F., Wen, Q., Luo, G. H., Wang, Y., & Jin, Y. (2006). Improvement of Fe/MgO catalysts by calcination for the growth of single-and double-walled carbon nanotubes. *Journal of Physical Chemistry B, 110*, 1201-1205.

Nishide, D., Kataura, H., Suzuki, S., Tsukagoshi, K., Aoyagi, Y., & Achiba, Y. (2003). High-yield production of single-wall carbon nanotubes in nitrogen gas. *Chemical Physics Letters, 372*, 45-50.

Noriler, D., Rosebrock, C. D., Mädler, L., Meier, H. F., & Fritsching, U. (2014). Influence of atomization and spray parameters on the flame spray process for nanoparticle production. *Atomization and Sprays, 24*, 495-524.

Novoselov, K. S., Fal'ko, V. I., Colombo, L., Gellert, P. R., Schwab, M. G., & Kim, K. (2012). A roadmap for graphene. *Nature, 490*, 192-200.

Novoselov, K. S., Geim, A. K., Morozov, S. V., Jiang, D., Zhang, Y., & Dubonos, S. V., et al. (2004). Electric field effect in atomically thin carbon films. *Science, 306*, 666-669.

Oberlin, A., Endo, M., & Koyama, T. (1976). Filamentous growth of carbon through benzene decomposition. *Journal of Crystal Growth, 32*, 335-349.

Okubo, S., Sekine, T., Suzuki, S., Achiba, Y., Tsukagoshi, K., & Aoyagi, Y., et al. (2004). Purification of single-wall carbon nanotubes synthesized from alcohol by catalytic chemical vapor deposition. *Japanese Journal of Applied Physics, 43*, L396-L398.

Oliveira, M. I. L. L., Chen, K., & Ferreira, M. F. J. (2002). Influence of the deagglomeration procedure on aqueous dispersion, slip casting and sintering of Si_3N_4-based ceramics. *Journal of the European Ceramic Society, 22*, 1601-1607.

Park, S. W., Kim, J.W., Choi, H.J., & Shim, J.H. (2014). Vibration atomic layer deposition for conformal nanoparticle coating. *Journal of Vacuum Science & Technology A, 32*, 01A115.

Patel, R. L., Jiang, Y.-B., & Liang, X. (2015). Highly porous titania films coated on sub-micron particles with tunable thickness by molecular layer deposition in a fluidized bed reactor. *Ceramics International, 41*, 2240-2246.

Paton, K. R., Varrla, E., Backes, C., Smith, R. J., Khan, U., & O'Neill, A., et al. (2014). Scalable production of large quantities of defect-free few-layer graphene by shear exfoliation in liquids. *Nature Materials, 13*, 624-630.

Pawinrat, P., Mekasuwandumrong, O., & Panpranot, J. (2009). Synthesis of Au–ZnO and Pt–ZnO nanocomposites by one-step flame spray pyrolysis and its application for photocatalytic degradation of dyes. *Catalysis Communications, 10*, 1380-1385.

Perez-Vaquero, J., Valverde, J. M., & Quintanilla, M. A. S. (2013). Flow properties of CO_2 sorbent powders modified with nanosilica. *Powder Technology, 249*, 443-455.

Petersen, M. A., Sale, T. C., & Reardon, K. F. (2007). Electrolytic trichloroethene degradation using mixed metal oxide coated titanium mesh electrodes. *Chemosphere, 67*, 1573-1581.

Pfeffer, R., Dave, R. N., Wei, D., & Ramlakhan, M. (2001). Synthesis of engineered particulates with tailored properties using dry particle coating. *Powder Technology, 117*, 40-67.

Philippe, R., Morançais, A., Corrias, M., Caussat, B., Kihn, Y., & Kalck, P., et al. (2007). Catalytic production of carbon nanotubes by fluidized-bed CVD. *Chemical Vapor Deposition, 13*, 447-457.

Plomp, A. J., Vuori, H., Krause, A. O. I., de Jong, K. P., & Bitter, J. H. (2008). Particle size effects for carbon nanofiber supported platinum and ruthenium catalysts for the selective hydrogenation of cinnamaldehyde. *Applied Catalysis A: General, 351*, 9-15.

Podczeck, F., Newton, J. M., & James, M. B. (1997). Influence of relative humidity of storage air on the adhesion and autoadhesion of micronized particles to particulate and compacted powder surfaces. *Journal of Colloid and Interface Science, 187*, 484-491.

Pokhrel, S., Birkenstock, J., Schowalter, M., Rosenauer, A., & Mädler, L. (2010). Growth of ultrafine single crystalline WO_3 nanoparticles using flame spray pyrolysis. *Crystal Growth and Design, 10*, 632-639.

Pokropivny, V. V., & Skorokhod, V. V. (2007). Classification of nanostructures by dimensionality and concept of surface forms engineering in nanomaterial science. *Materials Science and Engineering: C, 27*, 990-993.

Pollock, L. W. (1957). Process for production of carbon black. *U.S. Patent No. 2,796,332.*

Puurunen, R. L. (2005). Surface chemistry of atomic layer deposition: A case study for the trimethylaluminum/water process. *Journal of Applied Physics, 97*, 121301.

Puurunen, R. L. (2014). A short history of atomic layer deposition: Tuomo Suntola's atomic layer epitaxy. *Chemical Vapor Deposition, 20*, 332-344.

Qian, W., Liu, T., Wei, F., Wang, Z., & Li, Y. (2004). Enhanced production of carbon nanotubes: combination of catalyst reduction and methane decomposition. *Applied Catalysis A: General, 258*, 121-124.

Qian, W. Z., Wei, F., Wang, Z. W., Liu, T., Yu, H., & Luo, G. H., et al. (2003). Production of carbon nanotubes in a packed bed and a fluidized bed. *AIChE Journal, 49*, 619-625.

Qin, L., Gong, T., Hao, H., Wang, K., & Feng, H. (2013). Core-shell-structured nanothermites synthesized by atomic layer deposition. *Journal of Nanoparticle Research, 15,* 2150, doi:10.1007/s11051-013-2150-z.

Qiu, J., Wang, Z., Zhao, Z., & Wang, T. (2007). Synthesis of double-walled carbon nanotubes from coal in hydrogen-free atmosphere. *Fuel, 86*, 282-286.

Quevedo, J., Pfeffer, R., Shen, Y., Dave, R., Nakamura, H., & Watano, S. (2006). Fluidization of nanoagglomerates in a rotating fluidized bed. *AIChE Journal, 52*, 2401-2412.

Quevedo, J. A., & Pfeffer, R. (2010). In situ measurements of gas fluidized nanoagglomerates. *Industrial & Engineering Chemistry Research, 49*, 5263-5269.

Quintanilla, M. A. S., Valverde, J. M., Castellanos, A., Lepek, D., Pfeffer, R., & Dave, R. N. (2008). Nanofluidization as affected by vibration and electrostatic fields. *Chemical Engineering Science, 63*, 5559-5569.

Quintanilla, M. A. S., Valverde, J. M., Espin, M. J., & Castellanos, A. (2012). Electrofluidization of silica nanoparticle agglomerates. *Industrial & Engineering Chemistry Research, 51*, 531-538.

Radushkevich, L. V., & Lukyanovich, V. M. (1952). About the structure of carbon formed by thermal decomposition of carbon monoxide on iron substrate. *Soviet Journal of Physical Chemistry, 26*, 88–95. (in Russian)

Raganati, F., Ammendola, P., & Chirone, R. (2015). Role of acoustic fields in promoting the gas-solid contact in a fluidized bed of fine particles. *KONA Powder and Particle Journal, 32*, 23-40.

Rauwel, E., Nilsen, O., Galeckas, A., Walmsley, J., Rytter, E., & Fjellvaåg, H. (2012). ALD applied to conformal coating of nanoporous γ-alumina: Spinel formation and luminescence induced by europium doping. *ECS Transactions, 41*, 123-130.

Rick, C. E. (1955). Cooling and separating by condensation of hot gaseous suspensions. *U.S. Patent NO. 2721626A*. Du Pont.

Robichaud, C. O., Uyar, A. E., Darby, M. R., Zucker, L. G., & Wiesner, M. R. (2009). Estimates of upper bounds and trends in nano-TiO_2 production as a basis for exposure assessment. *Environmental Science & Technology, 43*, 4227-4233.

Roch, A., Jost, O., Schultrich, B., & Beyer, E. (2007). High-yield synthesis of single-walled carbon nanotubes with a pulsed arc-discharge technique. *Physica Status Solidi (B), 244*, 3907-3910.

Roch, A., Märcz, M., Richter, U., Leson, A., Beyer, E., & Jost, O. (2009). Multi-component catalysts for the synthesis of SWCNT. *Physica Status Solidi (B), 246*, 2511-2513.

Roebben, G., Rauscher, H., Amenta, V., Aschberger, K., Sanfeliu, A. B., & Calzolai, L., et al. (2014). *Towards a review of the EC recommendation for a definition of the term "nanomaterial" Part 2: Assessment of collected information concerning the experience with the definition.* European Commission, Joint Research Centre, doi: 10.2787/97286.

Roger, M. (1969). Method and apparatus for production of carbon black. *U.S. Patent NO.*3438732A. Morel Roger.

Romero, J. B., & Johanson, L. N. (1958). Factors affecting fluidized bed quality. *Chemical Engineering Progress Symposium Series, 58*, 28-37.

Rondet, E., Ruiz, T., & Cuq, B. (2013). Rheological and mechanical characterization of wet agglomerates processed in low shear mixer. *Journal of Food Engineering, 117*, 67-73.

Rosebrock, C. D., Riefler, N., Wriedt, T., Mädler, L., & Tse, S. D. (2013). Disruptive burning of precursor/solvent droplets in flame-spray synthesis of nanoparticles. *AIChE Journal, 59*, 4553-4566.

Rumpf, F. H., Taylor, R. W., & Toombs, A. E. (2010). Process for production of carbon black. *U.S. Patent NO. 7655209*. Cabot Corporation.

Sahm, T., Mädler, L., Gurlo, A., Barsan, N., Pratsinis, S. E., & Weimar, U. (2004). Flame spray synthesis of tin dioxide nanoparticles for gas sensing. *Sensors and Actuators B: Chemical, 98*, 148-153.

Salameh, S., Schneider, J., Laube, J., Alessandrini, A., Facci, P., & Seo, J. W., et al. (2012). Adhesion mechanisms of the contact interface of TiO_2 nanoparticles in films and aggregates. *Langmuir, 28*, 11457-11464.

Sanganwar, G. P., & Gupta, R. B. (2008). Enhancement of shelf life and handling properties of drug nanoparticles: Nanoscale mixing of itraconazole with silica. *Industrial and Engineering Chemistry Research, 47*, 4717-4725.

Sanganwar, G. P., Gupta, R. B., Ermoline, A., Scicolone, J. V., & Dave, R. N. (2009). Environmentally benign nanomixing by sonication in high-pressure carbon dioxide. *Journal of Nanoparticle Research, 11*, 405-419.

Sano, N., Nakano, J., & Kanki, T. (2004). Synthesis of single-walled carbon nanotubes with nanohorns by arc in liquid nitrogen. *Carbon, 42*, 686-688.

Sathe, T. R., Agrawal, A., & Nie, S. M. (2006). Mesoporous silica beads embedded with semiconductor quantum dots and iron oxide nanocrystals: Dual-function microcarriers for optical encoding and magnetic separation. *Analytical Chemistry, 78*, 5627-5632.

Schaumann, H. H. (1949a). Production of titanium oxide pigments. *U.S. Patent NO. 24882439A*. Du Pont.

Schaumann, H. H. (1949b). Titanium dioxide pigment production. *U.S. Patent NO. 2488440A*. Du Pont.

Schumacher, K., Schilling, R., Alff, H., & Roth, H. (2006). Titanium-aluminium mixed oxide powder. *WO2006067128A1*. Degussa AG.

Schwaiger, B., Niedermeier, W., Pelster, T., Schinkel, A. P., Teike, S., & Vogler, C. (2014). Carbon black compositions. *WO2014140228A1*. Orion Engineered Carbons Gmbh.

Scicolone, J. V., Lepek, D., Louie, L., & Davé, R. N. (2013). Fluidization and mixing of nanoparticle agglomerates assisted via magnetic impaction. *Journal of Nanoparticle Research, 15,* 1434, doi: 10.1007/s11051-013-1434-7.

Scicolone, J. V., Mujumdar, A., Sundaresan, S., & Davé, R. N. (2011). Environmentally benign dry mechanical mixing of nano-particles using magnetically assisted impaction mixing process. *Powder Technology, 209*, 138-146.

See, C. H., & Harris, A. T. (2007). A Review of Carbon Nanotube Synthesis via Fluidized-Bed Chemical Vapor Deposition. *Industrial & Engineering Chemistry Research, 46*, 997-1012.

Seekkuarachchi, I. N., & Kumazawa, H. (2008). Aggregation and disruption mechanisms of nanoparticulate aggregates. 2. Dispersion of aggregates using a motionless mixer. *Industrial and Engineering Chemistry Research, 47*, 2401-2413.

Selvaraj, S. K., Jursich, G., & Takoudis, C. G. (2013). Design and implementation of a novel portable atomic layer deposition/chemical vapor deposition hybrid reactor. *Review of Scientific Instruments, 84*, 095109.

Sen, R., Govindaraj, A., & Rao, C. N. R. (1997). Carbon nanotubes by the metallocene route. *Chemical Physics Letters, 267*, 276-280.

Seville, J. P. K., Willett, C. D., & Knight, P. C. (2000). Interparticle forces in fluidisation: A review. *Powder Technology, 113*, 261-268.

Shabanian, J., Jafari, R., & Chaouki, J. (2012). Fluidization of ultrafine powders. *International Review of Chemical Engineering, 4*, 16-50.

Shen, Y., & Lua, A. C. (2013). A facile method for the large-scale continuous synthesis of graphene sheets using a novel catalyst. *Scientific Reports, 3*, 3037, 3031-3036.

Shi, Z. J., Lian, Y. F., Liao, F. H., Zhou, X. H., Gu, Z. N., & Zhang, Y., et al. (2000). Large scale synthesis of single-wall carbon nanotubes by arc-discharge method. *Journal of Physics and Chemistry of Solids, 61*, 1031-1036.

Shimotani, K., Anazawa, K., Watanabe, H., & Shimizu, M. (2014). New synthesis of multi-walled carbon nanotubes using an arc discharge technique under organic molecular atmospheres. *Applied Physics A, 73*, 451-454.

Silvennoinen, R. J., Jylhä, O. J. T., Lindblad, M., Sainio, J. P., Puurunen, R. L., & Krause, A. O. I. (2007). Atomic layer deposition of iridium(III) acetylacetonate on alumina, silica–alumina, and silica supports. *Applied Surface Science, 253*, 4103-4111.

Singh, P., & Nanda, A. (2014). Enhanced sun protection of nano-sized metal oxide particles over conventional metal oxide particles: An in vitro comparative study. *International Journal of Cosmetic Science, 36*, 273-283.

Sinnott, S. B., Andrews, R., Qian, D., Rao, A. M., Mao, Z., & Dickey, E. C., et al. (1999). Model of carbon nanotube growth through chemical vapor deposition. *Chemical Physics Letters, 315*, 25-30.

Song, X., Liu, Y., & Zhu, J. (2007). Multi-walled carbon nanotubes produced by hydrogen DC arc discharge at elevated environment temperature. *Materials Letters, 61*, 389-391.

Soria-Hoyo, C., Valverde, J. M., van Ommen, J. R., Sánchez-Jiménez, P. E., Pérez-Maqueda, L. A., & Sayagués, M. J. (2015). Synthesis of a nanosilica supported CO_2 sorbent in a fluidized bed reactor. *Applied Surface Science, 328*, 548-553.

Stokes. (1951). Process of producing carbon black. *U.S. Patent 2,564,736*. Cabot Godfrey L Inc.

Stokes. (1954). Process of producing carbon black and synthesis gas. *U.S. Patent 2,672,402*. Cabot Godfrey L Inc.

Stramel, A. A., Gupta, M. C., Lee, H. R., Yu, J., & Edwards, W. C. (2010). Pulsed laser deposition of carbon nanotube and polystyrene–carbon nanotube composite thin films. *Optics and Lasers in Engineering, 48*, 1291-1295.

Strobel, R., Baiker, A., & Pratsinis, S. (2006). Aerosol flame synthesis of catalysts. *Advanced Powder Technology, 17*, 457-480.

Strobel, R., & Pratsinis, S. E. (2009). Direct synthesis of maghemite, magnetite and wustite nanoparticles by flame spray pyrolysis. *Advanced Powder Technology, 20*, 190-194.

Su, Y., Zhou, P., Zhao, J., Yang, Z., & Zhang, Y. (2013). Large-scale synthesis of few-walled carbon nanotubes by DC arc discharge in low-pressure flowing air. *Materials Research Bulletin, 48*, 3232-3235.

Sun, X., Bao, W., Lv, Y., Deng, J., & Wang, X. (2007). Synthesis of high quality single-walled carbon nanotubes by arc discharge method in large scale. *Materials Letters, 61*, 3956-3958.

Suntola, T. (1996). Surface chemistry of materials deposition at atomic layer level. *Applied Surface Science, 100-101*, 391-398.

Suntola, T., Lakomaa, E.-L., Knuuttila, H., Knuuttila, P., Krause, O., & Lindfors, S. (2003). Process and apparatus for preparing heterogeneous catalysts. U.S. Patent No. 6,534,431. Fortum Oil and Gas Oy.

Suvanto, M., & Pakkanen, T. A. (1998). Tungsten hexacarbonyl on alumina controlled deposition from gas phase. *Applied Catalysis A: General, 166*, 105-113.

Tahmasebpoor, M., de Martin, L., Talebi, M., Mostoufi, N., & van Ommen, J. R. (2013). The role of the hydrogen bond in dense nanoparticle-gas suspensions. *Physical Chemistry Chemical Physics, 15*, 5788-5793.

Tamadondar, M. R., Zarghami, R., Tahmasebpoor, M., & Mostoufi, N. (2014). Characterization of the bubbling fluidization of nanoparticles. *Particuology, 16*, 75-83.

Teleki, A., Wengeler, R., Wengeler, L., Nirschl, H., & Pratsinis, S. E. (2008). Distinguishing between aggregates and agglomerates of flame-made TiO_2 by high-pressure dispersion. *Powder Technology, 181*, 292-300.

Teoh, W. (2013). A perspective on the flame spray synthesis of photocatalyst nanoparticles. *Materials, 6*, 3194.

Teoh, W. Y., Amal, R., & Mädler, L. (2010). Flame spray pyrolysis: An enabling technology for nanoparticles design and fabrication. *Nanoscale, 2*, 1324-1347.

Teoh, W. Y., Amal, R., Mädler, L., & Pratsinis, S. E. (2007). Flame sprayed visible light-active Fe-TiO_2 for photomineralisation of oxalic acid. *Catalysis Today, 120*, 203-213.

Thess, A., Lee, R., Nikolaev, P., Dai, H., Petit, P., & Robert, J., et al. (1996). Crystalline ropes of metallic carbon nanotubes. *Science, 273*, 483-487.

Tian, B., Li, C., Gu, F., Jiang, H., Hu, Y., & Zhang, J. (2009). Flame sprayed V-doped TiO_2 nanoparticles with enhanced photocatalytic activity under visible light irradiation. *Chemical Engineering Journal, 151*, 220-227.

Tian, Y., Hu, Z., Yang, Y., Wang, X., Chen, X., & Xu, H., et al. (2004). In situ TA-MS study of the six-membered-ring-based growth of carbon nanotubes with benzene precursor. *Journal of the American Chemical Society, 126*, 1180-1183.

Tiznado, H., Domínguez, D., Muñoz-Muñoz, F., Romo-Herrera, J., Machorro, R., & Contreras, O. E., et al. (2014). Pulsed-bed atomic layer deposition setup for powder coating. *Powder Technology, 267*, 201-207.

To, D., Dave, R., Yin, X., & Sundaresan, S. (2009). Deagglomeration of nanoparticle aggregates via rapid expansion of supercritical or high-pressure suspensions. *AIChE Journal, 55*, 2807-2826.

To, D., Sundaresan, S., & Dave, R. (2011). Nanoparticle mixing through rapid expansion of high pressure and supercritical suspensions. *Journal of Nanoparticle Research, 13*, 4253-4266.

Tok, A. I. Y., Boey, F. Y. C., & Zhao, X. L. (2006). Novel synthesis of Al_2O_3 nano-particles by flame spray pyrolysis. *Journal of Materials Processing Technology, 178*, 270-273.

Tsapis, N., Bennett, D., Jackson, B., Weitz, D. A., & Edwards, D. A. (2002). Trojan particles: Large porous carriers of nanoparticles for drug delivery. *Proceedings of the National Academy of Sciences, 99*, 12001-12005.

Tully, J. N., & Olsen, C. M. (1954). Metal oxide production. *U.S. Patent No. 2,670,275*.

Ullmann, M., Friedlander, S., & Schmidt-Ott, A. (2002). Nanoparticle formation by laser ablation. *Journal of Nanoparticle Research, 4*, 499-509.

Valdesueiro, D., Meesters, G., Kreutzer, M., & van Ommen, J. (2015). Gas-phase deposition of ultrathin aluminium oxide films on nanoparticles at ambient conditions. *Materials, 8*, 1249-1263.

Valverde, J. M., & Castellanos, A. (2006). Fluidization of nanoparticles: A modified Richardson-Zaki law. *AIChE Journal, 52*, 838-842.

Valverde, J. M., & Castellanos, A. (2007). Types of gas fluidization of cohesive granular materials. *Physical Review E - Statistical, Nonlinear, and Soft Matter Physics, 75*, 1-6.

Valverde, J. M., & Castellanos, A. (2008). Fluidization of nanoparticles: A simple equation for estimating the size of agglomerates. *Chemical Engineering Journal, 140*, 296-304.

Valverde, J. M., Quintanilla, M. A. S., Castellanos, A., Lepek, D., Quevedo, J., & Dave, R. N., et al. (2008). Fluidization of fine and ultrafine particles using nitrogen and neon as fluidizing gases. *AIChE Journal, 54*, 86-103.

Van Bui, H., Helmer, R., Goulas, A., Grillo, F., & van Ommen, J. R. (2015). Atomic layer deposition of palladium nanoparticles on graphene. In *15th International Conference on Atomic Layer Deposition* (pp. 197). Portland, USA.

Van der Wal, R. L., Hall, L. J., & Berger, G. M. (2002). Optimization of flame synthesis for carbon nanotubes using supported catalyst. *The Journal of Physical Chemistry B, 106*, 13122-13132.

Van der Wal, R. L., & Ticich, T. M. (2001). Flame and furnace synthesis of single-walled and multi-walled carbon nanotubes and nanofibers. *The Journal of Physical Chemistry B, 105*, 10249-10256.

Van Norman, S. A., Tringe, J. W., Sain, J. D., Yang, R., Falconer, J. L., & Weimer, A. W. (2015). Using atomic layer deposited tungsten to increase thermal conductivity of a packed bed. *Applied Physics Letters, 106*, 153102.

van Ommen, J. R. (2013). Apparatus and process for atomic or molecular layer deposition onto particles during pneumatic transport. *U.S. Patent Application No. 13/254,854*.

van Ommen, J. R., Kooijman, D., Niet, M. D., Talebi, M., & Goulas, A. (2015). Continuous production of nanostructured particles using spatial atomic layer deposition. *Journal of Vacuum Science & Technology A: Vacuum, Surfaces, and Films, 33*, 021513.

van Ommen, J. R., Valverde, J. M., & Pfeffer, R. (2012). Fluidization of nanopowders: A review. *Journal of Nanoparticle Research, 14*, 737.

van Ommen, J. R., Yurteri, C. U., Ellis, N., & Kelder, E. M. (2010). Scalable gas-phase processes to create nanostructured particles. *Particuology, 8*, 572-577.

Vasudevan, S. A., Xu, Y., Karwal, S., van Ostaay, H. G. M. E., Meesters, G. M. H., & Talebi, M., et al. (2015). Controlled release from protein particles encapsulated by molecular layer deposition. *Chemical Communications, 51*, 12540-12543.

Vehring, R. (2008). Pharmaceutical particle engineering via spray drying. *Pharmaceutical Research, 25*, 999-1022.

Vehring, R., Foss, W. R., & Lechuga-Ballesteros, D. (2007). Particle formation in spray drying. *Journal of Aerosol Science, 38*, 728-746.

Venegoni, D., Serp, P., Feurer, R., Kihn, Y., Vahlas, C., & Kalck, P. (2002). Parametric study for the growth of carbon nanotubes by catalytic chemical vapor deposition in a fluidized bed reactor. *Carbon, 40*, 1799-1807.

Voll, M., Rothbuhr, L., & Kuhner, G. (1984). Process and apparatus for the production of carbon black. *U.S. Patent No. 4,439,401*. Manfred Full.

Vollath, D. (2008). Plasma synthesis of nanopowders. *Journal of Nanoparticle Research, 10*, 39-57.

Vuori, H., Silvennoinen, R., Lindblad, M., Österholm, H., & Krause, A. (2009). Beta zeolite-supported iridium catalysts by gas phase deposition. *Catalysis Letters, 131*, 7-15.

Wachs, I. E. (2005). Recent conceptual advances in the catalysis science of mixed metal oxide catalytic materials. *Catalysis Today, 100*, 79-94.

Wang, H. Y., & Moore, J. J. (2012). Low temperature growth mechanisms of vertically aligned carbon nanofibers and nanotubes by radio frequency-plasma enhanced chemical vapor deposition. *Carbon, 50*, 1235-1242.

Wang, X. S., Palero, V., Soria, J., & Rhodes, M. J. (2006). Laser-based planar imaging of nano-particle fluidization: Part II—mechanistic analysis of nanoparticle aggregation. *Chemical Engineering Science, 61*, 8040-8049.

Wang, X. S., Rahman, F., & Rhodes, M. J. (2007). Nanoparticle fluidization and Geldart's classification. *Chemical Engineering Science, 62*, 3455-3461.

Wang, Y., Wei, F., Luo, G. H., Yu, H., & Gu, G. S. (2002a). The large-scale production of carbon nanotubes in a nano-agglomerate fluidized-bed reactor. *Chemical Physics Letters, 364*, 568-572.

Wang, Y., Gu, G., Wei, F., & Wu, J. (2002b). Fluidization and agglomerate structure of SiO_2 nanoparticles. *Powder Technology, 124*, 152-159.

Wank, J. R., Buechler, K. J., Hakim, L., George, S. M., & Weimer, A. W. (2004). Coating fine iron particles with an oxidation-resistance γ-alumina nanolayer using ALD in a fluidized bed reactor. In U. Arena, M. Chirone, M. Miccio & P. Salatino (Eds.), *Fluidization XI - Present and Future of Fluidization Engineering* (pp. 603-610).

Wank, J. R., George, S. M., & Weimer, A. W. (2004a). Coating fine nickel particles with Al_2O_3 utilizing an atomic layer deposition-fluidized bed reactor (ALD–FBR). *Journal of the American Ceramic Society, 87*, 762-765.

Wank, J. R., George, S. M., & Weimer, A. W. (2004b). Nanocoating individual cohesive boron nitride particles in a fluidized bed by ALD. *Powder Technology, 142*, 59-69.

Waser, O., Büchel, R., Hintennach, A., Novák, P., & Pratsinis, S. E. (2011). Continuous flame aerosol synthesis of carbon-coated nano-LiFePO$_4$ for Li-ion batteries. *Journal of Aerosol Science, 42*, 657-667.

Wegener, S. L., Marks, T. J., & Stair, P. C. (2012). Design strategies for the molecular level synthesis of supported catalysts. *Accounts of Chemical Research, 45*, 206-214.

Wegner, K., & Pratsinis, S. E. (2003). Scale-up of nanoparticle synthesis in diffusion flame reactors. *Chemical Engineering Science, 58*, 4581-4589.

Wegner, K., Schimmoeller, B., Thiebaut, B., Fernandez, C., & Rao, T. N. (2011). Pilot plants for industrial nanoparticle production by flame spray pyrolysis. *KONA: Powder and Particle Journal*, 29, 251-265.

Wei, B. Q., Vajtai, R., Jung, Y., Ward, J., Zhang, R., & Ramanath, G., et al. (2002). Microfabrication technology: Organized assembly of carbon nanotubes. *Nature, 416*, 495-496.

Wei, D., Dave, R., & Pfeffer, R. (2002). Mixing and characterization of nanosized powders: An assessment of different techniques. *Journal of Nanoparticle Research, 4*, 21-41.

Weidenkaff, A., Ebbinghaus, S. G., Mauron, P., Reller, A., Zhang, Y., & Zuttel, A. (2002). Metal nanoparticles for the production of carbon nanotube composite materials by decomposition of different carbon sources. *Materials Science & Engineering C-Biomimetic and Supramolecular Systems, 19*, 119-123.

Weimer, M. A., Hakim, L. F., King, D. M., Liang, X., Weimer, A. W., & George, S. M., Li, P., et al. (2008). Ultrafast metal-insulator varistors based on tunable Al$_2$O$_3$ tunnel junctions. *Applied Physics Letters, 92*, 164101.

Weiss, R. J., Ly, H. C., Wegner, K., Pratsinis, S. E., & Steinfeld, A. (2005). H$_2$ production by Zn hydrolysis in a hot-wall aerosol reactor. *AIChE Journal, 51*, 1966-1970.

Wiedmann, M. K., Jackson, D. H. K., Pagan-Torres, Y. J., Cho, E., Dumesic, J. A., & Kuech, T. F. (2012). Atomic layer deposition of titanium phosphate on silica nanoparticles. *Journal of Vacuum Science Technology A, 30*, 01A134.

Xanthakis, E., van Ommen, J. R., & Ahrné, L. (2015). Flowability characterization of nanopowders. *Powder Technology, 286*, 156-163.

Xiao, B., Liu, J., Sun, Q., Wang, B., Banis, M. N., & Zhao, D., et al. (2015). Unravelling the role of electrochemically active FePO$_4$ coating by atomic layer deposition for increased high-voltage stability of LiNi$_{0.5}$Mn$_{1.5}$O$_4$ cathode material. *Advanced Science, 2*, 1500022, doi: 10.1002/advs.201500022.

Yan, H., Cheng, H., Yi, H., Lin, Y., Yao, T., & Wang, C., et al. (2015). Single-atom Pd_1/graphene catalyst achieved by atomic layer deposition: Remarkable performance in selective hydrogenation of 1,3-butadiene. *Journal of the American Chemical Society, 137*, 10484-10487.

Yan, Y., Miao, J., Yang, Z., Xiao, F. X., Yang, H. B., & Liu, B., et al. (2015). Carbon nanotube catalysts: Recent advances in synthesis, characterization and applications. *Chemical Society Reviews, 44*, 3295-3346.

Yang, J., Sliva, A., Banerjee, A., Dave, R. N., & Pfeffer, R. (2005). Dry particle coating for improving the flowability of cohesive powders. *Powder Technology, 158*, 21-33.

Yang, J., Wang, Y., Dave, R. N., & Pfeffer, R. (2003). Mixing of nano-particles by rapid expansion of high-pressure suspensions. *Advanced Powder Technology, 14*, 471-493.

Yang, W. (2005). Fluidization of fine cohesive powders and nanoparticles—A Review. *Journal of the Chinese Institute of Chemical Engineers, 36*, 1-15.

Yang, W., Chen, G., Shi, Z., Liu, C. C., Zhang, L., & Xie, G., et al. (2013). Epitaxial growth of single-domain graphene on hexagonal boron nitride. *Nature Materials, 12*, 792-797.

Yoon, J.-H., Jung, S.-C., & Kim, J.-S. (2011). Photocatalytic effects for the TiO_2-coated phosphor materials. *Materials Chemistry and Physics, 125*, 342-346.

Yu, Q., Dave, R. N., Zhu, C., Quevedo, J. A., & Pfeffer, R. (2005). Enhanced fluidization of nanoparticles in an oscillating magnetic field. *AIChE Journal, 51*, 1971-1979.

Yudasaka, M., Ichihashi, T., & Iijima, S. (1998). Roles of laser light and heat in formation of single-wall carbon nanotubes by pulsed laser ablation of $C_xNi_yCo_y$ targets at high temperature. *The Journal of Physical Chemistry B, 102*, 10201-10207.

Yudasaka, M., Kokai, F., Takahashi, K., Yamada, R., Sensui, N., & Ichihashi, T., et al. (1999a). Formation of single-wall carbon nanotubes: Comparison of CO_2 laser ablation and Nd:YAG laser ablation. *The Journal of Physical Chemistry B, 103*, 3576-3581.

Yudasaka, M., Yamada, R., Sensui, N., Wilkins, T., Ichihashi, T., & Iijima, S. (1999b). Mechanism of the effect of NiCo, Ni and Co catalysts on the yield of single-wall carbon nanotubes formed by pulsed Nd:YAG laser ablation. *The Journal of Physical Chemistry B, 103*, 6224-6229.

Yuill, W. A., Natalie, C. A., Flynn, H. E., & Fillipi, B. (2002). Process for producing and cooling titanium dioxide. *U.S. Patent No. 6,419,893.* Kerr-Mcgee Chemical Llc.

Zang, J. B., Lu, J., Qi, X. H., & Wang, Y. H. (2006). Characterization of silicon films grown by atomic layer deposition on nanocrystalline diamond. *Diamond and Related Materials, 15*, 1434-1437.

Zeng, X., Sun, X., Cheng, G., Yan, X., & Xu, X. (2002). Production of multi-wall carbon nanotubes on a large scale. *Physica B: Condensed Matter, 323*, 330-332.

Zhan, G.-D., Du, X., King, D. M., Hakim, L. F., Liang, X., & McCormick, J. A., et al. (2008). Atomic layer deposition on bulk quantities of surfactant-modified single-walled carbon nanotubes. *Journal of the American Ceramic Society, 91*, 831-835.

Zhang, Q., Huang, J. Q., Zhao, M. Q., Qian, W. Z., & Wei, F. (2011). Carbon nanotube mass production: Principles and processes. *Chemsuschem, 4*, 864-889.

Zhang, Q., Zhao, M.-Q., Huang, J.-Q., Liu, Y., Wang, Y., & Qian, W.-Z., et al. (2009). Vertically aligned carbon nanotube arrays grown on a lamellar catalyst by fluidized bed catalytic chemical vapor deposition. *Carbon, 47*, 2600-2610.

Zhang, Q., Zhao, M.-Q., Huang, J.-Q., Nie, J.-Q., & Wei, F. (2010). Mass production of aligned carbon nanotube arrays by fluidized bed catalytic chemical vapor deposition. *Carbon, 48*, 1196-1209.

Zhang, X., & Ahmandi, G. (2011). Effects of electrostatic and capillary forces and surface deformation on particle detachment in turbulent flows. *Journal of Adhesion Science and Technology, 25*(11), 1175-1210.

Zhang, Y., Gu, H., & Iijima, S. (1998). Single-wall carbon nanotubes synthesized by laser ablation in a nitrogen atmosphere. *Applied Physics Letters, 73*, 3827.

Zhao, T., & Liu, Y. (2004). Large scale and high purity synthesis of single-walled carbon nanotubes by arc discharge at controlled temperatures. *Carbon, 42*, 2765-2768.

Zhao, T., Liu, Y., & Zhu, J. (2005). Temperature and catalyst effects on the production of amorphous carbon nanotubes by a modified arc discharge. *Carbon, 43*, 2907-2912.

Zhao, X., Ohkohchi, M., Inoue, S., Suzuki, T., Kadoya, T., & Ando, Y. (2006). Large-scale purification of single-wall carbon nanotubes prepared by electric arc discharge. *Diamond and Related Materials, 15*, 1098-1102.

Zhong, G., Hofmann, S., Yan, F., Telg, H., Warner, J. H., & Eder, D., et al. (2009). Acetylene: A key growth precursor for single-walled carbon nanotube forests. *Journal of Physical Chemistry C, 113*, 17321-17325.

Zhou, D., Cui, Y., Xiao, P. W., Jiang, M. Y., & Han, B. H. (2014). A general and scalable synthesis approach to porous graphene. *Nature Communications, 5*, 4716.

Zhou, Y., King, D. M., Li, J., Barrett, K. S., Goldfarb, R. B., & Weimer, A. W. (2010a). Synthesis of photoactive magnetic nanoparticles with atomic layer deposition. *Industrial & Engineering Chemistry Research, 49*, 6964-6971.

Zhou, Y., King, D. M., Liang, X., Li, J., & Weimer, A. W. (2010b). Optimal preparation of Pt/TiO$_2$ photocatalysts using atomic layer deposition. *Applied Catalysis B: Environmental, 101*, 54-60.

Zhu, C., Liu, G., Yu, Q., Pfeffer, R., Dave, R. N., & Nam, C. H. (2004). Sound assisted fluidization of nanoparticle agglomerates. *Powder Technology, 141*, 119-123.

Zhu, C., Yu, Q., Dave, R. N., & Pfeffer, R. (2005). Gas fluidization characteristics of nanoparticle agglomerates. *AIChE Journal, 51*, 426-439.

Zhu, T., & Li, J. (2010). Ultra-strength materials. *Progress in Materials Science, 55*, 710-757.

Zhu, X., Zhang, Q., Wang, Y., & Wei, F. (2015). Review on the nanoparticle fluidization science and technology. *Chinese Journal of Chemical Engineering, 24*(1), 9-22.